Synthesis, Characterisation and Dissolution of Brannerite. A Uranium Titanate Mineral.

A thesis submitted in fulfilment of the requirements for the degree of

DOCTOR OF PHILOSOPHY

Fiona Anne Charalambous

Bachelor of Science (Applied Chemistry) (Honours)

School of Applied Sciences

RMIT UNIVERSITY

APRIL 2013

Declaration of Authenticity

I certify that except where due acknowledgement has been made, the work is that of the author alone; the work has not been submitted previously, in whole or in part, to qualify for any other academic award; the content of the thesis is a result of work which has been carried out since the official commencement date of the approved research program; and, any editorial work, paid or unpaid, carried out by a third party is acknowledged.

Fiona Anne Charalambous

April 2013

Acknowledgments

I am grateful to many people for their support during the course of my thesis. Firstly I would like to thank my primary supervisor, Prof. Suresh K. Bhargava; whose patience, kindness, limitless support and academic and industrial experience have been irreplaceable to me.

I would like to thank Dr. James Tardio. There are no words to describe the amount of effort you have put into my research project. Your continuous guidance as well as your persevering understanding throughout my PhD has been a pillar of strength (even if you are a bombers supporter!). I really am appreciative of your patience, and the knowledge you have given me to mature into a researcher is unspoken.

A thank you must go to Dr. Mark Pownceby from CSIRO. Your approach and knowledge on mineralogy has been indispensable during my PhD. When I first read your paper on EPMA analysis all those years ago, I thought to myself, finally a technique that could do some serious analysing. I'm very glad I showed the group that paper! Thank you for collaborating with our group and being the friendly and humble scientist we know.

My next thank you is to Dr. Lathe Jones, for your input and patience. Thank you for helping me gain a grasp on electrochemistry, for without it, I would be lost. I cannot wait to work on other areas of electrochemistry with you in the near future.

I would also like to thank the Australian research council-linkage and BHP Billiton for giving me the opportunity to work on this challenging project. Special thanks goes to Dr. Bill Birch (Melbourne Museum), Dr. Robert Gee and Dr. Stephen Grocott for their valuable feedback on all things uranium.

To the uranium crew; Rahul Ram, Scott McMaster and Hailey Reynolds thank you for all the memories working in the radiation lab. It can get pretty crazy at times in there!

I would also like to thank my colleagues in the Centre for Advanced Materials and Industrial Chemistry (CAMIC) for all your support during my PhD. Thank you for all the technical support from the staff at RMIT. I especially want to thank the analytical / technical support from Frank Antolasic, Paul Morrison, Phil Francis, Dr. Johan Du Plessis and Peter Rammul.

The path to becoming a doctor is plagued with distractions. I'd like to thank those distractions for making me the person I am. So a very big thank you to my friends (distractions); Elizabeth Kulikov, Kat Foertig, Vivian Li, Andrew Basile, Nick Nola, Blake Plowman, Rajesh Ramanathan, Jarrod Newnham, Jos Cambell, David Tonkin, Steve Barrow, Hemant Daima, Andrew Pearson and Emma Goethals at RMIT University. To my friends and other distractions back on the Mornington Peninsula; Steph Gregory, Alicia Dikkenberg, Vicky Coyle, Faith Mitchell, Michelle Guest, Samantha Eastwood, Chelsea Vela, Elisha Dowsett, Emma Eddington, Hayley Moss and the Bevilles crew; thank you for keeping me sane and grounded. What would I have done without my dinners with you all!

I would like to thank my family, both immediate and extended for the constant support they have given me over this journey. I thank you for always being there for me and the overwhelming support you have given. To my parents and brother, who have to put up with me every day; you have seen my ups and downs in research. Thank you for just being who you are and supporting me. I have watched and learned from your constant work ethic and I think that is what has made this PhD possible. To my husband Phil; thank you for always knowing what not to say. You have been my rock and have consoled me on numerous occasions while endearing to fix the issues I face. What would I do without you!

To everyone who has supported me throughout my PhD, thank you for helping me be the person I am today. My sincerest thanks to all of you.

This thesis is dedicated to my parents

"Learn from yesterday, live for today, hope for tomorrow.

The important thing is to not stop questioning."

Albert Einstein

Publications

Leaching behaviour of natural and heat-treated brannerite-containing uranium ores in sulfate solutions with iron(III)

F. Charalambous, R. Ram, S. McMaster, M. Pownceby, J. Tardio and S.K. Bhargava

Accepted by Mineral Engineering

An investigation on the dissolution of natural uraninite ores

Minerals Engineering, Volumes 50–51, September 2013, Pages 83-92

R. Ram, F.A. Charalambous, S. McMaster, M.I. Pownceby, J. Tardio and S.K. Bhargava

An investigation on the dissolution of synthetic brannerite (UTi_2O_6)

Hydrometallurgy, Volume 139, July 2013, Pages 1–8

F.A. Charalambous, R. Ram, S. McMaster, J. Tardio and S.K. Bhargava

Chemical and microstructural characterisation studies on natural uraninite and associated gangue minerals

Minerals Engineering, Volume 45, May 2013, Pages 159-169

R. Ram, F.A. Charalambous, S. McMaster, M.I. Pownceby, J. Tardio and S.K. Bhargava

An investigation on the effect of several anions on dissolution of synthetic uraninite (UO_2)

Hydrometallurgy, Volume 136, April 2013, Pages 93-104

R. Ram, F.A. Charalambous, S. McMaster, J. Tardio and S.K. Bhargava

Chemical and microstructural characterisation studies on natural and heat treated brannerite samples

Minerals Engineering, Volume 39, December 2012, Pages 276-288

F.A. Charalambous, R. Ram, M.I. Pownceby, J. Tardio and S.K. Bhargava

An investigation on the effects of Fe (FeII & FeIII) and oxidation reduction potential on the dissolution of synthetic uraninite (UO_2)

Hydrometallurgy, Volume 109, Issue 12, 2011, pp.125-1308

R. Ram, F.A. Charalambous, J. Tardio and S.K. Bhargava

Characterisation of a uranium ore using multiple X-ray diffraction based methods

Mineral engineering, Volume 23, Issue 9, August 2010, pp.1-8

H.S. Reynolds, R. Ram, F.A. Charalambous, F. Antolasic, J. Tardio and S.K. Bhargava

Chemical and Microstructural Characterisation Studies on Naturally Occurring Uranium Minerals - Implications for Processing

GEOMET AUSIMM 2013, Australia, 30/09/2013-02/10/2013

R. Ram, F.A. Charalambous, S. McMaster, M.I. Pownceby, J. Tardio and S.K. Bhargava

Characterisation studies on natural and heated betafite

Proceedings of Chemeca 2013, Australia, 30/09/2013-02/10/2013

R. Ram, S. McMaster, F.A. Charalambous, J. Tardio and S.K. Bhargava

Dissolution of the Uranium Mineral Brannerite

Proceedings of Chemeca 2012, New Zealand, 23-26/09/2012

F.A. Charalambous, R. Ram, S. McMaster, J. Tardio and S.K. Bhargava

Characterisation and Dissolution studies on the Uranium Mineral Betafite

Proceedings of Chemeca 2012, New Zealand, 23-26/09/2012

S. McMaster, R. Ram F.A. Charalambous, J. Tardio and S.K. Bhargava

Characterisation on a brannerite containing mineral samples

Proceedings of Chemeca 2011, Australia, 18-21/09/2011, pp.1-11

F.A. Charalambous, R. Ram, J. Tardio and S.K. Bhargava

An Investigation on the synthesis of the uranium mineral brannerite

Proceedings of Chemeca 2011, Australia, 18-21/09/2011, pp.1-8

M. Amin, F.A. Charalambous, J. Tardio and S.K. Bhargava

Characterisation and dissolution studies on varying forms of brannerite

Proceedings of the 3rd International conference on Uranium, Saskatoon, Saskatchewan, Canada, 15-18th August, 2010, pp. 597-608

F.A. Charalambous, R. Ram, J. Tardio and S.K. Bhargava

The effect of various halides on dissolution of synthetic uranium dioxide

Proceedings of the 3rd International Conference on Uranium, Saskatoon, Saskatchewan, Canada, 15-18/08/2010, pp.585-595

R. Ram, F.A. Charalambous, J. Tardio and S.K. Bhargava

Investigation of dissolutions kinetics of synthetic uraninite (UO_2/UO_2^{2+})

Proceedings of Chemeca 2009 Perth, Australia, 27-30/09/2009, pp.1-10

R. Ram, F.A. Charalambous, J. Tardio, A. Hussein and S.K. Bhargava

Table of Content

List of Tables

List of Figures

Glossary of Terms and Abbreviations

A

a.u	Arbitrary Units

B

BSE	Back Scatter Electron

C

CP	Carbon Paste
CPE	Carbon Paste Electrodes
CV	Cyclic Voltammetry

E

E	Potential
EDX	Energy Dispersive Spectroscopy
EPMA	Electron Probe Micro-Analyser
eV	electron Volts (units for the measure of Binding Energy)

F

Feed	The sample which is to go into that process

H

HNBCW	Heated Natural Brannerite Crockers Well
HNBRD	Heated Natural Brannerite Roxby Downs

I

i	Current
IR	Infrared Spectroscopy
ICP-MS	Inductively Coupled Plasma Mass Spectrometry

L

LSV	Linear Sweep Voltammetry

N

NBCW	Natural Brannerite Crockers Well
NBRD	Natural Brannerite Roxby Downs

O

ORP	Oxidation-Reduction Potential

P

ppm	Parts per Million

R

REE	Rare Earth Elements

S

SEM	Scanning Electron Microscope/Microscopy
T	
TG/DTA	Thermogravimetry / Differential Thermal Analysis
W	
WA	Wavelength Dispersive
X	
XRD	X-ray Diffraction
XPS	X-ray Photoelectron Spectroscopy

Abstract

A number of different uranium minerals are processed in different regions of the world to produce the uranium based fuel that is used to generate electricity. Potential future increases in demands for uranium based fuel have led to increased interest in the extraction of uranium from minerals that to date have not been mined / processed as extensively as the most widely mined / processed uranium mineral uraninite. The uranium titanate mineral brannerite (UTi_2O_6), which is found in numerous uranium ore bodies around the world, is one such mineral that may be a potential future source for increased uranium production.

In this thesis the characteristics and dissolution chemistry of both natural and synthetic brannerites have been investigated in detail. Natural samples were investigated to identify the major minerals that are in close association with naturally occurring brannerite. Leaching chemistry of all natural and synthetic brannerites have been studied under conditions that are used in uranium minerals processing. An electrochemical leaching study of synthetic brannerite was undertaken to examine the surface behaviour of synthetic brannerite suspended in tank based leaching conditions similar to those used in uranium mineral processing.

Characterisation studies conducted on two naturally occurring brannerites ore bodies from South Australia, focussed on their chemistry and mineralogy, and involved the use of use of multiple characterisation techniques (X-ray Diffraction Analysis, Raman Spectroscopy, Scanning Electron Microscopy and Electron Probe Micro Analysis). Recrystallization of the natural brannerite samples (via heat treatment) were also investigated. From the results obtained, the natural brannerite samples contained brannerite

that was rich in thorium and also uranothorite and thorianite-uraninite phases. Gangue mineralogy phases found in both mineral samples were rutile quartz, aluminosilicates, unidentified REE-containing phosphates, zircon, titanates and apatite. After heat treatment the natural brannerite samples contained a high-Th brannerite and the thorianite-uraninite phase in the unheated samples was decomposed into separate ThO_2 and UO_2 phases.

One of the research aims of this thesis was to synthesise and characterise a brannerite that has little impurities (rutile and uraninite) as possible and use this synthetic product to investigate the maximum extraction of uranium. This investigation was undertaken to gain detailed knowledge into the rate of dissolution of the synthesised brannerite over a range of conditions (temperature, $[H_2SO_4]$ and [Fe] / ORP). One for the major findings from this research indicated that [Fe(III)] (over the range 3 – 12 g/L) did not have a significant influence on dissolution at a reaction temperature of 50 °C (in 15 g/L H_2SO_4). Yet at 95 °C in 15 g/L H_2SO_4, increasing [Fe(III)] (over the range 3 – 12 g/L) leads to significant increases in the dissolution rate.

These aforementioned dissolution tests were conducted to probe the mechanism of synthetic brannerite dissolution and were compared with respect to the electrochemical behaviour of this synthetic mineral. An investigation was undertaken to determine the reason why this uranium mineral is not readily leachable under mild conditions and to determine if any type of passivation was occurring on the surface of synthetic brannerite. Tafel curves reveal that acid concentrations from 15 to 50 g/L H_2SO_4 show limited leaching, with only a modestly active region corresponding to dissolution. H_2SO_4 concentrations of 100 to 150 g/L show a well-defined active region, ranging from approximately 0.45 to 0.55 V vs Ag/AgCl, where dissolution proceeds readily, but further scanning in the anodic direction leads to surface passivation, and a rapid drop off of the dissolution current.

When dissolution tests for the two natural brannerite samples were conducted under identical conditions investigated for synthetic brannerite, the results showed that the effect of increasing [Fe(III)], [H_2SO_4], and temperature was to increase the solubility of uranium from brannerite. The natural brannerite samples that were heat treated to 1200 ºC to restore crystallinity resulted in poor uranium extraction under identical conditions, with maximum uranium extraction rates of < 10 % uranium observed. The lower extraction rates were attributed to the heat treatment causing chemical and structural (recrystallisation) changes to the brannerite.

Uranium recovery processes from brannerite is not straightforward with the efficiency of uranium recovery being greatly influenced by the mineralogical characteristics of the ore. Synthetic and natural brannerites can achieve high uranium extraction rates providing that acid strength, oxidant strength and temperatures are maintained at high levels.

Chapter 1

Introduction and Literature Review

This chapter provides an overview of the field of uranium processing; a brief history of uranium mining and processing in Australia: a discussion of the chemistry of uranium minerals and the importance of the uranium bearing mineral brannerite. The synthesis of synthetic versions of brannerite is also discussed.

Global warming concerns have led to significant interest in processes for generating electrical energy that do not generate significant quantities of carbon dioxide. The generation of electricity via uranium based nuclear fuel is a well-established technology that does not result in the production of significant quantities of carbon dioxide and hence is considered by many as a replacement for fossil fuel based processes. Hence the element uranium (and the minerals in which it is found) may receive significantly increased interest in the near future.

The nuclear energy market is expected to grow substantially over the next 20 years, for example in the U.S. alone it is predicted to rise by 50 % by 2030, whilst worldwide electricity consumption is expected to double by 2030 according to the Department of Energy (World Nuclear Association, 2012a).

Due to the predicted increase in uranium demands and with a decrease in the availability of numerous high quality grade ores, a greater understanding and awareness is needed to improve the mining technology of refractory ores to meet future uranium demands without increasing environmental impact. For industrial companies to achieve such demands with minimal environmental impact, an enhanced fundamental understanding of chemical processes is essential. Areas that are essential in understanding the aforementioned are; composition / structure of uranium minerals and their effects on the processing of uranium, as well as the chemical / mechanism reactions that are involved in the dissolution of uranium minerals that influence leaching, by the liberation of gangue minerals and the uranium speciation in aqueous solutions.

The major objective of this thesis was to improve the understanding of the fundamental chemistry of the uranium titanate mineral, brannerite by gaining knowledge of its composition / structure of natural and synthetic samples and to gain an improved understanding of the dissolution behaviour of this refractory mineral.

1.1. Literature Review

1.1 Historical background of Uranium

Uranium was discovered in the mineral pitchblende (U_3O_8) in 1789 by the German chemist, Martin Heinrich Klaproth (to date uranium has been identified as a major constituent in over 200 naturally occurring minerals) (Clark, et al., 2006; Burns and Finch, 1999; Finch and Murakami, 1999). In 1841 French scientist, Eugene Peligot first isolated uranium in the metallic state. In 1896, the French physicist Antoine Becquerel discovered the radioactive properties of uranium, and in 1898 Marie and Pierre Curie carried out further pioneering work on atoms, radioactivity and uranium. Research by Enrico Fermi and others starting in 1934 led to its use as a fuel for the generation of the electricity industry. In the 1940s a team of scientists created the world's second artificial nuclear reactor but the first reactor that was continuous. By the late 1950s, several nuclear reactors were in commercial use generating electricity for towns around, The Soviet Union, England and The United States of America.

1.1.2. Uranium mining production in Australia

Uranium minerals have been mined in Australia since 1954 and currently there are four operating mines in Australia. Australia has 31 % of the world's uranium reserves (World Nuclear Association, 2012b) and the world's largest single uranium deposit, located at the Olympic Dam Mine in South Australia.

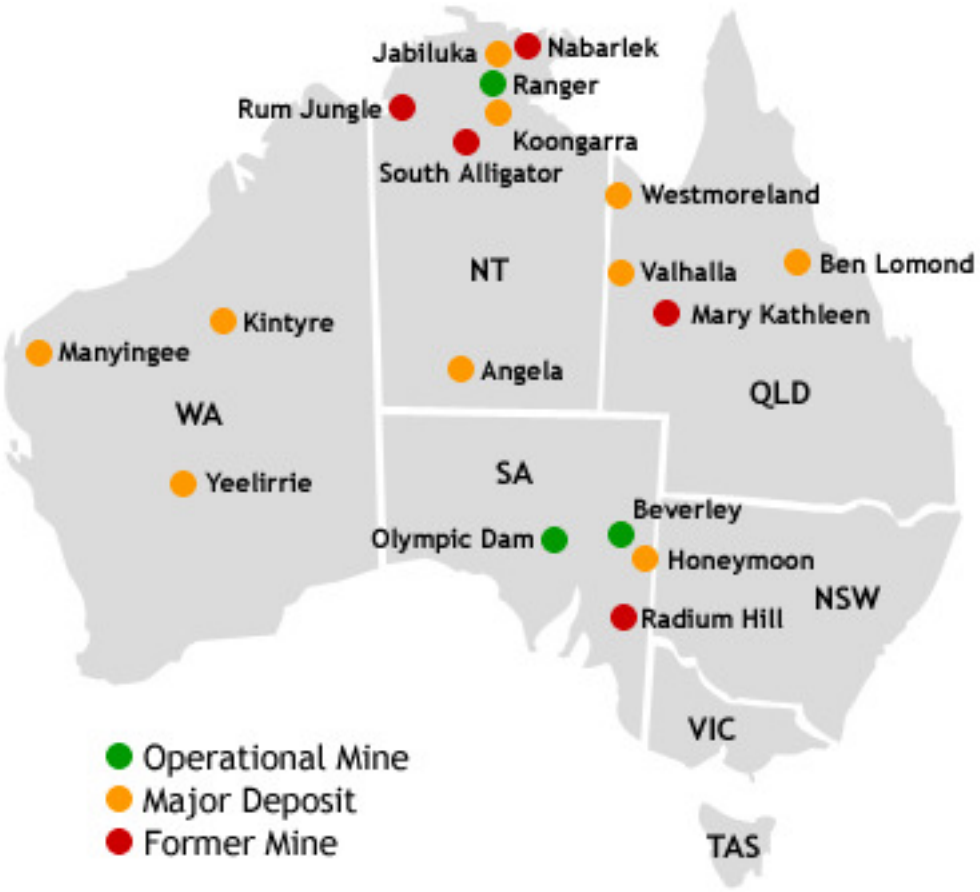

Figure 1.1: Map of Australia's past and present mines and deposits (Australian Uranium, 2013).

The three largest uranium mines in Australia are Olympic Dam, Ranger Uranium Mine and Beverley Uranium Mine. Future production is expected from Honeymoon Uranium Mine and the planned Four Mile uranium mine (shown in Figure 1.1 (Australian Uranium, 2013)).

Radium Hill in South Australia was the first uranium mine and where the mineral davidite was discovered. Ores containing radium and uranium at high concentrations were found, as well as camotite and trace amounts of ilmenite, rutile, magnetite, hematite,

pyrite, chalcopyrite inter-grown with quartz and biotite, chromium, vanadium and molybdenum.

The Rum Jungle uranium deposit in the Northern Territory operated from 1954 to 1971, were the major metals processed were uranium and copper.

The Mary Kathleen open-cut uranium mine in Queensland operated from 1958 to 1963 and then re-opened again in 1976 to 1982.

Olympic Dam (OD), located at 265 km north of Port Augusta in South Australia, commenced operations in 1988 and was acquired by BHB-Billiton in 2005 (World Nuclear Association, 2008). It is potentially the world's largest uranium producer, with estimated ore reserves of 195, 883 tonnes of uranium, 7.5 million tonnes of copper and significant amounts of gold and silver (Agency, O.N.E. and Agency, I.A.E., 2006).

Ranger Uranium Mine in the Northern Territory is surrounded by the Kakadu National Park. It is operated by Energy Resources of Australia and the Rio Tinto Group. The operation began processing of the uranium ore body in 1980 (ore is ground and sulphuric acid leached) and in 2006 an expansion was announced to process low grade ore material.

Beverley Uranium Mine in South Australia is Australia's first in-situ mine located in the Flinders Rangers. It first opened in 2001 and the major uranium mineral, coffinite is hosted by loose sands in the channel of a former river.

Honeymoon Uranium Mine is Australia's fourth uranium deposit to go into production and its second in-situ recovery mine (ABC News, 2009).

The Four Mile Mine deposit in South Australia is the fifth uranium deposit to go into production in Australia. In 2009, Alliance Resources publicized that the deposit contained 28,000 tonnes of uranium oxide and the ore grade was ten times that of Olympic Dam mine and double that of the Ranger mine (Tasker, 2009). Approval of the mine was given in 2009 after Australia's three-mine policy (established in 2007) had been abolished.

In 2010-2011, Kazakhstan, Canada and Australia produced concentrated uranium oxides of 33%, 18% and 11% of world production respectively.

1.2. Uranium mineral deposits / uranium minerals

Concentrated deposits of uranium minerals are found in various regions of the world. There are 15 different types of deposits that have been identified (shown in Table 1.1), which have been further categorised according to their geological setting and genesis of mineralisation.

Table 1.1: Types of uranium deposits.

Deposit type	Location	Ore / Mineral type	Ore grade
Unconformity-related deposits	Saskatchewan, Canada and Northern Territory, Australia	Quartz-rich sandstones	Highest grade
Sandstone deposits	Australia, Mongolia, South America and Africa	Pitchblende, coffinite and secondary minerals.	Low to medium grade.
Quartz-pebble conglomerate deposits	Ontario, Canada and South Africa	Uraninite, uranothorite, brannerite and coffinite	Low grade with high tonnages
Breccia complex deposits	South Australia, Queensland, Australia, Chile, Brazil and Southern Peru	Uraninite, brannerite and coffinite	Low grade
Vein deposits	France, Germany, Czech Republic, Canada and Africa	Uraninite and pitchblende	Low grade
Intrusive deposits	Namibia, Greenland and South Africa	Betafite and uraninite	Low grade
Phosphorite deposits	United States and Morocco	Torbernite	Low grade
Collapse breccia pipe deposits	United States	Uraninite and pitchblende	Medium grade
Volcanic deposits	Russia, Mongolia, Nevada and Siberia	Pitchblende	Low grade
Metasomatite deposits	Ukraine, Brazil, United States and Queensland, Australia	Uraninite and brannerite	Low grade
Metamorphic deposits	Queensland, Australia and Austria	Uraninite	Low grade
Lignite	Greece and United State		Not commercially viable
Black shale deposits	Sweden, United States, Brazil and Germany*	Uranium oxide minerals	Low grade
Other types of deposits - (Jurassic Todilto Limestone, Permian hard coal (and host rocks) and uranium extraction from fly ash)	United States, Germany, Hungry and China	Jurassic Todilto Limestone, Permian hard coal (and host rocks) and uranium extraction from fly ash	Low grade

* High grade

Olympic Dam in Southern Australia is the only iron-ore-copper-gold (IOCG-U) deposit known as a Breccia complex deposit. There are many types of uranium ores around the world, as a result of the differing ores, different minerals processing procedures are applied and it is therefore very important to understand the type of ore being processed.

As mentioned previously there have been over 200 minerals discovered to date that contain uranium as major constituent. The most common uranium mineral is known as uraninite (UO_2) or pitchblende (UO_3, U_2O_5) or collectively referred to as U_3O_8. Other primary uranium minerals include coffinite ($U(SiO_4)_{1-x}(OH)_{4x}$), brannerite (UTi_2O_6), davidite ($(REE)(Y, U)(Ti,Fe^{3+})_{20}O_{38}$, betafite ($(Ca,U)_2(Ti,Nb,Ta)_2O_6$) and thucholite (uranium-bearing pyrobitumen). Secondary uranium minerals include autunite ($Ca(UO_2)_2(PO_4)_2$ x 8-12H_2O), carnotite ($K_2(UO_2)_2(VO_4)_2$ x 1-3H_2O), gummite (a mixture of oxides, silicates and hydrates of uranium), seleeite ($Mg(UO_2)_2(PO_4)_2$ x 10H_2O), torbernite ($Cu(UO_2)_2(PO_4)_2$ x 12H_2O), tyuyamunite ($Ca(UO_2)_2(PO_4)_2$ x 8-10H_2O) and Zeunerite ($Cu(UO_2)_2(AsO_4)_2$ x 8-10H_2O).

Most uranium minerals can be separated into two groups; the reduced species- which contain uranium as U^{4+} - and the oxidized species- which contain uranium as U^{6+}. There are very few mixed valence (4+ / 6+) minerals and at least one uranium mineral that contains U^{5+} (Burns and Finch, 1999). Uranium ore deposits predominately contain reduced uranium species. The reduced uranium minerals are often more chemically complicated that their original structures due to isomorphous substitution of elements such as Th^{4+} and REE^{3+} and U^{4+}. The addition of substituting elements such as Th^{4+} and REE^{3+} for U^{4+} is common in reduced uranium minerals.

There are a number of commercially important uranium minerals (from which uranium is extracted to produce uranium based nuclear fuel). The three most important uranium

minerals from a uranium minerals processing perspective are uraninite, coffinite and brannerite.

Uraninite

Uraninite (UO_{2+x}) is the most common U^{4+} mineral and is the main ore mineral in many uranium deposits found around the world. Uraninite has a fluorite structure, where the uranium is coordinated by eight oxygen atoms in cubic arrangement, in which each oxygen atom bonds with four uranium atoms. The structure of natural uraninite contains many defects due to oxidation and substitution on the uranium site, as well as radiation damage.

Coffinite

Coffinite is a tetragonal orthosilicate with U^{4+} coordinated by eight oxygen atoms in the form of a distorted cube-like polyhedron. The chemical formula of coffinite is still controversial with respect to the existence of water molecules $USiO_4 \cdot nH_2O$) or hydroxyl groups ($U(SiO_4)_{1-x}(OH)_{4x}$).

Brannerite

Brannerite is an archetype structure and adopts a monoclinic symmetry where the anatase-like edge TiO_6 octahedra shares corners and edges to the $U^{4+}O_6$ octahedra. The chemical formula of brannerite is $U^{4+}Ti_2O_6$, where the uranium in brannerite is partly oxidized. Brannerite crystals are metamict and recovering their crystallinity requires annealing to produce an X-ray diffraction pattern.

1.3. Uranium minerals processing

In Australia there are three types of mines in operation at the present, in-situ leaching (Beverley, Honeymoon and the soon to be open Four Mile mine), open-pit mining (Ranger Mine) and an underground mine (Olympic Dam).

Olympic Dam is an extremely large site which produces copper, uranium, gold and silver. The deposit itself is known as an iron oxide copper gold deposit and is the fourth largest copper deposit and the largest known single deposit of uranium in the world. The site hosts an underground mine as well as an intergraded metallurgical processing plant.

The metallurgical processing plant processes uranium containing ore into yellow cake is achieved using a combination of processes (characterisation, preconcentation / leaching and treatment of the liquor. Yellow cake is then shopped off shore to countries such as the United States of America, to where the purification of yellow cake to UF_6 and preparation of UO_2 nuclear fuel used in nuclear fuel rods. Of these processes the characterisation and leaching process is of considerable interest to this thesis, which is discussed in detail as follows.

1.3.1. Characterisation

To recover uranium from ores, a series of steps is required, but ultimately the aforementioned depends on the nature of the ore involved. Characterisation techniques are used to identify the host gangue mineralogy such as quartz- which is chemically inactive or calcite- an acid consuming mineral. Highly refractory ores require intensive processing whereas others break down between the mine and the mill. It is therefore important to understand the mineralogy before extraction has been begun.

1.3.2. Preconcentration / leaching

After thoroughly characterising the gangue mineralogy and uranium minerals in the orebody, a pre-treatment is essential to enrich a low-grade ore to be processed economically.

The high grade, run-of-mine ore is crushed and ground to liberate the mineral particles to prepare the ore for leaching. For low grade ores, floatation is commonly used as a pre-concentration step prior to leaching. Size reduction of the ore is necessary and is adequate for most types of ores which use sulphuric acid in their process, however finer grinding is needed for only alkali treated ores.

The leaching process is carefully chosen according to the mineralogical nature investigated in the characterisation of the ore (section 1.3.1).

For acid treatment of ores dilute sulphuric acid is always used, where the rate of dissolution is dependent on acid concentration, temperature and surface area of the particles within the ore. Highly concentrated acid is only used in ores that contain feldspar and clay, since the high concentration will dissolve any aluminium silicates. If tetravalent uranium is present (minerals such as uraninite, coffinite and brannerite), an oxidising agent such as sodium chlorate or manganese dioxide with dissolved iron acting as a catalyst; is added to the leaching solution (Peehs, et al., 2012). The following reactions that occur during the dissolution process are listed in equations 1-5 (Clark, 2006):

$$2\,H_2SO_4 + MnO_2 + UO_2 \rightarrow UO_2SO_4 + MnSO_4 + 2\,H_2O \qquad \text{(Equation 1.1)}$$

$$3\,H_2SO_4 + NaClO_3 + 3\,UO_2 \rightarrow 3\,UO_2SO_4 + NaCl + 3\,H_2O \qquad \text{(Equation 1.2)}$$

$$UO_2 + 2\,Fe^{3+} \rightarrow UO_2^{2+} + 2\,Fe^{2+} \qquad \text{(Equation 1.3)}$$

$$2\,Fe^{2+} + MnO_2 + 4\,H^+ \rightarrow 2\,Fe^{3+} + Mn^{2+} + 2\,H_2O \qquad \text{(Equation 1.4)}$$

$$6\,Fe^{2+} + ClO_3^- + 6\,H^+ \rightarrow 6\,Fe^{3+} + Cl^- + 3\,H_2O \qquad \text{(Equation 1.5)}$$

Complex anions such as $[UO_2(SO_4)_3]^{4-}$ are also formed at high concentrations but do not cause problems in later processing (Clark, 2006).

For alkaline treatment an alkaline solution is used on more finely ground ores. For alkaline treated ores, it is considered to be slower than acid leaching but is more effective with ores containing gangue minerals such as calcium compounds or other acid-consuming minerals. Carbonate leaching is selectively leached and is carried out using sodium carbonate. If tetravalent uranium is present as an oxidant, such as oxygen (as air) or permanganate is typically used to generate a more soluble hexavalent uranium species (Peehs, et al., 2012). The dissolution of simple uranium oxide follows the reactions shown in equations 6-8 (Clark, 2006). Biocarbonate is used to kept the hydroxide concentration low and avoid the precipitation of urinates (equation 9).

$$2\,UO_2 + O_2 \rightarrow 2\,UO_3 \qquad \text{(Equation 1.6)}$$

$$UO_3 + 3\,CO_3^{2-} + H_2O \rightarrow UO_2(CO_3)_3^{4-} + 2\,OH^- \qquad \text{(Equation 1.7)}$$

$$OH^- + 2\,HCO_3^- \rightarrow CO_3^{2-} + H_2O \qquad \text{(Equation 1.8)}$$

$$2\,UO_2(CO_3)_3^{4-} + 6\,OH^- + 2Na^+ \rightarrow Na_2U_2O_7 + 6\,CO_3^{2-} + 3\,H_2O \qquad \text{(Equation 1.9)}$$

1.3.3. Recovery of uranium from leach solutions to refining to a high-purity product

Ion exchange, solvent extraction and the Eluex process (a combination of the aforementioned two processes) can be used to remove uranium from the leached liquor. Removed first from the liquor are the undissolved solids (which would have a negative effect) by sedimentation or decanting or with hydro cyclones, filters or centrifuges (Peehs, et al., 2012).

Ion exchange

In ion exchange, an anion exchange resin is used to selectively adsorbs the hexavalent uranium into either the anionic sulfato or the carbonato complex from leached solutions (Peehs, et al., 2012). In carbonate solution the uranyl species is thought to be the *tris*-carbonato complex, $UO_2(CO_3)_3^{4-}$ and from sulphate solutions the anion is likely to be $UO_2(SO_4)_n^{2-2n}$ (n is either 3 or 2). Strongly basic ion exchanger is generally used to extract these complexes (equations 10 and 11), where the R is the matrix and X is the functional basic group of the ion exchanger (Clark, 2006).

$$4\,RX + [UO_2(CO_3)_3]^{4-} = R_4[UO_2(CO_3)_3] + 4\,X^- \quad \text{(Equation 1.10)}$$

$$4\,RX + [UO_2(SO_4)_3]^{4-} = R_4[UO_2(SO_4)_3] + 4\,X^- \quad \text{(Equation 1.11)}$$

The sulphate solution is acidified and the carbonate solution is kept slightly basic with addition of bicarbonate (Merritt, 1971.). From this solution the uranium is precipitated and recovered as a fairly pure uranium concentrate.

Solvent Extraction

In solvent extraction two types of solvents are used in the extraction process; the first includes alkylated phosphoric acids and pyrophosphoric acids and the second, higher aliphatic amines (Peehs, et al., 2012). During the process, both types are dissolved in inert hydrocarbons, mostly high-purity kerosene. The mechanism of extraction is based on ion exchange in the liquid phase.

Eluex process

In the Eluex process, uranium is separated by ion-exchange resin subsequently by solvent extraction (Merritt, 1971.). The ion exchange resin collects uranium quantitatively and the breakthrough of foreign ions is tolerated since these are removed easily in the solvent extraction stage. In this process, the first stage has the useful effect of increasing the concentration of uranium, with consequent reduction in the mass flow and the second stage improves the purification effect of this step as the uranium concentration in the feed is higher (Clark, 2006; Peehs, et al., 2012).

Refining to a high-purity product

Yellow cake (65-85 % U_3O_8) product of uranium milling operations is not generally pure enough for use in most nuclear applications and therefore refining yellow-cake into a product of satisfactory purity for use in the nuclear industry is required. From the abovementioned process, yellow-cake is refined from these solutions where by the uranium in the form of its sulphate complex or the carbonato complex (Peehs, et al., 2012). Yellow cake is then produced by precipitation from the acid liquor with ammonia or $Mg(OH)_2$ or by precipitation from alkaline liquor with NaOH. The dried uranium concentrate product obtained is called yellow cake due to its colour and form, where the precipitation is carried out in large, agitated vessels.

1.3.4. Purifying yellow cake to UF_6

In a wet treatment process, the refined high-purity product, the obtained yellow cake is dissolved in nitric acid and then purified using solvent extraction. The resulting solution of uranium in nitric acid can then be reacted chemically to form UO_2 or UO_3 by using either the ammonium diuranate or the ammonium uranyl carbonate process, or by denitrating evaporation (Peehs, et al., 2012). The intermediate product is then calcined to form UO_2. In

a two stage process UO_2 is then converted to UF_6, by treating UO_2 produced with HF to form UF_4 is then converted into UF_6 by treatment with fluorine gas. The dry UF_6 product must then be purified by fractional distillation (Peehs, et al., 2012).

1.3.5. Preparation of UO_2 nuclear fuel pellets

The preparation of UO_2 nuclear fuel pellets entails the purified UF_6 product to be enriched by either wet methods such as ammonium diuranate or the ammonium uranyl carbonate process and / or dry methods such as Integrated Dry Route, Direct Conversion, General Electric Dry conversion to obtain a UO_2 powder (Peehs, et al., 2012). The powder must be pretreated, except in the ammonium uranyl carbonate process, only after pretreatment do the various steps of pelletization, such as compression, sintering, and grinding; give an end product with the preferred properties (Peehs, et al., 2012).

1.4. Brannerite

As mentioned previously brannerite is a uranous titanate mineral that occurs naturally in many uranium ore bodies (Zhang, et al., 2001). The structure and composition of naturally occurring and synthetic brannerite; synthesis of synthetic versions of brannerite and the dissolution of brannerite are discussed in detail in the proceeding sections.

1.4.1. Structure, composition and preparation of synthetic forms

Brannerite's crystal structure is monoclinic and both the U and Ti atoms are in distorted octahedral coordination (Zhang et al., 2001). Figure 1.2 shows the distorted polyhedral diagram of UTi_2O_6 projected along the [0 1 0] direction. The TiO_6 octahedra form a zigzag sheet by sharing common edges and the neighbouring sheets are connected by UO_6

octahedra (Lian, et al., 2002). The structure of synthetic brannerite was determined by Szymanski and Scott (1982), and contains both U^{4+} and Ti^{4+} in octahedral coordination ($U_{r\Phi6}$ hexagonal bipyramid).

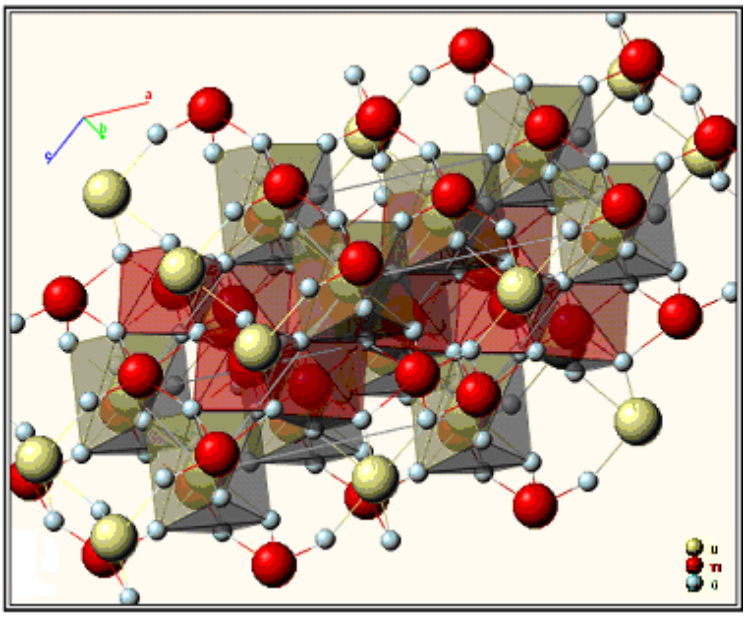

Figure 1.2: Crystal structure of Brannerite (Szymanski and Scott, 1982).

Natural brannerite generally contains impurity elements including Pb, Ca, Th, Y and REE on the U-site, and Si, Al and Fe on the Ti-site (Lian, et al., 2002). Natural brannerite is completely metamict (amorphous) as a result of the α-decay damage from the constituent U and Th (Lian, et al., 2002) and requires annealing to reconstitute the crystal structure and thus produce an XRD pattern. The recrystallisation of natural amorphous brannerite on annealing at ~1000 °C has been confirmed by X-ray diffraction (XRD) (Zhang, et al., 2006; Patchett and Nuffield, 1960). Thermogravitry along with differential thermal analysis (TG/DTA) (Zhang, et al., 2006; Balek, et al., 2007) and emanation thermal analysis (ETA) (Balek, et al., 2007) has been used to investigate and characterise the thermal reactivity / recrystallisation of amorphous brannerite. Also a study of an

amorphous natural brannerite has been conducted with the details of its thermal recrystallisation and the effect of radiation damage on its chemical durability reported (Zhang et al., 2006). Figure 1.3 is an image of natural brannerite from the Crockers Well region in South Australia.

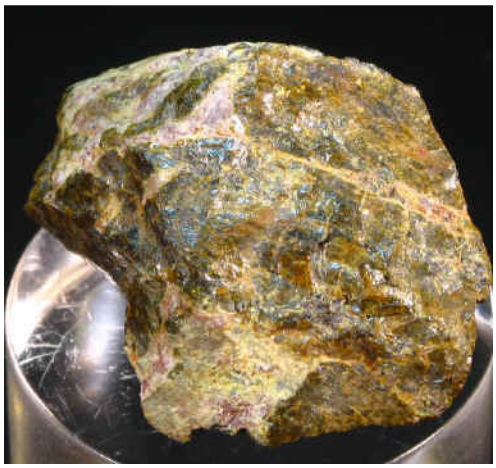

Figure 1.3: Brannerite from Crockers Well East, Olary Ranges, South Australia, Australia (sample size: 2.5 x 2 x 1 cm) (Mineral Atlas, 2012).

The U in natural brannerite is nearly always partly oxidized (Burns and Finch, 1999). The presence of Pb is mainly due to the radioactive decay of U and Th (e.g. ^{238}U and ^{232}Th series) (Zhang, et al., 2006). Brannerite also exists, as a minor phase, in the ceramic formulations designed for the immobilization of spent nuclear fuel and surplus plutonium (Zhang, et al., 2006). From compositional and leach studies, sufficient evidence exists to support the presence of coffinite ($U[SiO_4]_{1-x}[OH]_{4x}$) as an alteration product inter-growing with brannerite (Zhang, et al., 2003).

There is very little information available in the open literature on the mineralogy of brannerite containing ore bodies. Analysis of ore samples from the Sunshine Mine in Idaho, USA, which is a silver and base metal vein deposit, showed that most of the

uranium occurs in a prismatic UTi_2O_6 mineral, commonly in aggregates of 5–50 μm long lath-like crystals, identified as originally being brannerite. Subsequently, the brannerite has exsolved into extremely fine-grained uraninite and a TiO_2 polymorph (Zartman and Smith, 2009). Quantitative microprobe spot analyses were made on different areas of the prismatic crystals all of which revealed uranium and titanium, reported as UO_2 and TiO_2, in the approximate molar ratio of 1:2 (Zartman and Smith, 2009). An X-ray diffraction confirmation of the U–Ti phase has not yet been achieved, but brannerite with the idealized formula UTi_2O_6 satisfies both the chemical and crystallographic attributes of the mineral (Zartman and Smith, 2009). Analysis on other areas showed a particularly large brannerite crystal with considerable variation in backscatter electron (BSE) intensity; three separate spot analyses give slightly different compositions with the highest uranium and lowest titanium concentrations occurring in the lightest area (Zartman and Smith, 2009). This region also contained several uraninite grains, some apparently replacing the brannerite, and others proposed to have formed from uranium that migrated out of the brannerite. Except for its presence as a fine-grained product of brannerite un-mixing, this one minor and apparently secondary occurrence represents the only positive identification of uraninite encountered in the study (Zartman and Smith, 2009).

A recent study on brannerite mineralogy was conducted on gold deposits in the Vaal River region in South Africa. Analysis in this study showed that uraninite as well as brannerite-type minerals are jointly responsible for the major portion of uranium carriers in ore from the Witwatersrand basin. 80–90% of the uranium in the ores is contained as uraninite, 8–19% as brannerite, and the balance as traces of coffinite and uranium phosphates (Lottering, et al., 2008). Liebenberg (1955) distinguished between two uraniferous titanates in Witwatersrand ore: uraniferous leucoxene and brannerite which have UO_2:TiO_2 mole ratios of <1 and >1, respectively (Lottering, et al., 2008). Previous

work done by Glatthaar and Duchovny (Glatthaar and Duchovny, 1979) indicated that Vaal River ores mostly consist of brannerite associated with leucoxene and other titaniferous minerals (termed uraniferous leucoxene) which have a more loosely knit appearance and probably are more readily available for dissolution as compared to brannerite associated with silicates (termed brannerite), which occurs as minute, compact crystals intergrown in the siliceous material (Lottering, et al., 2008). This however, is not indicative that the different types of brannerite minerals will dissolve. Minerals with exposed surface area are technically leachable as they can be accessed by a lixiviant. 71% to 86% of the brannerite particles have more than 10% of their surfaces exposed, and even higher proportions have more than 5% of their surfaces exposed (Lottering, et al., 2008).

Synthetic brannerite is often associated with rutile and in many cases with anatase as a natural alteration product (Zhang, et al., 2003). Previously reported experimental studies on the syntheses of brannerite have shown that the prepared brannerite contains minor rutile inclusions (~5% TiO_2 and trace amounts of reduced Ti oxide) and trace amounts of UO_2 (<0.1%) (Zhang, et al., 2001; Zhang, et al., 2003; Zhang, et al., 2004; Zhang, et al., 2001; Thomas and Zhang, 2003). There are many methods that have been reported for preparing synthetic brannerite. The most common method reported is known as the alkoxide/nitrate route (Ringwood, 1988). This method involves the following main reaction steps:

- Preparation of an aqueous solution containing stoichiometric amounts of U and Ti
- Co-precipitation of U and Ti hydroxides
- Heating of hydroxides to remove water, nitrate and alcohol
- Wet milling and drying
- Hot-pressing the milled product at 1260°C for 2 h under 21 MPa in graphite dies (Zhang, et al., 2001).

Synthetic brannerite can also be prepared by wet grinding for 1 hour and fired at 1450 °C for 24h in air (Lu, 2006). A mechano-chemical method for preparing brannerite involves dry mixing of high purity uranium oxide and anatase (TiO_2) which is then ball-milled, pressed into a pellet and fired at 1350 °C for 300 hours in a mixture of CO (5%) and CO_2 gas (Donaldson, et al., 2005).

For the preparation of doped brannerite; a mixture of oxides is dried and calcined in air at 700-750 °C for 1 hour, followed by wet milling for long periods, followed by drying. The dried product is then ground and hot-pressed at 1260 °C or cold-pressed and then fired at 1200-1300 °C for 14-15 hours (James, 2002; Shatalov, et al., 2007). In contrast to the preparation of brannerite, the synthesis of lithium tungsten vanadates, which are iso-structural to uranium titanate, are performed at low temperature, via a wet chemistry route (Amdouni, et al., 2003).

Synthetically doped brannerites that have been substituted with Ca^{2+}, La^{3+}, Gd^{3+}, Y^{3+}, Hf^{4+} and Pu^{4+} onto the U site has allowed the synthesis to take place in an air or argon atmosphere (Vance et al., 2001, James and Watson, 2002 and Finnie et al., 2003).

From studies conducted by Vance et al (2001), the substitution of Ca^{2+}, La^{3+}, Gd^{3+}, Y^{3+}, Hf^{4+} and Pu^{4+} on the U site within the brannerite structure, $U_{1-x}M_xTi_2O_6$ and the incorporation of these other impurity ions provides a means of stabilizing brannerite phases produced in air. The doping of lower valence $\boldsymbol{M}$ atoms; Ca and La in particular, into these brannerite phases occurs in concurrence with the oxidation of U^{4+} to U^{5+} (James and Watson, 2002).

1.4.2. Dissolution chemistry of brannerite

1.4.2.1. Dissolution of Synthetic brannerite

There have been studies on the leaching of synthetic brannerites that have predominantly focussed on determining the stability of this mineral when used as a storage material for radioactive waste, such as to immobilise surplus plutonium (Jostsons et al., 1999) (where it is commonly referred to as synroc) (Zhang et al., 2001). The conditions used in these studies (simulated environmental conditions) are however significantly different to those used in uranium minerals processing.

However a study by Shatalov et al (2007) investigated the dissolution of synthetic brannerite under conditions relevant to minerals processing. They reported that synthetic brannerite can be completely dissolved in 10-15 g/L of [H_2SO_4] at 140 °C in an oxidative autoclave leaching process (Shatalov et al., 2007).

1.4.2.2. Dissolution of Natural brannerite

There have been a number of studies on the leaching of natural brannerites under minerals processing conditions reported in the open literature. It must be noted that the high potential for variations in the composition of this complex mineral across a single ore body and different ore bodies makes it impossible to accurately compare the leaching results reported for brannerite in different studies (and in some cases it might not be accurate to compare brannerite leaching from different grains in the same ore sample).

Ifill et al (1996) conducted a detailed study on oxidative acid leaching of brannerite and allied titaniferous assemblages in uranium ores from Elliot Lake, Ontario. The results obtained from this study, which was conducted using a rotating-disc (polished section) method in H_2SO_4 and HCl solutions with added Fe^{3+}/$NaClO_3$ at 25 to 70 °C were however qualitative. Some of the main qualitative findings from this study reported were:

- Regardless of its morphology and texture (laths or needles, reticulate or blocky) brannerite was not readily leachable under the conditions studied
- Regardless of the process conditions the rate controlling step appears to be initial leach-pit formation. These pits expand radially throughout the aggregate as leaching proceeds – this dissolution mode is independent of the relative amounts of brannerite and titania
- Secondary coffinite growths which are readily leachable enhance the overall leaching kinetics of brannerite by accelerating leach-pit formation

From their studies on the leaching of a composite grain aggregate (which consisted of a brannerite rich core surrounded by uraniferous titania) Ifill et al (1996) reported that brannerite leaching from this composite grain was complete under the following conditions: 75 g/L H_2SO_4, 5 g/L $NaClO_3$, 4 g/L Fe^{3+}, as $Fe_2(SO_4)_3$, 60 °C, 1 h.

Lottering and Lorenzen (2009; 2008) investigated the leaching of brannerite from low grade uranium ores from South Africa. The results reported for brannerite leaching from these ores are summarised in Table 1.2. A number of interesting results were reported on brannerite leaching in the aforementioned study. Firstly solution ORP had a significant effect on brannerite leaching with maximum leaching being achieved for all of the ores at the highest ORP tested (700 mV). Interestingly for one of the ores there was a significant decrease in extent of brannerite leaching when the ORP was increased from ~416 to 500 mV. Uraninite leaching however also decreased (albeit marginally) for this same ore sample when the ORP was increased from ~416 to 500 mV (as opposed to the reasonable increase that was observed for the other 2 ores) and hence this result may have been an outlier. Another interesting finding from the study conducted by Lottering and Lorenzen (2008) was the significant difference in the extent of brannerite leaching observed for the

three different ores when an ORP of ~416 mV (vs SCE) was used (63.8%, 83.0% and 29.0%). This result was in complete contrast to the results obtained for uraninite leaching at the same ORP where the extent of leaching of uraninite was very similar for all three ores (87.4%, 82.1% and 81.7% respectively). This result could have been due to the composition / structure of brannerite being significantly different across the three different ores and the extent of leaching of this mineral being highly dependent on these factors at conditions of low-moderate ORP.

Table 1.2 Brannerite leaching results reported by Lottering and Lorenzen (2008).

Ore	Initial brannerite (ppm as U) in sub samples used for tests at varied ORP	% Extent of leaching at different ORP (vs SCE)		
		~416 mV	500 mV	700 mV
A	30.2, 46.1, 31.4	63.8	86.5	86.7
B	59.3, 56.7, 65.5	83.0	72.2	86.3
C	34.3, 36.6, 50.0	29.0	39.7	82.9

Reaction conditions: T = 60 ° C, [H_2SO_4] = 16.3 kg/t, [MnO_2] = 4 kg/t, pH 0.5 – 1.2, H_2O_2 and HNO_3 used to obtain ORP of 500 mV and higher, t = 24 h.

Uranium leaching from "brannerite ores" has been investigated by Shatalov et al (2007) and Muralikrishna et al (1991). In the aforementioned studies no uranium mineral characterisation data was given, hence the proportion of uranium minerals present as brannerite is not known. The results obtained by Shatalov et al (2007) are given in Table 1.3. In this study leaching tests were conducted at high temperature (160 °C) in a corrosion resistant steel autoclave equipped with an anchor type mixing apparatus (280 rpm) with added oxygen (oxygen partial pressures 300-800 kPa (total pressure 900 – 1500 kPa). >97% uranium leaching was achieved in 3h from the brannerite ore studied over the range of conditions studied (refer to Table 1.3).

Table 1.3: Brannerite ore leaching results reported by Shatalov et al (2007). Note: Tests conducted at 160 ° C for 3 h.

Experiment	Initial acid concentration, g/dm3	Liquid phase of the pulp			Solid phase of the pulp					Degree of oxidation of the sulfide sulphur (pyrite), %	Degree of uranium extraction into solution, %
		Concentration, g/liter		Oxidation-reduction potential, mV	Yield, %	Content, %					
		H_2SO_4	Fe^{3+}			U	$S_{sulfide}$	$S_{sulfate}$	Fe		
1	0	6.3	2.2	600	88.1	0.020	1.32	1.70	12.2	82.6	97.4
2	~3	7.9	2.0	620	83.8	0.015	3.67	1.42	12.2	56.1	97.9
3	5	11.5	2.5	620	81.5	0.010	4.76	2.26	10.7	38.7	98.9
4	10	12.0	2.5	640	81.5	0.008	1.83	3.45	10.5	75.9	98.9
5	15	14.4	3.3	700	87.3	0.005	1.14	3.31	9.75	98.3	99.5

Muralikrishna et al (1991) investigated the effect of using a pre-concentration process on the leaching of uranium from a brannerite ore over a range of conditions. The results obtained for the same ore when the pre-concentration process was not used revealed that <4% of the uranium was leached under the following conditions: pH = 1.4, [H_2SO_4] = 30.7 kg/t, t= 6h, (temperature not reported, however based on other tests conducted was most likely 50 or 80 ° C). The results obtained when the pre-concentration process was used are given in Table 1.4. The pre-concentrate was obtained using a wet high intensity magnetic separator. The results reported by Muralikrishna et al showed that acid concentration has a significant effect on brannerite leaching from the ore they studied. They also showed that increasing the residence time from 6 to 12 hours lead to a significant increase in leaching at a lower acid concentration. No residence time effect was observed after 6 hours when a higher acid concentration was used and no further effect of residence time occurred beyond 12 hours when a lower acid concentration was used. Muralikrishna et al (1999) also reported that sulphuric acid was able to leach a higher extent of uranium from the brannerite ore compared to nitric acid and hydrochloric acid under the conditions used (Table 1.4).

Table 1.4: Results on brannerite ore leaching reported by Muralikrishna et al (1991).

Time in hours	Temperature °C	ROM kg H_2SO_4/t	Concentrate kg H_2SO_4/t	CeO_2 in liquor g/l	% brannerite leached (as $U_3O_{8)}$
12	50	2.74	68.4	nd	16.0
12	50	5.48	136.8	nd	28.5
12	50	8.20	205.2	nd	36.6
6	80	16.4	410.0	nd	57.0
12	80	16.4	410.0	1.6	71.0
24	80	16.4	410.0	2.0	69.0
6	80	25.0	612.0	nd	75.0
12	80	25.4	610.0	nd	74.0
6	80	49.0	1224.0	nd	80.0

(nd = not detected; ROM = Run of the mill ore)

Table 1.5: Effect of acid type on leaching of uranium from a brannerite ore (1991).

Leachant	Time in hours	Temperature °C	Quantity of acid	% U_3O_8 leached
HCl	6	80	Tonne/Tonne	62
HNO_3	6	80	Tonne/Tonne	63
H_2SO_4	6	80	Tonne/Tonne	70

Based on the studies that have been published in the open literature on brannerite leaching using minerals processing conditions it is difficult to determine which parameter(s) have the most influence on brannerite leaching. Each of the studies that have been reviewed in detail confirm the influence of a different parameter: Temperature (Shatalov, et al., 2007); ORP (Lottering and Lorenzen, 2008); and acid concentration and residence time (Muralikrishna, et al., 1991). The fact that brannerite composition / structure can vary considerably and that this most likely influences leaching makes it extremely difficult to draw general conclusions on the effects of individual parameters on brannerite leaching. It is most likely that the influence of various parameters on leaching will be highly dependent on the composition / structure of the brannerite studied.

1.4.2.3. Electrochemical studies of brannerite

Studies on minerals such as chalcopyrite in carbon paste electrodes have been shown to be a reliable way to observe the leaching behaviour, particularly in regards to the effects of electrolyte and temperature on dissolution processes, surface passivation and the study of a possible leaching mechanism. The use of carbon paste electrodes to measure minerals by electrochemically means has been previously applied predominantly to sulphide minerals. Such studies include; simulation of conditions under which industrial leaching of sulphide minerals take place (Cruz et al., 2005), determining the differences in kinetics for chalcopyrite in the leaching process within different acidic media (Lazaro et al., 1995) and optimising individual leaching processes for the electrochemical activity of galena (Ahlbery and Asbjornsson, 1993).

There have been no studies specific to investigating the abovementioned on the mineral brannerite and therefore to gain a greater understanding on the optimum leaching conditions of this mineral of such high refractory nature would be a great achievement.

1.5. Summary of literature review

Although brannerite is nominally given the simple formula UTi_2O_6, naturally occurring brannerite in ores is chemically complex. Naturally occurring brannerite is heavily substituted with other cations and is always X-ray amorphous requiring calcination to achieve a diffraction pattern. With regards to the dissolution of stoichiometric, pure brannerite there have only been studies conducted on this form of brannerite pertaining to its use as a radioactive waste host (these conditions are generally referred to as "environmental" conditions and are significantly different from those used in uranium minerals processing). The combined effects of chemical modifications such as structure,

oxidation, alteration and gangue mineralogy, undoubtedly explains the differences often reported / observed in leaching studies of natural brannerite bearing ores and makes it essential to consider unique processing conditions for different brannerite ore bodies in order to gain optimal uranium extraction during processing. While numerous uranium extraction studies have been conducted on naturally occurring brannerite ores, this review has demonstrated that results are variable, being strongly dependent on differences in structure and chemistry of the host brannerite, the composition of any associated uranium containing minerals and the gangue mineral content. The differences in chemistry also makes it essential that before any extraction process takes place, detailed ore characterisation studies are of major importance in order to fully understand the interrelationship between chemistry, mineralogy, mineral liberation and therefore a possible indication in the potential leaching characteristics / behaviour / mechanism of the uranium with in the brannerite containing orebody.

1.6. Objectives

As discussed previously there have been a number of studies conducted on a number of aspects of synthetic and natural brannerite reported in the literature. This includes studies on structure, composition and occurrence, and also studies on the stability of synthetic brannerites under environmental conditions as well as natural brannerites under minerals processing conditions. However these studies have been varied and limited in their scope due to the differences that occur across brannerite bearing ore bodies. Furthermore there have been no relevant studies conducted on synthetic UTi_2O_6 dissolution under conditions of relevant to minerals processing. There is also very little information on the mechanism of dissolution of this mineral under these conditions.

The main aim of this thesis was to investigate the dissolution of brannerite and obtain information that could contribute to improvements in the processing of this important uranium bearing mineral. Specific aims of this project included are:

- Investigating the chemistry and mineralogy of two naturally occurring brannerite samples using multiple characterisation techniques to gain a greater understanding on the structure and gangue minerals associated with brannerite bearing ores.
- Investigating the rate of dissolution of synthetic brannerite over a range of conditions including conditions similar to those used in tank based leaching of uranium minerals as well as probing the mechanism of synthetic brannerite dissolution by electrochemical means.
- Investigating the rate of dissolution of naturally occurring brannerite over a range of conditions including temperature, [H_2SO_4] and [Fe(III)].

1.7. References

ABC News, 2009. Work begins on Honeymoon uranium mine. [online] Available at: <http://abc.net.au/news/2009-04-24/work-begins-on-honeymoon-uranium-mine/1661896> [Accessed 21 April 2013].

Agency, O.N.E. and Agency, I.A.E. 2006. Forty Years of Uranium Resources, Production and Demand in Perspective: The Red Book Retrospective, Nuclear Energy Agency, Organisation for Economic Co-operation and Development.

Ahlberg, E. and Asbjornsson, J., 1993. Carbon paste electrodes in mineral processing: an electrochemical study of galena. Hydrometallurgy, 34: 171-185.

Amdouni, N., Zarrouk, H. and Julien, C.M., 2003. Synthesis, structure and intercalation of brannerite $LiWVO_6$ wet-chemical products. Journal of Materials Science, 38: p. 4573 – 4579.

Australian Uranium, 2013. Map of Australian Uranium Deposits and Mines. [online] Available at: <http://www.australianuranium.com.au/uranium-map.html> [Accessed 21 April 2013].

Balek, V., Vance, E.R., Zelenak, V., Malek, Z. and Subrt, J., 2007. Use of emanation thermal analysis to characterize thermal reactivity of brannerite mineral. Journal of Thermal Analysis and Calorimetry, 88(1): p. 93-98.

Burns, P.C. and Finch, R.J., 1999. Uranium: Mineralogy, Geochemistry and the Environment. Reviews in Mineralogy, ed. P.H. Ribbe. Vol. 38., Mineralogical Society of America: Washington, DC.

Clark, D.L., Neu, M.P., Runde, W. and Keogh, D.W., 2006. Uranium and Uranium Compounds, in Kirk-Othmer Encyclopedia of Chemical Technology. John Wiley and Sons, Inc.

Cruz, R., Luna-Sanchez, R.M., Lapidus, G.T., Gonzalez, I. and Monroy, M., 2005. An experimental strategy to determine galvanic interactions affecting the reactivity of sulphide mineral concentrates. Hydrometallurgy, 78 (3-4): 198-208.

Donaldson, M., Stevens, R., Lang, B.E., Boerio-Goates, J., Woodfielda, B.F., Putnam, R.L. and Navrotsky, A., 2005. Heat capacities and absolute entropies of UTi_2O_6 and $CeTi_2O_6$. Journal of Thermal Analysis and Calorimetry, 81(3): p. 617-625.

Finch, R.J. and Murakami, T., 1999. Systematics and paragenesis of uranium minerals. In: Burns, P.C., Finch, R.J. (Eds), Uranium: Mineralogy, Geochemistry and the Environment. Reviews in Mineralogy, vol. 38, pp. 91–180.

Glatthaar, G.W. and Duchovny, M., 1979. Mode of occurrence of uranium in Western Deep levels and Vaal Reefs sample. AR Report, Project No. R54, Ref No. M/79/304. CONFIDENTIAL.

Ifill, R.O., Cooper, W.C. and Clark, A.H., 1996. Mineralogical and process controls on the oxidative acid-leaching of radioactive phases in Elliot Lake, Ontario, uranium ores: II – Brannerite and allied titaniferous assemblages. Metullurgy, p. 93-103

James, M. and Watson, J.N., 2002.The synthesis and crystal structure of doped uranium brannerite phases $U_{1-x}M_xTi_2O_6$ (M = Ca^{2+}, La^{3+} and Gd^{3+}). Journal of Solid State Chemistry, 165: p. 261-265.

Lazaro, I., Martinez-Medina, N., Rodriguez, I., Arce, E. and Gonzalez, I., 1995. The use of carbon paste electrodes with non-conducting binder for the study of minerals: Chalcopyrite. Hydrometallurgy, 38: 277-287.

Lian, J., Wang, L.M., Lumpkin, G.R. and Ewing, R.C., 2002. Heavy ion irradiation effects of brannerite-type ceramics. Nuclear Instruments and Methods in Physics Research, 191: p. 565-570.

Liebenberg, W.H., 1955. The occurrence and origin of gold and radioactive minerals in the Witwatersrand system, the Dominion Reef, the Venetersdorp Reef and the Black Reef. Trans. Proc. Geol. Soc. S. Afr., 58, p. 101-254.

Lottering, M.J. and Lorenzen, L., 2008. The development of a diagnostic leaching method for South African low grade uranium ores. Proceedings of [the] International Mineral Processing Congress, 24th, Beijing, China, 2: p. 2899-2904.

Lottering, M.J., Lorenzen, L., Phala, N.S., Smit, J.T. and Schalkwyk, G.A.C., 2008. Mineralogy and uranium leaching response of low grade South African ores. Minerals Engineering, 21: p. 16-22.

Lu, D.Y., Toda, M. and Sugano, M., 2006. High-Permittivity double rare-earth-doped barium titanate ceramics with diffuse phase transition. Journal of the American Ceramic Society, 89(10): p. 3112-3123.

Merritt, R.C., 1971. The Extractive Metallurgy of Uranium. Colorado School of Mines Research Institute and USAEC, Golden, Colo.

Muralikrishna, N., Mohanty, K.B. and Viswamohan, K., 1991. Extraction of uranium from refectory type of ores – a case study of Brannerite from Ramsinggpura, Sikar district, Rajasthan, India. Exploration and Research for Atomic Minerals, 4: p. 203-208.

Peehs, M., Walter, T., Walter, S. and Zemek, M., 2012. Uranium, Uranium Alloys, and Uranium Compounds. In Ullmann's Encyclopaedia of Industrial Chemistry. John Wiley and Sons, Inc.

Patchett, J.E. and E.W. Nuffield, 1960. The synthesis and crystallography of brannerite, [Part] 10 of Studies of radioactive compounds. The Canadian Mineralogist, 6(4): p. 483-490.

Ringwood, A.E., 1988. Radioactive Waste Forms for the Future. North-Holland, Amsterdam. 233.

Shatalov, V., Pirkovskii, S. and Smirnov, K., 2007. Oxidation of pyrite by oxygen and concurrent leaching of uranium from ore under the condition of an autogenous autoclave process. Atomic Energy, 102(2): p 146-150.

Szymanski, J. T. and Scott, J. D., 1982. A crystal structure refinement of synthetic brannerite UTi_2O_6 and its bearing, on rate of alkaline-carbonate leaching of brannerite in ore. The Canadian Mineralogist, 20, p.271-280.

Tasker, S.J., 2009. Uranium industry emerges a key player. [Online in: The Australian] Available at: <http://m.theaustralian.com.au/news/uranium-industry-emerges-a-key-player/story-e6frg6n6-1225750626161> [Accessed on 21 April 2013].

Thomas, B.S. and Y. Zhang, 2003. A kinetic model of the oxidative dissolution of brannerite, UTi_2O_6. Radiochimica Acta, 91: p. 463-472.

Van Nostrand, 2006. Uranium. Van Nostrand's Scientific Encyclopedia. John Wiley and Sons, Inc.

Mineral Atlas, 2012. Vibrational Spectroscopy and Photo Atlas of minerals: Brannerite. [online] Available at: <http://www.mineralatlas.com/mineral%20photos/B/branneritecp.htm> [Accessed 21 April 2013].

World Nuclear Association, 2008. Australia's Uranium. [online] Available at: <http://world-nuclear.org/education/mining.htm> [Accessed 22 October 2008].

World Nuclear Association, 2012a. World Energy Needs and Nuclear Power. [online] Available at: <http://www.world-nuclear.org/info/Current-and-Future-Generation/World-Energy-Needs-and-Nuclear-Power/#.UXPLIrX-GSo> [Accessed 21 April 2013].

World Nuclear Association, 2012b. Australia's Uranium. [online] Available at: <http://world-nuclear.org/info/Country-Profiles/Countries-A-F/Australia--Uranium/#.UXD3RLX-GSo> [Accessed 19 April 2013].

Zartman, R.E. and J.V. Smith, 2009. Mineralogy and U–Th–Pb age of a uranium-bearing jasperoid vein, Sunshine Mine, Coeur d'Alene district, Idaho, USA. Chemical Geology, 261: p. 185-195.

Zhang, Y., Hart, K.P., Bourcier, W.L., Day, R.A., Thomas, B.S., Aly, Z. and Jostsons, A., 2001. Kinetics of uranium release from Synroc phases. Journal of Nuclear Materials 2001. 289: p. 254-262.

Zhang, Y., Hart, K.P., Thomas, B.S., Aly, Z., Li, H. and Carter, M., 2001. Dissolution of Synthetic Brannerite at 90 °C. Materials Research Society Symposium Proceedings, 663: p. 341-346.

Chapter 2

Experimental

This chapter provides information on the materials and methods that were used to conduct research that is presented in more than one chapter of this thesis.

2.1. Materials

Two naturally occurring brannerite samples were obtained from the Victorian Museum, Melbourne, Australia. The samples were originally sourced from the Crockers Well uranium prospect in South Australia and from the Roxby Downs region, also in South Australia. These samples are hereafter referred to as NBCW and NBRD respectively.

High grade brannerite leach feed ore sample was obtained from BHP Billiton. The sample was sourced from Roxbury Downs in South Australia.

Other materials used were as follows; Uranyl acetate ($UO_2(CH_3COO)_2.2H_2O$) (97.5%) and titanyl sulphate dihydrate ($TiOSO_4.2H_2O$) (97 %) were used as received. Sulphuric acid (H_2SO_4) (Aldrich Chemical), iron sulphate ($Fe_2(SO_4)_3$) (Aldrich Chemical), nitric acid (HNO_3) (70 % AR grade) (Merck Led) and 1000 ppm uranium ICP-MS standard (AccuStandard).

Milli-Q water (H_2O) (18 MΩ) was used in all experimental procedures / experiments.

2.2 Methods

2.2.1 Dissolution test procedure

A 1 L glass reaction vessel with a five-necked glass lid equipped with a thermometer, a mechanical stirrer and a reflux condenser was used as the dissolution reaction vessel. The reaction vessel was heated by a thermostatically controlled mantle to reach and maintain the preferred temperature within ±1 °C. For each run, 500 mL of [H_2SO_4] and [Fe(III)] solution of predetermined molarity was charged into the reaction vessel and heated to the desired temperature. A known amount of uranium bearing sample was then added and the contents were well agitated. Solution samples of 0.25 mL were taken at pre-determined times during a run and analysed for uranium by ICP-MS.

2.2.2 Digestion method for determination of elemental composition

100 mg of powdered brannerite (NBCW and NBRD) samples were weighed out into separate Teflon vessels. The sides of these vessels were rinsed down with a small amount of Milli-Q water. 4 mL of concentrated hydrochloric acid was added slowly to each vessel and left to subside, followed by 3 mL of concentrated nitric acid and left to subside. Next 2 mL of concentrated sulphuric acid and 3 mL of concentrated hydrofluoric acid was then added to each vessel and they were then placed on aluminium heating blocks at 110 °C where the solutions were heated until incipient dryness. The temperature was raised to 160 °C to bring each sample to complete dryness. A further 1 mL of concentrated sulphuric acid was added to each vessel where each sample was heated to 160 °C to complete dryness.

Once each sample was dry 1 mL of concentrated nitric acid and 2 drops of concentrated sulphuric acid were added to each vessel and the reaction was left to subside. 19 mL of 2 % nitric acid were added to each vessel and were capped and placed into a drying oven at 110 °C for 2 h.

The samples were prepared for ICP-MS by diluting each sample which was then acidified. Using a multi elemental environmental standard full quantitative analysis was completed for the all-natural brannerite samples.

2.3. Characterisation and analytical techniques

2.3.1 X-ray Diffraction (XRD)

2.3.1.1 Theory

X-ray diffraction (XRD) is a non-destructive method used to identify the differing phases / structure of crystalline materials, which utilizes the wave properties of X-rays. The positions and intensities of the X-rays diffracted by the crystalline solid can provide a wealth of information such as crystal structure, composition of a solid, particle size, evidence of decomposition, polymorphism, preferred orientation and order-disorder relationships (Whiston et al., 1987). Modern devices for producing X-rays are called X-ray tubes. These produce an intense characteristic line spectrum superimposed on a less intense continuous spectrum known as white or background radiation. Characteristic X-rays are produced when high-speed electrons remove inner K, L or M electrons from target atoms, and outer electrons fill the vacancies and in consequence release energy in the form of x-rays. The continuous spectrum arises from the conversion of the electron's kinetic energy to radiant energy on impact.

An X-ray beam of original intensity I_o becomes reduced to intensity I on passing through a distance x of absorbing medium of density ρ. The intensities are related by the equation:

$$I = I_o e^{-\mu_m \rho x} \qquad \text{(Equation 2.1)}$$

Where μ_m is called the mass absorption coefficient, μ_m is characteristic to a particular medium but is independent of its state.

Mass absorption generally increases with increasing wavelength, but the graph of μ_m versus λ shows a number of vertical discontinuities called absorption edges. These correspond to the ionisation energies of the K, L and M electrons of the absorbing medium.

The X-rays having wavelengths less than these absorption edges have sufficient energy to displace inner electrons resulting in the emission of characteristic radiation (Whiston et al., 1987). When electrons with sufficient energy to dislodge inner shell electrons of are directed towards the target material such as copper (Cu), the characteristic X-ray spectra of copper are produced.

These spectra consist of several components, the most common being K_α and K_β (Whiston et al., 1987). The specific wavelengths are characteristic of the target material and the most widely used is Cu. The important x-ray lines for Cu are $K\alpha_1$ and $K\alpha_2$ with wavelengths of 1.5405 and 1.544 Å respectively. These X-rays are used to determine crystallographic parameters such as lattice constants, which are, in turn, used to identify the crystallographic structure of a sample (Whiston et al., 1987).

Families of planes of atoms in a crystal have the ability to reflect an X-ray beam when the Bragg equation:

$$2d\ sin\ \theta = n\lambda \qquad \text{(Equation 2.2)}$$

is fulfilled, where d is the inter-planar spacing, θ is the angle between the planes and the X-ray beam (Bragg angle), λ is the X-ray wavelength, and n is an integer called the order of reflection.

Families of planes are identified by a system of Miller Indices (*hkl*). Miller Indices take integer values which correspond to the number of times a set of crystal planes with *a*, *b* and *c* edges of the unit cell intercept (Whiston et al., 1987). In principle XRD measurements are basically applied to measuring distances between planes with X-ray waves. When (CB + BD) in Figure 2.1 equals 2d sin θ, the Bragg condition ($2d \sin\theta = n\lambda$) is satisfied and an x-ray peak will be measured.

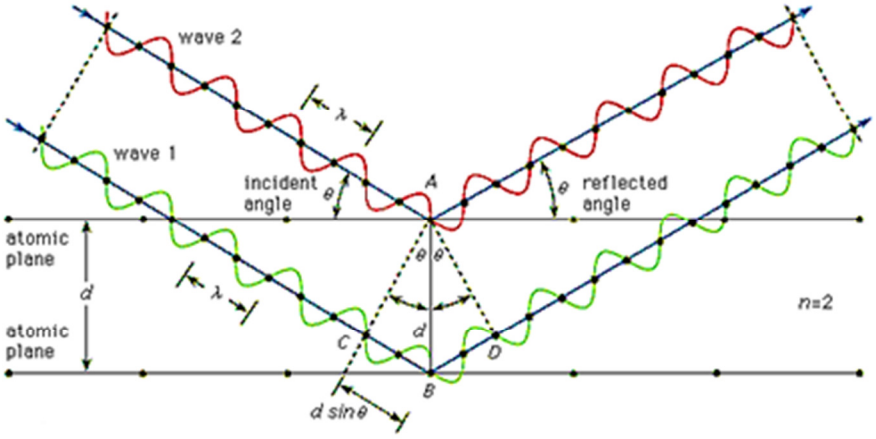

Figure 2.1: X-ray diffraction Bragg condition when $2d\ sin\ \theta = n\lambda$.

The Bragg law indicates the angle at which this strong diffraction peak is observed and depends on the distance between the planes in the crystal lattice, and is called the d spacing (Whiston et al., 1987). The values of the d spacing are calculated from appropriate equations. The crystal structure of the sample is determined from the crystallographic databases available from the Joint Committee on Powder Diffraction Standards (JCPDS) files (Whiston et al., 1987).

2.3.1.2 Sample preparation and instrument details

Whole rock samples containing natural brannerite were prepared for XRD analysis as follows: samples were crushed using a mortar and pestle to form a powder, this was then placed into a circular poly methyl methacrylate holder and the sample was evenly placed onto a glass flat plate within the holder and covered by Kapton film. The same process, excluding the crushing step, was used to prepare all synthetic brannerite samples. X-ray powder diffraction patterns were obtained on a Bruker D8 Advance diffractometer fitted with a copper tube (copper Kα radiation), an incident beam monochromator, and a scintillation detector. The diffractometer was operated at a voltage of 40 kV and current of

35 mA. Diffraction patterns were collected over the range 10-60 ° 2θ using a 1 ° fixed divergence slit, a step size of 0.015 °, and counting times of 2.5 s per step (total pattern collection time of 138 minutes per sample). The instrument was calibrated using quartz and corundum calibration standards prior to use.

2.3.2. X-Ray Photoelectron Spectroscopy (XPS)

2.3.2.1 Theory

X-ray photoelectron spectroscopy (XPS) is a quantitative spectroscopic technique that can be used to analyse the surface chemistry of a material through a single photon in / electron out process.

In XPS, spectra are obtained using a monochromatic source via radiation (i.e. photons of fixed energy given $E = hv$) by irradiating a material with a beam of X-rays, which leads to the ionisation of the atom (A) and the emission of core (inner shell) electrons called photoelectrons from the top layer of the materials surface (Figure 2.2) (Van Der Heide, 2011).

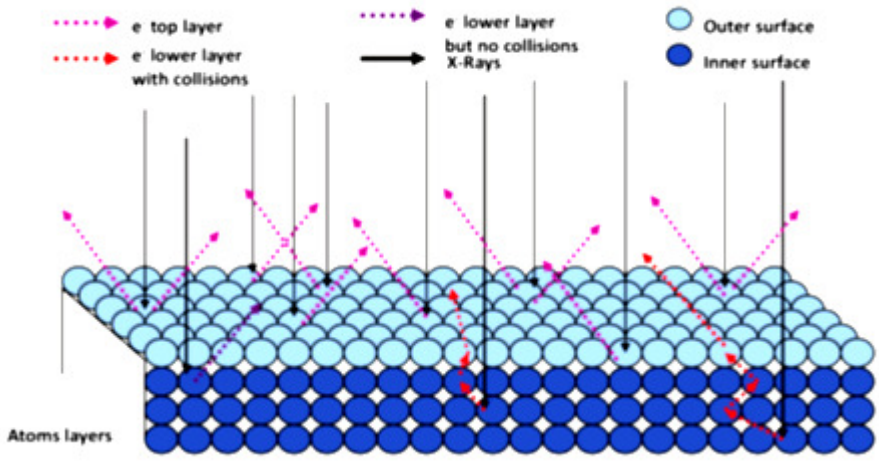

Figure 2.2: Path flow of electrons when X-rays of fixed photon energy is bombarded on a target surface in XPS.

While the irradiation is taking place, simultaneous measurements are taken of the kinetic energy distribution of the emitted photoelectrons and number of electrons that escape from the top 1 to 10 nm of the material being analysed. The photoionization process can be given as:

$$A + hv = A^+ + e^- \quad \text{(Equation 2.3)}$$

Conservation of energy requires:

$$E(A) + hv = E(A^+) - E(e^-) \quad \text{(Equation 2.4)}$$

Since the number of electrons that escaped from the top 1 to 10 nm of the material is observed to possess kinetic energy (KE), the below expression can be rearranged in terms of kinetic energy as:

$$KE = kv - (E(A^+) - E(A)) \quad \text{(Equation 2.5)}$$

The final term $(E(A^+) - E(A))$, represents the difference in energy between the ionised and neutral atoms is generally called the binding energy (BE) of the electron which is represented in the equation below:

$$KE = hv - BE \quad \text{(Equation 2.6)}$$

The electron binding energy levels of the material are measured with respect to the Fermi-level of the solid. The below equation has now accounted for the work function (ϕ) of the material:

$$KE = hv - BE - \phi \quad \text{(Equation 2.7)}$$

The precise binding energy of an electron is determined not only by the level from which photoemission is occurring, but also on the formal oxidation state of the atom and the local chemical and physical environment. This gives rise to small shifts in the peak position seen in the spectrum which are known as chemical shifts.

2.3.2.2 Sample preparation and instrument details

Samples were prepared for XPS analysis by firstly pressing the particles in a die press. The pressed samples were then placed onto a carbon tape / silicon substrate, which were placed into a condenser to remove air from carbon tape / silicon substrate. XPS measurements were carried out using a Thermo Scientific K-Alpha X-ray Photoelectron Spectrophotometer instrument at a pressure lower than 1 x 10^{-9} Torr). All scans were recorded with un-monochromatized Mg Kα radiation (photon energy of 1253.6 eV) at pass energy of 20 eV and an electron take off angle of 90 °. The overall resolutions for all XPS measurements were 0.1 eV. The core level spectra were background corrected using the Shirley algorithm and chemical distinct species were resolved using a nonlinear least squares fitting procedure.

2.3.3. Inductively Coupled Plasma Mass Spectrometry (ICP-MS)

2.3.3.1 Background and Theory

Inductively Coupled Plasma Mass Spectrometry (ICP-MS) is a technique used for determining the elemental composition of samples. Most instruments are only capable of analysing aqueous samples however solid samples can also be analysed directly using a technique known as laser ablation ICP-MS. ICP-MS can be used to precisely identify and measure quantitatively a number of elements in the periodic table including elements that are often difficult to analyse. This technique can also be used to measure individual isotopes of an analyte, and also can be used to detect and measure concentrations of analytes in solution at very low levels (Taylor, 2001).

In this technique, positive ions generated by the high temperatures in an inductively coupled plasma (ICP) are extracted via a differentially pumped interface, into a low-

resolution mass analyser to scan a wide mass range very rapidly (Taylor, 2001). This provides near simultaneous determination of most elements down to $pg.ml^{-1}$ levels.

ICP-MS instruments consist of several components including the ICP, a sample introduction system, a mass spectrometer with ion detector, and a data acquisition/readout system as seen in Figure 2.3 (Taylor, 2001 and Thomas, 2008).

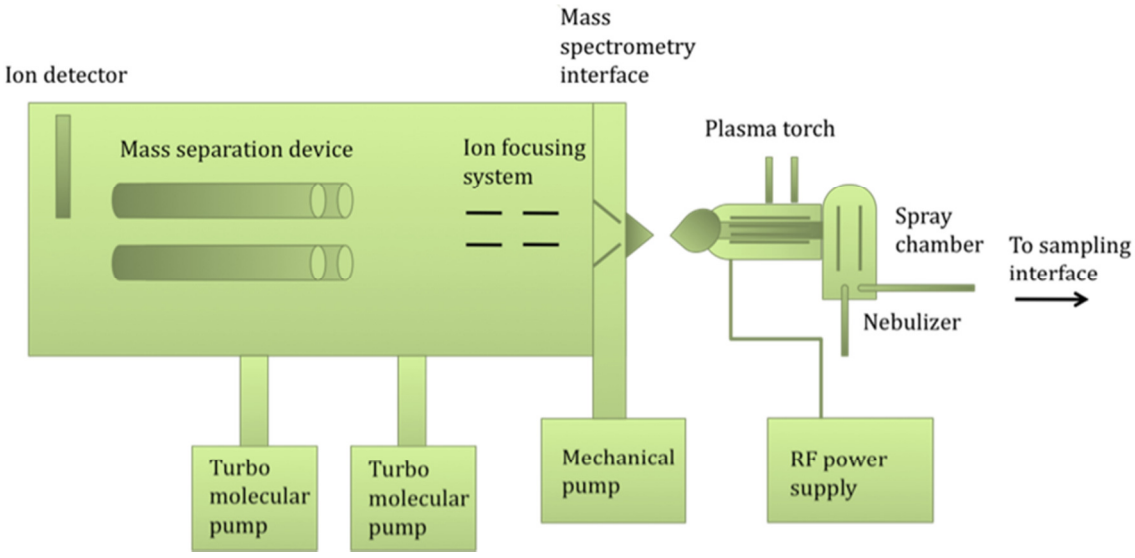

Figure 2.3: Schematic diagram of an ICP-MS (Thomas, 2008).

The sample as an aqueous solution is introduced into the nebuliser which converts it into an aerosol, which passes through to the argon plasma torch, where it is rapidly vaporized, dissociated, atomised and ionised (Taylor, 2001). The sample leaves the torch as a mixture of ions, atoms, un-dissociated molecular fragments and un-volatilised particles. The function of the interface is to representatively sample ions produced in the ICP, deliver them from the high-temperature atmospheric pressure argon plasma, and facilitate their transport into the mass spectrometer (Taylor, 2001). Semi-quantitative analysis is a method used to qualitatively determine the elemental composition of an unknown sample.

2.3.3.2 Sample preparation and instrument details

Uranium concentrations were measured using an Agilent HP 7700 ICP-MS. The instrument was calibrated prior to sample analysis using uranium calibration standards. These standards were prepared using a uranium standard solution. An internal standard (terbium) was also added to all calibration and test samples. Solution samples of 0.25 mL were taken at pre-determined times during dissolution tests where they were diluted to 100 mL in a volumetric flask with 0.715 mL of HNO_3 followed by analyses for uranium by ICP-MS. The calculated percentage error for uncertainty in all dissolution tests was ± 2.64 %.

2.3.4. Scanning Electron Microscopy (SEM)

2.3.4.1 Background and Theory

The scanning electron microscope (SEM) is an electron microscope used to image a sample surface by scanning it with a high-energy beam of electrons in a programmed scan pattern. The electrons interact with the atoms that make up the sample producing signals that contain information about the sample's surface topography, composition and other properties such as electrical conductivity (Goldstein et al., 2003). In the Environmental SEM instrument (ESEM), a series of pressure limiting apertures (PLAs) are placed down the column, across each of which a pressure differential is maintained as shown in the schematic diagram in Figure 2.4. The microscope column is shown in Figure 2.4. The difference between the ESEM and the SEM is that environmental scanning electron microscopy is a form of electron microscopy that can be carried out under atmospheric pressure, while the SEM requires vacuum in the specimen chamber. Also ESEM permits the imaging of wet samples with minimal sample preparation (Goldstein et al., 2003). Consequently, despite the relatively high pressure in the chamber, this design allows

ESEMs to operate with LaB_6 filaments as well as tungsten, and field emission guns are also becoming available to give superior quality imaging (McDonald, 2002).

The vacuum system is employed which offers greater control of the specimen environment as well as the ability to control the higher pressures up to 20 torr (McDonald, 2002). This pressure range is achieved by having several successive levels of differential apertures and intermediate pumps to minimize gas flow back to the gun region. The ESEM has a facility to flood the sample chamber with water mist prior to experiments in which liquids or hydrated materials are being observed to ensure that full saturation is achieved so that no drying occurs during the pump down of the system (McDonald, 2002). This system maintains a high vacuum in the column while allowing higher pressures and water vapour to be present in the specimen chamber. The sample sits on a Peltier stage, which maintains the sample temperature a few degrees above freezing. The coolness of the sample plus the water vapour in the chamber can keep the sample completely hydrated (McDonald, 2002).

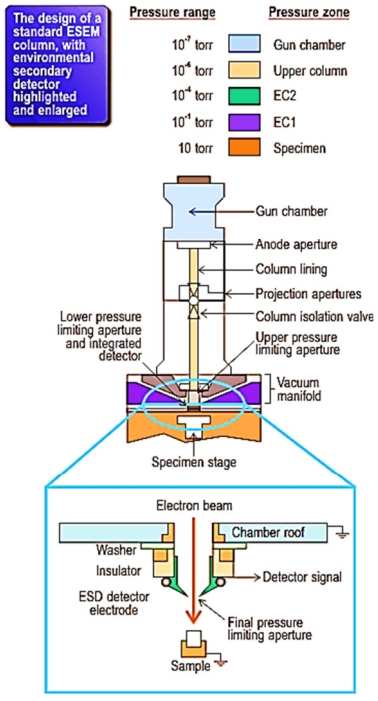

Figure 2.4: Diagram of a standard ESEM column (McDonald, 2002).

Water vapour in the chamber is ionised by secondary electrons reflected from the sample. The freed electrons amplify the signal from the sample, while positive ions drift to the sample and suppress charging, as schematically represented in Figure 2.5 (McDonald, 2002). As a result, ESEM can examine non-conductive, uncoated samples under low vacuum.

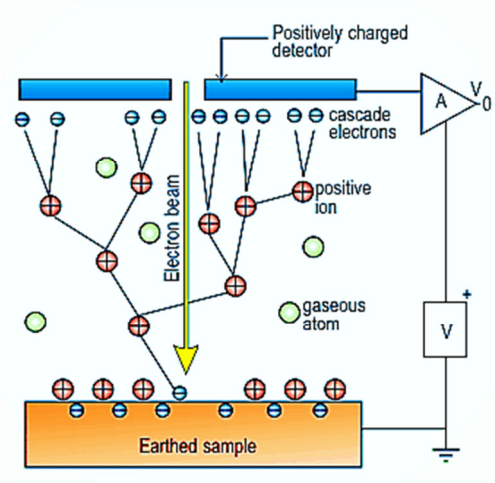

Figure 2.5: SEM column (McDonald, 2002).

2.3.4.2 Sample preparation and instrument details

Samples were prepared for SEM analysis by placing grains of the sample onto a stainless steel holder that was covered in carbon tape. Samples were then carbon coated.

Scanning electron microscopy was performed on a FEI Quanta 200 Environmental Scanning Electron Microscope (SEM) fitted with an AMETEK Si(Li) Energy Dispersive X-ray (EDX) detector system EDX system (refer to next section). The instrument was operated under high vacuum at an accelerating voltage of 25 kV.

2.3.5. Energy Dispersive X-ray Spectroscopy (EDX)

2.3.5.1 Background and Theory

The Energy-dispersive X-ray spectrometer (EDX) is an analytical technique used for qualitative elemental x-ray microanalysis. Due to the short period of time taken to acquire the total spectrum of interest, the beam energy allows for a rapid evaluation of the specimen constituents. This technique is particularly suited for the identification of unknown samples. It is useful to consider the appearance of the K, L and M lines in EDX spectra as a function of position in the SEM/x-ray microanalysis field to study x-ray spectra from pure elements and simple compounds (Vaughan, 1989).

In EDX each emitted x-ray produces a charge pulse in a semiconductor detector. This tiny and short-lived current is converted first into a voltage pulse, then into a digital signal reflecting the energy of the original X-ray, which is schematically represented in Figure 2.6 (Vaughan, 1989). The digital signal, in turn, adds a single count to the appropriate channel of a multichannel analyser (MCA).

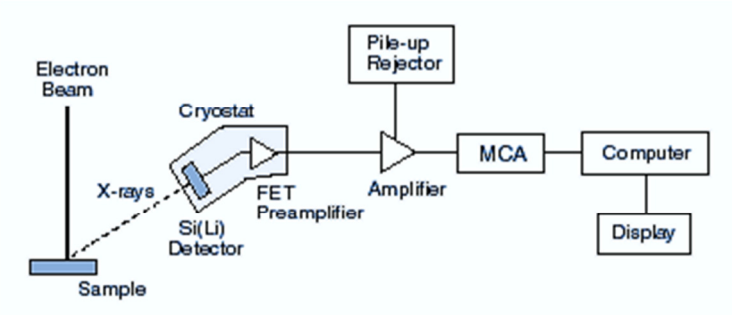

Figure 2.6: Schematic diagram of an EDX system.

X-ray Mapping using EDX is a technique which is specifically used to gain the elemental distribution of a desired sample area. This involves recording and displaying the total x-ray count in an energy window of a sample as a scaled grey level, to rigorous

quantitative compositional mapping in which a complete compositional analysis is performed at each location in a matrix scan (Vaughan, 1989). In quantitative compositional mapping, the grey or colour scale at a particular pixel displayed on an analogy device such as a CRT is related to the actual concentration of each constituent (Goldstein et al., 2003).

2.3.5.2 Sample preparation and instrument details

Samples were prepared for EDX analysis by placing grains of the sample onto a stainless steel holder that was covered in carbon tape. Samples were then carbon coated.

An environmental scanning electron microscope ESEM FEI XL30 equipped with an Oxford energy dispersive spectroscope (EDX) attachment was used to determine the composition of selected samples.

2.3.6. Electron Probe Micro-Analyser (EMPA)

2.3.6.1 Background and Theory

The electron Probe Micro-Analyser (EPMA) is an analytical instrument used to determine the chemical composition of small volumes of solid materials (Figure 2.7). It works in the same way as a scanning electron microscope where the sample is bombarded with an electron beam, emitting x-rays at wavelengths characteristic to the elements being analysed. This enables the abundances of elements present within small sample volumes (typically 10-30 cubic micrometres or less) to be determined (Wittry, 1958). The concentrations of elements from boron to plutonium can be measured at levels as low as 100 parts per million (ppm) (Wittry, 1958).

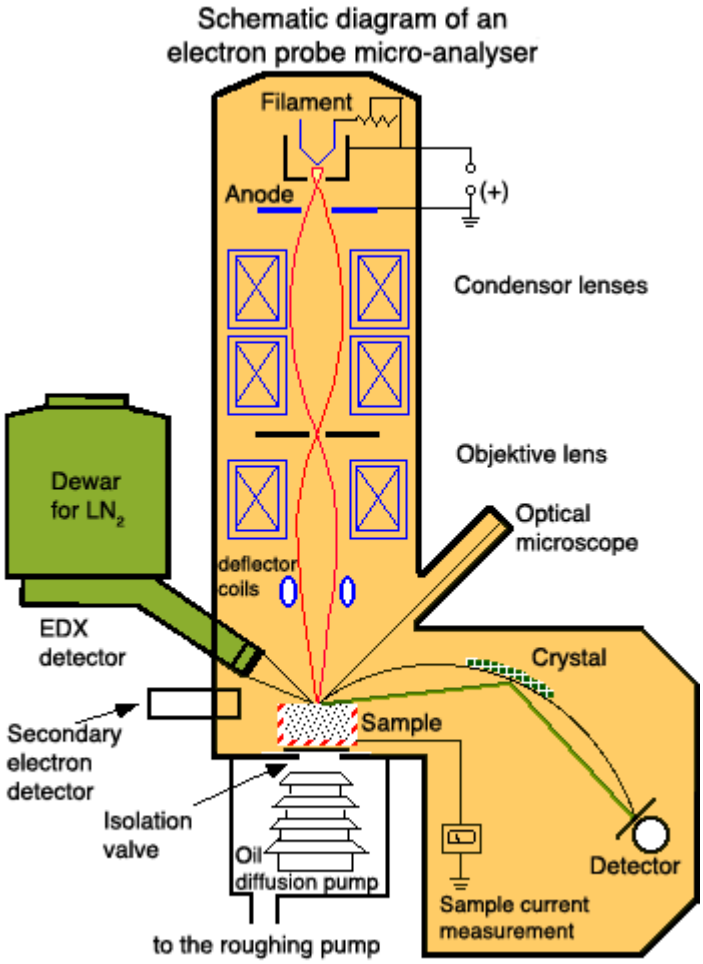

Figure 2.7: Schematic diagram of an EPMA system (Heidelberg University, 1994).

A beam of electrons is fired at a sample. The beam causes each element in the sample to emit X-rays at a characteristic frequency; the X-rays can then be detected by the electron microprobe. The size of the electron beam determines the trade-off between resolution and scan time.

2.3.6.2 Sample preparation and instrument details

Samples were prepared for EPMA mapping analysis by dispersing grains of the natural uncrushed brannerite samples in epoxy resin and mounting into 2.5 cm round blocks. The blocks were cured overnight, sectioned to expose a fresh surface, and then polished flat

using successively finer diamond paste cutting compounds down to a final cutting size of 1 µm. Immediately prior to analysis, each sample was coated with a 15 nm thick carbon film to prevent charge build-up on the surface of the sample when probed by the electron beam.

Two types of EPMA information were obtained. Initially, the two samples containing natural brannerite were mapped using a high resolution Field Emission Gun (FEG) equipped EPMA (JEOL 8500F Hyperprobe). This was done in order to: 1) locate individual brannerite grains and examine their distribution and, 2) to examine the chemical homogeneity of the brannerite grains. Following mapping by FEG-EPMA, the samples were examined by quantitative EPMA techniques using a JEOL 8900 Superprobe to determine the chemistry of the brannerites.

To locate regions of high uranium, the samples were initially inspected using high contrast back scattered electron (BSE) imaging and then selected areas on each of the polished sample mounts were mapped using a combination of wavelength dispersive (WD) and energy dispersive (ED) spectroscopic techniques. The elements mapped using the WD spectroscopic techniques were Fe, Si, U, Ti and Pb. The elements Si and Pb were included in the mapping dataset to check for the presence of coffinite ($U[SiO_4]_{1-x}[OH]_{4x}$) and also for the presence of secondary lead (a decay product from uranium). Standards used to calibrate the EPMA WD spectrometers prior to mapping were: hematite (Fe_2O_3), wollastonite ($CaSiO_3$), uranium oxide (UO_2), rutile (TiO_2) and anglesite ($PbSO_4$). Elements that were not measured by WD spectroscopy were measured using two energy-dispersive (ED) spectrometers operating in parallel. Measuring both ED and WD signals simultaneously ensured that the complete chemical spectrum, at each step interval in the map, was obtained. This additional information was important when trying to identify phases that contained elements not present in the main WD element map suite. Operating conditions for the microprobe during mapping were an accelerating voltage of 12 kV, a

current of 50 nA, a step size of between 0.2-1.0 μm and counting times of 25 msec per step. The choice of step size was based on a compromise between maximising the number of particles analysed and ensuring any fine-grained U-rich mineral phases were located.

After mapping, the element distribution data were manipulated using the software package CHIMAGE (Harrowfield et al., 1993) which incorporates an automated clustering algorithm that identifies chemical groupings (Wilson and MacRae, 2005). The clustering procedure used was a multi-element data analysis approach whereby the groupings of elements identified via the clustering algorithm represented statistically different chemical/mineral phases. These phases were then overlaid onto the mapped region to provide a "phase-patched" map showing the distribution of all chemical/mineral phases within the mapped area.

2.3.7. Raman Spectroscopy

2.3.7.1 Background and Theory

Raman spectroscopy is a spectroscopy technique that is used to study the vibrational, rotational and other low-frequency modes in a material, which assists in the determination of a materials chemical composition (Gardiner et al., 1989). It is also a complementary technique to infrared spectroscopy (IR). In contrast to IR a change of polarisation potential (i.e. deformation of the electron cloud) is essential for a molecule to exhibit a Raman effect. The intensity of the scattered light is dependent on the amount of the polarisation potential change, i.e. photons are scattered by the interaction with vibrational and rotational transitions in molecules (Nasdala et al., 2004). Figure 2.8 visually demonstrates the states involved in a Raman signal. The energy level diagram shows a line thickness is roughly proportional to the signal strength from the different transitions.

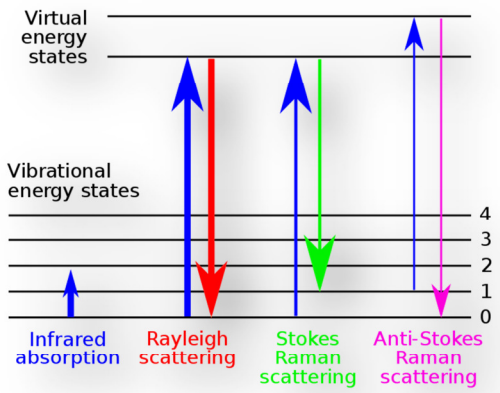

Figure 2.8: Energy level diagram showing the states involved in Raman signal. The line thickness is roughly proportional to the signal strength from the different transitions (Sharma, 1981).

2.3.7.2 Sample preparation and instrument details

Samples were prepared by dispersing the crushed and powdered samples onto a gold coated glass plate. Raman measurements were carried out with a PerkinElmer RamanStation 400 at an excitation wavelength of 785 nm and recorded at a resolution of 4 cm^{-1} in the range between 50 cm^{-1} and 3000 cm^{-1}.

2.3.8. Electrochemical techniques

2.3.8.1 Linear Sweep Voltammetry

2.3.8.1.1 Background and Theory

Linear sweep voltammetry (LSV) is a voltammetric method where the current of the working electrode is measured while the potential between the working electrode and a reference electrode is swept linearly in time (Figure 2.9). Oxidation or reduction of a species is registered as a peak in the current signal at the potential at which the species begins to be oxidised or reduced (Bard et al., 2001). Figure 2.9 is a typical representation

of analytes in solutions where the peak shape and position gives information about the thermodynamics and kinetics of the redox process, as well as diffusion processes. In mineral samples either solid samples (when the mineral is conducting) or carbon paste electrodes (CPE) are used as the working electrode. It has been established that the electrochemical behaviour of the CPE can represent the conditions under which real leaching processes are conducted (Lazaro, et al., 1995). In this thesis, carbon paste electrodes were used for brannerite as the sample is in a powder form of limited conductivity.

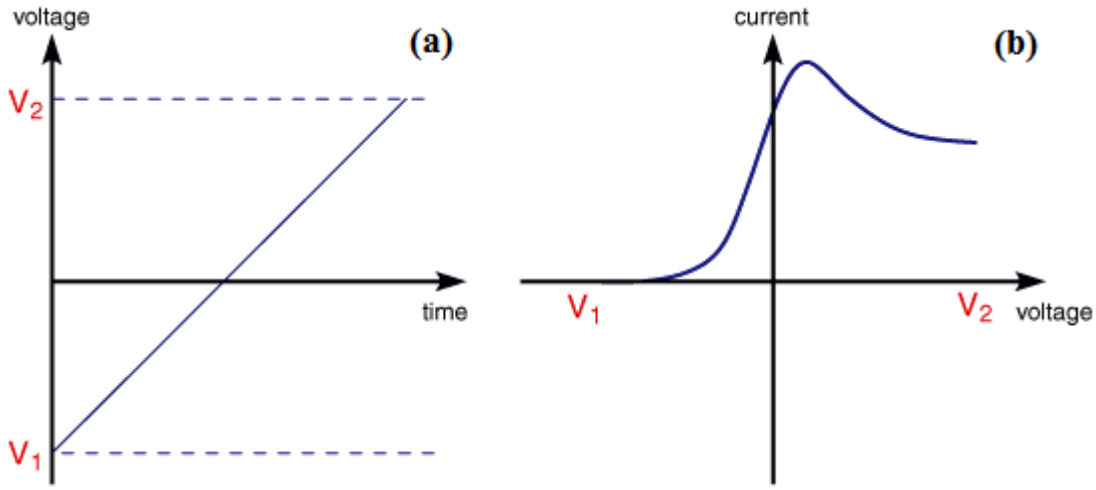

Figure 2.9: (a) LSV the voltage is scanned from a lower limit to an upper limit and (b) Voltammogram for a single voltage scan using an electrolyte solution.

2.3.8.2. Cyclic Voltammetry

2.3.8.2.1. Background and Theory

Cyclic voltammetry (CV) is a potentiodynamic electrochemical measurement. In CV, the working electrode potential is ramped linearly versus time (Figure 2.10), where the ramping is known as the scan rate (V/s). A potential is applied between the reference

electrode and the working electrode, in which the current is measured between the working electrode and the counter electrode, where the data is plotted as current (i) vs. potential (E).

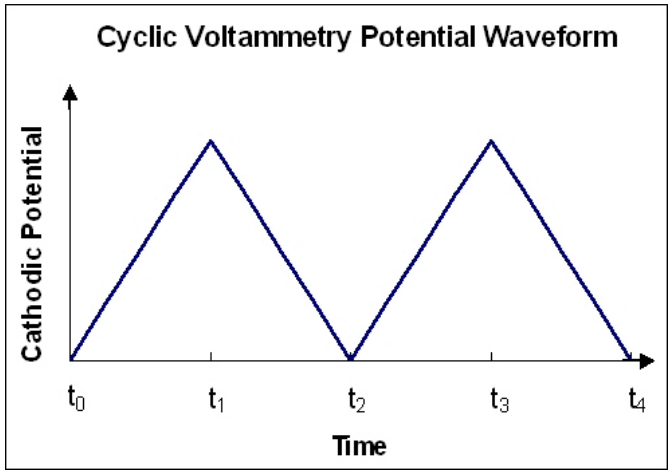

Figure 2.10: Cyclic voltammetry waveform.

The forward scan (waveform) produces a current peak for any analytes that can be reduced / or oxidised depending on the initial scan direction, through the range of the potential scanned. For a solution based process, there is an increase in current as the potential reaches the reduction potential of the analyte, this will fall as the concentration of the analyte is depleted close to the electrode surface. The oxidation peak will have a similar peak shape to the reduction peak when the process is chemically and electrochemically reversible, and detailed studies of voltametric curves can give information about the mechanism, thermodynamics and kinetics of a redox process (Figure 2.11).

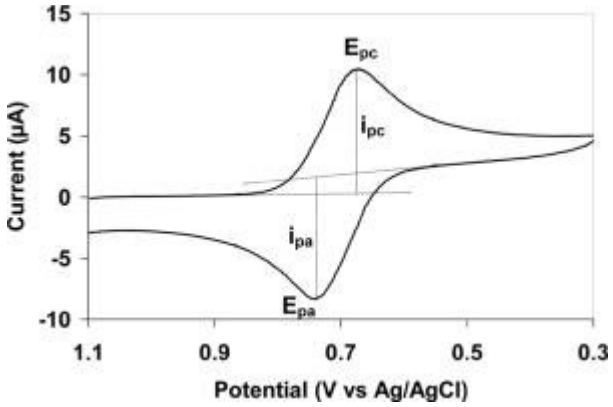

Figure 2.11: CV where i_{pc} and i_{pa} show the peak cathodic and anodic current respectively for a reversible reaction.

Traditional electrochemical techniques such as CV have been used on pure mineral samples, yet a tendency to fracture in the polishing procedure, an irregular and heterogeneous surface, and varying resistivities of mineral samples can affect the confidence of data recorded (Horta, et al., 2009). Therefore in solid state electrochemical analysis used in this thesis, the mineral sample is ground together with a carbon paste to produce a mixture that has been shown to give reliable results in electrochemical studies.

2.3.8.3. Tafel Curve

2.3.8.3.1. Background and Theory

The Tafel curve in electrochemistry is used predominately to study corrosion. Using the Tafel curve the determination of the corrosion potential and the rate of corrosion can be achieved as well as prediction of mechanistic information. Tafel curves are a convenient method to observe active dissolution and surface passivation based on redox processes. The coefficient of charge transfer can also be determined as the slope of the Tafel curve. Figure 2.12 shows the current-potential curve on the left and the Tafel curve ($\log_{10}$(current) vs. potential) on the right.

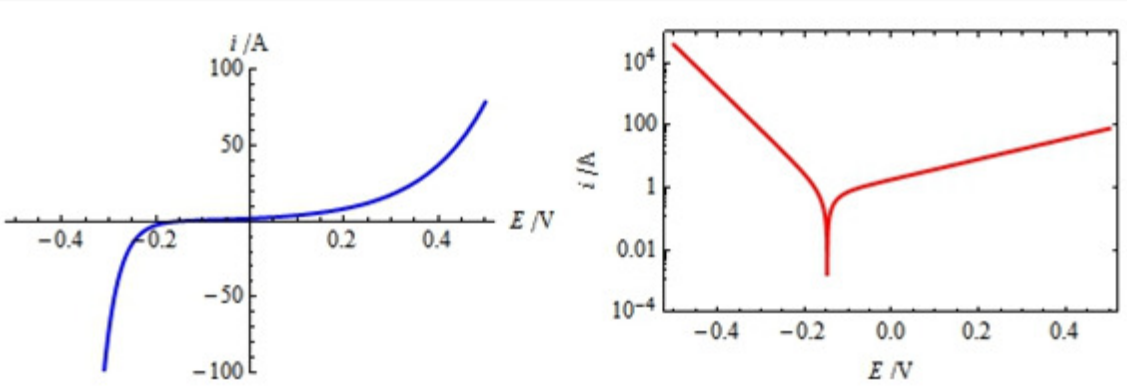

Figure 2.12: Current-potential curve on the left and Tafel curve on the right.

From the literature, the mineral chalcopyrite has been quite extensively studied using Tafel curves to determine the corrosion potential of the system. Viramontes, et al (2007) describes how the passivation of chalcopyrite can be studied by voltammetry by looking at the shape of the Tafel curves.

2.3.9. Sample preparation and instrument details for electrochemical studies

Carbon Paste (CP) consisting of uniform graphite particles mixed with a paraffin binder, was purchased from Bioanalytical Systems (West Lafayette, USA), and used as received. To prepare the working formula, a 1:1 ratio of Carbon Paste: Synthetic Brannerite (by weight) was freshly prepared by grinding in a mortar and pestle, to obtain a homogeneous paste. This paste was placed in a working electrode with a diameter of approximately 0.3 cm, levelled with a spatula and polished on low roughness paper to obtain a flat, reproducible surface.

All experiments were undertaken under a nitrogen atmosphere in a 100 mL temperature controlled glass reactor with a Pt wire as a counter electrode, an Ag/Ag/Cl reference

electrode held at ambient (22 °C) temperature by separation from the reaction vessel with a salt bridge, and a compressed and polished Carbon Paste-brannerite mixture as the working electrode. The reactor was maintained at the desired temperature with a circulating hot water bath. Electrochemical experiments were undertaken with a CH Instruments CH920D potentiostat. Solutions of varying concentrations of H_2SO_4 and were prepared with Milli-Q water (H_2O). For potential scanning experiments in H_2SO_4 the Carbon Paste-brannerite working electrode was initially rested in the electrolyte solution for 10 min before scanning as practice showed that this resulted in the most reproducible results.

2.4. References

Bard, A.J. and Faulkner, L.R., 2001. Electrochemical Methods: Fundamentals and Applications. Wiley.

Gardiner, D.J., Graves, P.R. and Bowley, H.J., 1989. Practical Raman spectroscopy. Springer-Verlag.

Goldstein, J., 2003. Scanning Electron Microscopy and X-ray Microanalysis. Springer London Limited.

Harrowfield, I.R., MacRae, C.M. and Wilson, N.C., 1993. Chemical imaging in electron microprobes. In Proceedings of the 27th Annual MAS Meeting, Microbeam Analysis Society, New York, 547-548.

Heidelberg University, 1994. Electron probe micro-analyser (EPMA). [online] Available at: <http://www.rzuser.uni-heidelberg.de/~hb6/labor/ems/index_en.html> [Accessed 21 March 2013.

Lazaro, I., Martinez-Medina, N., Rodriguez, I., Arce, E. and Gonzalez, I., 1995. The use of carbon paste electrodes with non-conducting binder for the study of minerals: Chalcopyrite. Hydrometallurgy, 38: 277-287.

McDonald, A.M., 2002. Environmental Scanning Electron Microscopy – ESEM. [online] Available at: <http://www.azom.com/details.asp?ArticleID=1556> [Accessed 21 March 2013].

Nasdala, L., Smith, D.C., Kaindl, R. and Zieman, M.A. 2004. Raman spectroscopy: analytical perspectives in mineralogical research. In Spectroscopic methods in mineralogy (Beran, A. and Libowitzky, E., Eds.). EMU Notes in Mineralogy, 6: 281-343.

Sharma, B.K., 1981. Spectroscopy. Krishna Prakashan.

Van Der Heide, P., 2011. X-ray Photoelectron Spectroscopy: An introduction to Principles and Practices. Wiley.

Taylor, H.E., 2001. Inductively Coupled Plasma-Mass Spectrometry: Practices and Techniques, Acad. Press.

Thomas, R., 2008. Practical Guide to ICP-MS: A Tutorial for Beginners, 2nd edition, Taylor and Francis.

Vaughan, D. (ed.), 1989. Energy-dispersive X-ray microanalysis. An introduction. Kevex Instruments, San Carlos, CA.

Viramontes-Gamboa, G., Rivera-Vasquez, B.F, and Dixon, D.G., 2007. The active-passive behavior of chalcopyrite. Comparative study between electrochemical and leaching responses. Journal of The Electrochemical Society, 154 (6), 299-311.

Wilson, N.C. and MacRae, C.M., 2005. An automated hybrid clustering technique applied to spectral data sets. Microscopy and Microanalysis, 11, Suppl. 2, 434CD.

Whiston, C., Prichard, E. and ACOL, 1987. X-ray Methods, John Wiley and Sons.

Wittry, D.B., 1958. Electron Probe Microanalyzer. US Patent No 2916621, Washington, DC: U.S. Patent and Trademark Office.

Chapter 3

Characterisation studies on a uranium ore and natural brannerite samples

In this chapter a uranium bearing ore and two mineral samples containing natural brannerite were extensively characterised to identify the key impurities / gangue mineralogy that are associated with natural brannerite. Heat treatment of the aforementioned samples was also investigated.

3.1. Introduction

As mentioned in Chapter 1 the uranium titanium oxide species, brannerite (nominally UTi_2O_6), has the potential to be a source for maintaining or increasing uranium production. Given the increased emphasis on brannerite as a primary source of uranium, there have been several studies undertaken on various aspects of the composition, structure and physical occurrence of this mineral.

Brannerite is typically found in alkali-metasomatic ore bodies formed at medium-high hydrothermal temperatures (i.e. temperatures approaching 400-600 °C) as well as in numerous uraninite and coffinite containing uranium deposits where it has been identified in both unconformity-type and hydrothermal-vein deposits (Finch, 1996). It forms via precipitation from oxidised U-bearing fluids where the uranium is transported as the uranyl ion, UO_2^{2+}, and its complexes, until changes in solution chemistry lead to precipitation of brannerite (Finch and Murakami, 1999). In some deposits however, brannerite is believed to have formed following adsorption of uranium onto Ti oxides (McCready and Parnell, 1998).

As mentioned earlier (section 1.2) the mineral brannerite is commonly represented by the chemical formula, $U^{4+}Ti_2O_6$ although the uranium in brannerite is nearly always partly oxidised and sometimes hydrated (Finch and Murakami, 1996).

Due to the varied chemical composition of natural brannerites such as ($(U_{0.629}Th_{0.039}Ca_{0.20})(Ti_{2.199}Fe_{0.13})O_{69}$) in Ontario (Ifill et al., 1996), ($U(Ti, Fe)_2O_6$) from Olympic Dam in South Australia (Macnaughton et al., 1999) and ($(U, Th, Ca)(Ti, Fe)_2O_6$) from Vaal river ore bodies in South Africa (Lottering et al., 2008); the formula for brannerite is thus considerably more complex than the ideal UTi_2O_6 and is therefore more commonly reported as $[U,Ca,Th,Y,REE][Ti,Si,Fe,Al]_2O_{6-8}[OH]_x$.

The chemistry of natural brannerites has been previously investigated by Hess and Wells (1920), Pabst (1954), Hewett et al. (1957), Lumpkin et al. (2000), Colella et al. (2005) and Polito et al. (2009). A recent Scanning Electron Microscopy-Energy Dispersive X-ray (SEM-EDX) study on twelve natural brannerite samples by Lumpkin et al. (2012) demonstrated that unaltered natural brannerite typically had Ti and U contents ranging from 1.8 to 2.1 and 0.4 to 0.9 atoms per formula unit, respectively (based on a total of three metal cations). Other cations on the U-site included Ca, Th, Y and REE while Fe, Si, Al, Nb, Mn and Ni were present on the Ti site. Where there was evidence of alteration, significant amounts of Si and other elements were able to be incorporated and up to 40-90 % of the original U could be lost. An examination of the valence state of uranium in a range of natural brannerite samples by Colella et al. (2005) indicated the presence of minor U^{5+} and/or U^{6+} (in addition to U^{4+}) suggesting partial solid solution with orthobrannerite, $[U^{6+},U^{4+}]Ti_2O_6[OH]$. Typical alteration phases associated with natural brannerite include: TiO_2 phases such as rutile and anatase, galena and unidentified Th-rich phases (Lumpkin et al., 2012).

All natural brannerites are metamict (Smith, 1984) due to destruction of crystallinity through alpha-radiation decay from the constituent U (Lian et al., 2002). The presence of Pb in many brannerite samples is mainly due to the decay of the contained U and Th (e.g. ^{238}U and ^{232}Th series decay). Zhang et al. (2006) heated natural brannerite samples at a range of temperatures up to 1100 °C and examined the thermally recrystallised products by XRD, SEM and TEM. Heating resulted in the formation of UO_2 particles among the recrystallised brannerite grains as well as the formation of Pb-rich aluminosilicate glass films at grain boundaries. According to Zhang et al. (2006), the transition from amorphous (metamict) to crystalline brannerite occurs between 900-1100 °C. The recrystallisation of

natural amorphous brannerite on annealing at ~ 1000 °C confirms previous studies using XRD (Patchett and Nuffield, 1960, Vance et al., 2000), thermogravimetry / differential thermal analysis (TG/DTA) (Vance et al., 2000, Balek et al., 2000) and emanation thermal analysis (Balek et al., 2000, 2007). The crystal structure parameters of naturally occurring brannerite are not known with certainty due to the loss of crystallinity associated with metamictization. The crystal structure of synthetic, stoichiometric UTi_2O_6 however, indicates the unit is monoclinic with space group C2/m and both the U and Ti atoms are in distorted octahedral coordination (Szymanski and Scott, 1982).

The main aim of the research reported in this chapter was to investigate the chemistry and mineralogy of two naturally occurring brannerite samples using multiple characterisation techniques including X-ray Diffraction (XRD) analysis, Scanning Electron Microscopy (SEM), Raman spectroscopy, Inductively Coupled Plasma Mass Spectrometry (ICP-MS) and Electron Probe Microanalysis (EPMA). In addition, the natural brannerite samples were heat treated to examine the effect of temperature on the chemistry, texture and microstructural properties of the two samples. Results were also compared with a brannerite containing leach feed sample (derived directly from a uranium bearing ore) from Roxbury Downs, South Australia. Results will provide an evaluation of the key differences between natural and heat treated brannerite samples and the likely impact of these parameters on the composition and structure of this mineral.

3.2. Materials and Methods

3.2.1. Materials

The details of the samples that are used in this Chapter: NBCW, NBRD and high grade brannerite leach feed sample are described in section 2.1 in Chapter 2.

3.2.2. Methods

Details of the following methods used in this chapter: XRD, EPMA mapping, ICP-MS, SEM, XPS and Raman spectroscopy are given in Chapter 2.

2.2.1. Heat treatment of samples

All heat treatments were conducted in a Carbolite HTF 18/8 furnace. The temperatures ranged from 100-1200 °C in air, at 100 °C intervals. All samples were individually placed in a platinum boat and the furnace was heated to the required temperature at a steady ramp rate of 6 °/min. Upon reaching the required temperature, the sample was held at the designated temperature for 3 h, before cooling. This procedure was then repeated for the same sample at the next allocated temperature.

2.2.2. Quantitative EPMA

The chemical composition of the natural brannerite samples was quantitatively determined using a JEOL 8900 Superprobe Electron Probe Microanalyser (EPMA, JEOL 8900). The accelerating voltage and beam current were 15 kV and 10 nA, respectively. All analysis positions were verified as being homogeneous and flat by viewing the secondary electron image of the area to be analysed (at 5000 × magnification). The electron beam diameter was defocused to 4 μm for all analyses. The following suite of elements was analysed: Fe, Pb, Si, U, Ti, Th, Al, P, Ca, Y, S and O. A separate Energy Dispersive (ED) x-ray detector system was used during the analyses to check for the presence of other elements. For each element, the counting time on the peak was 20 s and half of that time

was measured on both sides of the peak (to measure the background). The standards used for calibration, the x-ray peak used, and the calculated detection limits (2σ, listed in ppm) were as follows: synthetic hematite (Fe_2O_3) for Fe(Kα), 2000 ppm, natural thorianite (ThO_2) for Th(Mα), 1000 ppm, natural wollastonite ($CaSiO_3$) for Si(Kα), 270 ppm, natural rutile for Ti(Kα), 3000 ppm, natural wollastonite for Ca(Kα), 370 ppm, synthetic magnesium aluminate spinel ($MgAl_2O_4$) for Al(Kα), 150 ppm, natural anglesite ($PbSO_4$) for Pb(Mα), 1300 ppm, synthetic yttrium vanadate (YVO_4) for Y(Lα), 420 ppm, cerium oxide (CeO_2) for Ce(Lα), 550 ppm, natural UO_2 for U(Mα), 1700 ppm. Oxygen was measured directly using the Kα x-ray line. The oxygen peak position was calibrated using the natural uraninite standard and detection limits (2σ) were calculated to be 2600 ppm.

All elemental analyses were corrected for atomic number (Z), absorption (A) and fluorescence (F) using the CITZAF *Phi-Rho-Z* matrix correction procedure (Armstrong, 1995) implemented on the JEOL 8900 EPMA. In order to determine the possible influence of different matrix correction procedures, the PAP procedure of Pouchou and Pichoir, (1985, 1991) was also used to calculate the element abundances. There was no significant difference in results obtained from either matrix correction procedure.

3.3. Results and Discussion

3.3.1. X-Ray Diffraction and Effect of Calcination Temperature on Crystallinity of Natural brannerite samples

The two natural brannerite samples were initially analysed to determine the bulk mineralogy of the powdered material. The XRD patterns that were obtained are shown in Figure 3.1a (NBCW) and Figure 3.1c (NBRD). Both patterns were characterised by having a broad, low intensity hump extending from 10-60 ° 2θ that lacked any recognisable diffraction peaks. Such patterns are characteristic of amorphous materials indicating: a) the brannerite in both samples was highly metamict, and, b) both samples had little contamination by individual gangue mineral phases that were crystalline. Note however, if contamination by extraneous phases was present, it was generally at levels below the detection limits of the XRD technique which are typically < 1-2 wt %.

To confirm that the samples contained brannerite, each was calcined at 1200 °C for 24 hours in air to recrystallise any amorphous brannerite present. Calcination conditions were selected on the basis of conditions used in previous studies to convert amorphous brannerite into a crystalline form (e.g. Vance et al., 2000). The XRD patterns for the heated NBCW and NBRD samples are shown in Figure 3.1b (NBCW) and Figure 3.1d (NBRD). Analysis of the XRD patterns using the ICDD library database indicated that the metamict natural samples were both successfully converted to crystalline brannerite (Database of the International Centre for Diffraction Data (ICDD) pattern 12-0477).

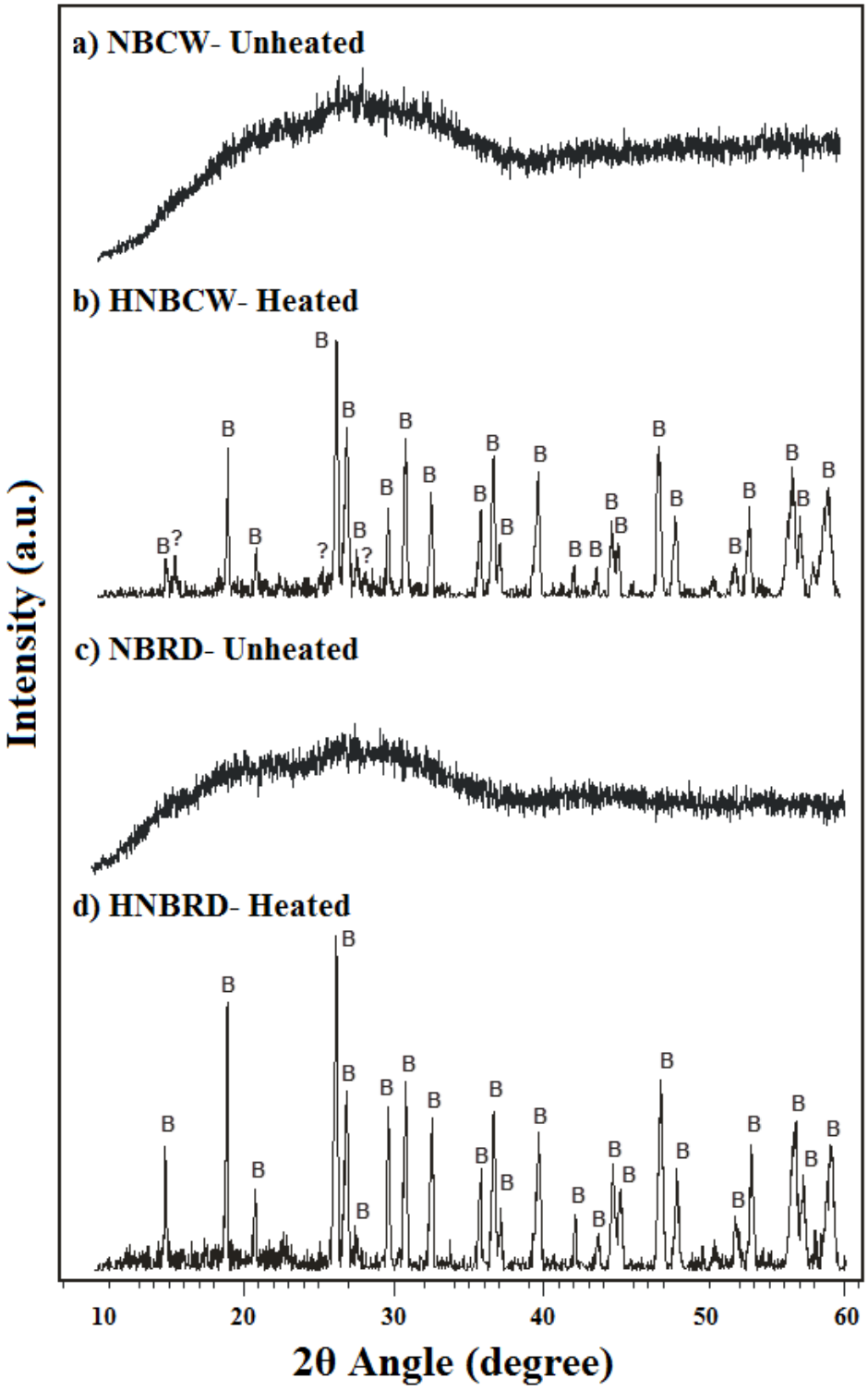

Figure 3.1: X-ray diffraction patterns comparing data obtained from the unheated and calcined brannerite samples. Peaks labelled 'B' indicate brannerite peaks while peaks labelled '?' are unknown (see text for details). In both samples, the unheated material produced patterns consistent with an amorphous, metamict sample whereas the effect of calcination at 1200 °C for 24 h in air was to produce well-crystallised brannerite.

For sample NBCW, the XRD pattern obtained for the calcined sample contained three diffraction lines at ~ 15.5 °, 25 ° and 27.5 ° 2θ that were not characteristic of recrystallised brannerite, nor were observed in the unheated sample (Figure 3.1b). The diffraction line at ~ 27.5 ° 2θ was most likely due to the presence of rutile/anatase (TiO_2) which is typically associated with brannerite-rich ores while the peak at 25 ° 2θ was a possible match for uranothorite ($[Th,U]SiO_4$). It is unclear as to the origin of the peak at 15.5 ° 2θ. In comparison, the calcined NBRD sample appeared to consist almost exclusively of recrystallised brannerite plus a minor amount of rutile/anatase (Figure 3.1d).

The effects of calcining the two natural brannerite containing samples at temperatures from 100 – 1200 °C in air, at 100 °C intervals, was investigated. The main focus of these tests was to understand the effect of radiation damage on the stability of brannerite through the recrystallisation process. Results are shown in Figures 3.2 (NBCW) and 3.3 (NBRD).

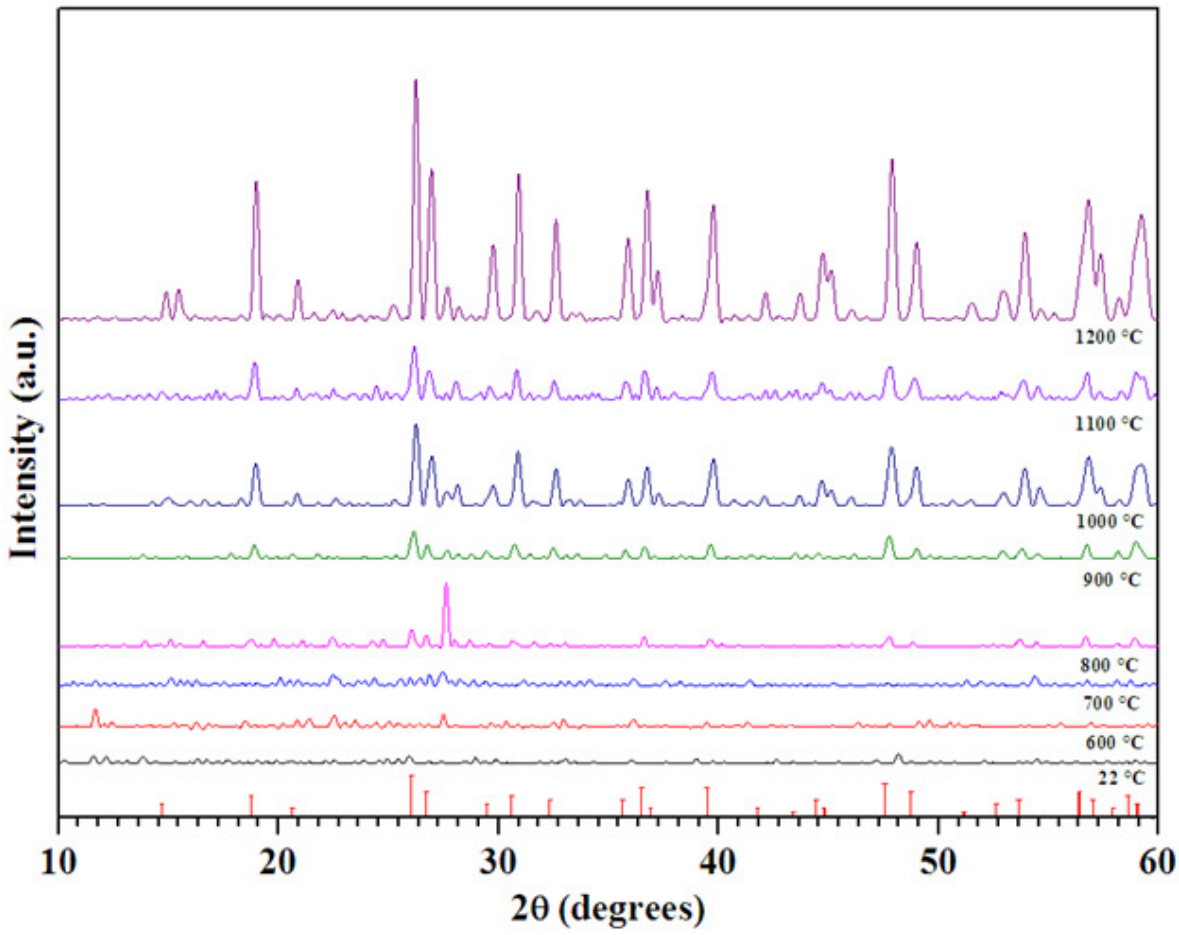

Figure 3.2: XRD patterns obtained for NBCW calcined at different temperatures for 24 h in air. All patterns have been background corrected to remove the broad hump characteristic of metamict material. Peak positions corresponding to brannerite (ICDD pattern number 12-477) are shown as sharp lines along the x-axis.

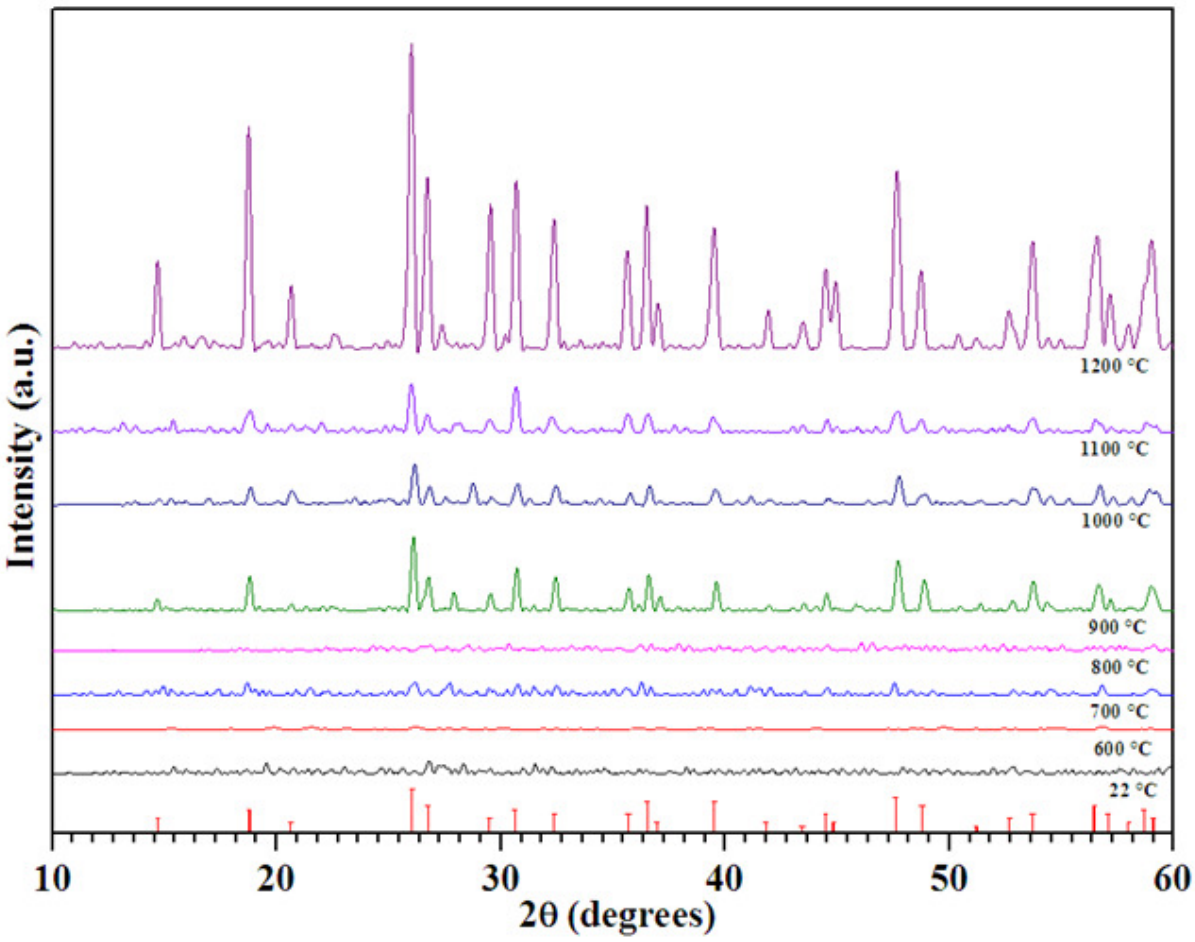

Figure 3.3: XRD patterns obtained for NBRD calcined at different temperatures for 24 h in air. All patterns have been background corrected to remove the broad hump characteristic of metamict material. Peak positions corresponding to brannerite (ICDD pattern number 12-477) are shown as sharp lines along the x-axis.

For the NBCW sample, radiation damage annealing began at temperatures as low as 800 °C with brannerite peaks just beginning to become visible. In comparison, the NBRD sample did not begin to show evidence of brannerite recrystallisation until an annealing temperature of 900 °C was reached. Results are consistent with previous annealing measurements made by Vance et al. (2000) and Zhang et al. (2006) who both determined the metamict-crystalline transition in natural brannerite samples occurred at temperatures of around 900-1000 °C. It is unclear however, as to why the NBCW showed evidence of

recrystallisation at temperatures up to 100 °C lower than the NBRD sample. Vance et al. (2000) speculated that the recrystallisation temperature was related to the purity of the sample with the presence of impurities such as rare earths and calcium stabilising the brannerite structure (in air). If so, the current results indicate the NBCW sample may contain more impurities than the NBRD sample.

3.3.1.1. Elemental compositions of Natural Brannerites

The two natural brannerite samples were digested using a multi acid digestion discussed in Chapter 2 and analysed by ICP-MS to determine the elements present in both natural samples (Table 3.1).

The two natural brannerite samples were digested in order to determine the bulk chemistry of the NBCW and NBRD samples. A summary of the bulk chemistry for each sample is provided in Table 5.1. Stoichiometric brannerite contains ~ 55 % U however both samples contained levels of uranium well below the theoretical content. Of the two natural brannerite samples, NBCW contained the lowest amount of uranium (24.16 % U) indicating the sample had impurities and contained other mineral phases. The high levels of elements Th, Cu, Zn, Al and Ca could suggest the occurrence of mineral phases of thorium oxides, sulphides and aluminium oxides with the natural brannerite sample.

Table 3.1: Summary of bulk chemical analysis data determined by ICP-MS for the natural brannerite samples NBCW and NBRD (in average weight % concentrations).

Elements	NBCW	NBRD
Na	0.00	0.47
Al	1.70	2.63
K	0.00	10.20
Ca	1.36	2.23
Ti	19.30	21.04
V	0.05	0.05
Mn	0.04	0.15
Fe	0.00	0.00
Cu	2.41	0.00
Zn	1.13	0.17
Nb	0.31	0.77
Mo	0.02	0.02
Ag	0.01	0.02
Sb	0.06	0.06
Ba	0.01	0.00
Ta	0.04	0.07
Tl	0.02	0.02
Pb	0.49	0.57
Th	6.85	6.68
U	24.16	26.45

3.3.2. Raman Spectroscopy

Raman spectroscopy was used to investigate any potential structural differences between the two brannerite containing samples, pre- and post-calcination. The samples were scanned between a range of 50 cm^{-1} to 3000 cm^{-1}.

The Raman spectra of the unheated brannerite samples are shown in Figures 3.4a and 3.4b. In previous work, the brannerite Raman spectrum has been throughly analysed between 100-1100 cm^{-1}, with the vibration modes fitted by Raman data from known uranyl titanate minerals holfertite, davidite and betafite and from known uranyl oxyhydroxide minerals (Frost et al., 2009, Frost and Reddy, 2010, Frost, 2011, Frost and Reddy, 2011).

As well, the RRUFF™ Project online database (http://rruff.info/) also contains reference spectra for a natural (RRUFF ID: R060613) and heated (RRUFF ID: R080091) brannerite sample sourced from Crockers Well. The heated sample had been calcined in air at 1000 °C for 18 hours.

For the unheated samples, both spectra may be conveniently divided into sections according to the position and intensity of the Raman bands. These are between 50-900 cm^{-1} and 900-2100 cm^{-1}. The bands observed in the region 50-900 cm^{-1} are typically associated with UO_2^{2+} and Ti-O stretching vibrations while the broad Raman bands in the 1000 to 2100 cm^{-1} region are attributed to U-OH bending modes and overtones (Frost et al., 2009). Normally, the UO stretching and bending modes are very intense and sharp in the Raman spectra of uranyl minerals (Frost et al., 2010). However, in both natural brannerite samples examined in the current study, these bands tended to be broad and of low intensity. It is likely therefore, that metamictisation has affected the Raman spectrum of brannerite causing the bands to become broad and overlapping. As well, it was observed that the intensity of bands in the 50-900 cm^{-1} region for the NBCW sample were more reduced in intensity than for the NBRD sample. These differences may indicate possible differences in the degree of metamictisation between samples.

The Raman spectra for both samples after high temperature heating are shown in Figures 3.4c and 3.4d. Compared to the unheated samples, the effect of heating was to sharpen and intensify the Raman peaks. The heated Crockers Well spectrum (Figure 3.4c) is in excellent agreement with the Raman spectrum provided in the RRUFF™ database for a heated brannerite sample.

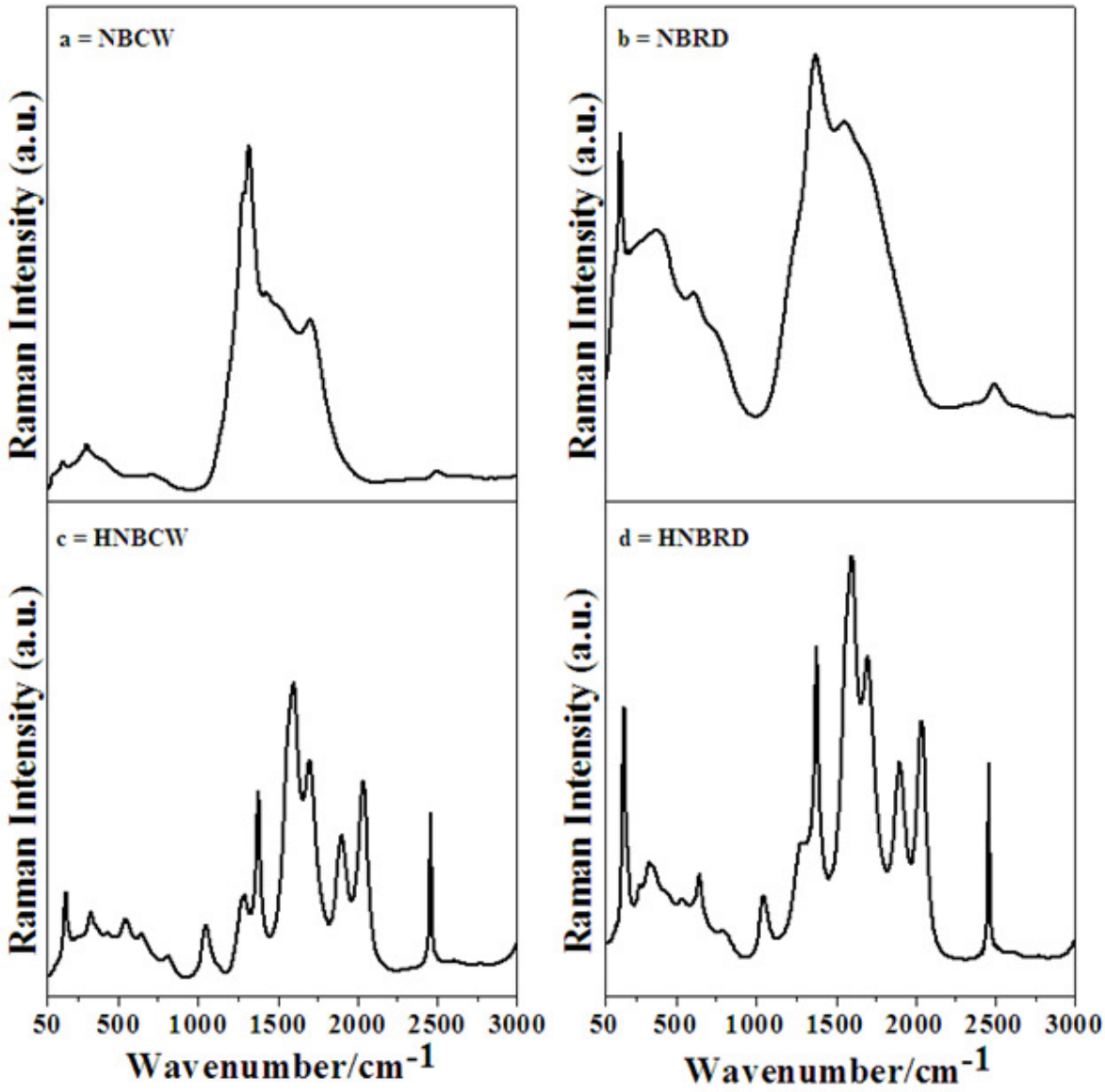

Figure 3.4: Raman spectra for the natural and heated brannerite samples: (a) natural brannerite, Crockers Well (NBCW), (b) natural brannerite, Roxby Downs (NBRD), (c) heated natural brannerite, Crockers Well (HNBCW), and, (d) heated natural brannerite, Roxby Downs (HNBRD). Y axes is in arbitrary units.

3.3.3. Scanning Electron Microscopy (SEM) and EPMA Mapping

The four samples (NBRD, NBCW, Heated NBRD and Heated NBCW) were examined by SEM and also mapped by EPMA to determine the key minerals associated with the brannerite, to examine the distribution of phases, and to examine the textures of individual

particles. Results are shown in Figures 3.5 and 3.6 for the Crockers Well sample and in Figures 3.7 and 3.8 for the sample from Roxby Downs.

3.3.3.1. Crockers Well (NBCW and HNBCW)

The unheated Crockers Well sample exhibited complex, heterogeneous microstructural features including evidence for alteration – most likely through interaction with an aqueous fluid – formation of secondary alteration products, and the presence of cracks and fractures within the brannerite grains and in adjacent minerals (Figures 3.5a-3.5d). The brannerite was intimately mixed with uranothorite ($[Th,U]SiO_4$) and a solid solution of thorianite-uraninite ($[Th,U]O_2$) (Figure 3.6). The uranothorite typically formed large, porous bright patches within brannerite particles (Figure 3.5d) while the thorianite-uraninite typically was present as smaller grains (inclusions) within brannerite. Energy Dispersive (ED) analysis of the brannerite indicated a composition rich in thorium, consistent with the Crockers Well brannerite commonly being reported as Th-brannerite (Whittle, 1954, Ashley, 1984, Lumpkin et al*.,* 2012). Throughout the sample there was clear evidence for alteration of the Th-brannerite e.g. the dark grey particle slightly below centre in Figure 3.6a and the particle shown in Figure 3.6d. Alteration of the Th-brannerite was associated with an increase in P, Si, and Al (determined by ED analysis) compared to less altered regions.

Rutile was common in the Crockers Well sample and was typically distributed as fine-grained crystals throughout the Th-brannerite and uranothorite dominated particles (dark grey mineral phase in Figures 3.5a and 3.5c and Figure 3.6). In rare cases, rutile was present as large, (~100-150 μm) particles. Other gangue mineral phases present in the Crockers Well sample included: quartz (upper dark particle in top left quadrant of Figure

3.5b), biotite (bottom dark phase in Figure 3.5b), unidentified REE-containing phosphates (not shown), and zircon.

Textures within the heated Crockers Well sample were less heterogeneous compared to the unheated sample with much of the alteration that was apparent in Figures 3.5a-3.5d being homogenised by the heating process. The main phases present in the heated sample included Th-brannerite, thorianite (ThO_2 – brightest phase in Figure 3.5e) and small crystals of uraninite (UO_2 – bright grains in Figure 3.5g). Heating the sample to 1200°C caused extensive recrystallisation of the brannerite to produce clusters of 2-3 μm sized, prismatic grains (e.g. Figures 3.5g and 3.5h). The crystalline form of the heated brannerite grains is of the monoclinic space group observed in synthetic brannerite (Szymanski and Scott, 1982). After heating, the composition of the brannerite remained Th-rich although patches of brannerite appeared to have more thorium than others. The presence of uraninite indicates that the thorianite-uraninite ($[Th,U]O_2$ phase present in the unheated sample was decomposed into a ThO_2 phase and a UO_2 phase (note however, the ThO_2 contained minor U in solid solution whereas the UO_2 contained negligible Th - determined by ED analysis). Larger gangue mineral phases such as rutile (Figure 3.5f) remained unaffected by the heating process although the smaller rutile grains that were originally present within the Th-brannerite appear to have undergone some recrystallisation forming small equant crystals (Figure 3.5h).

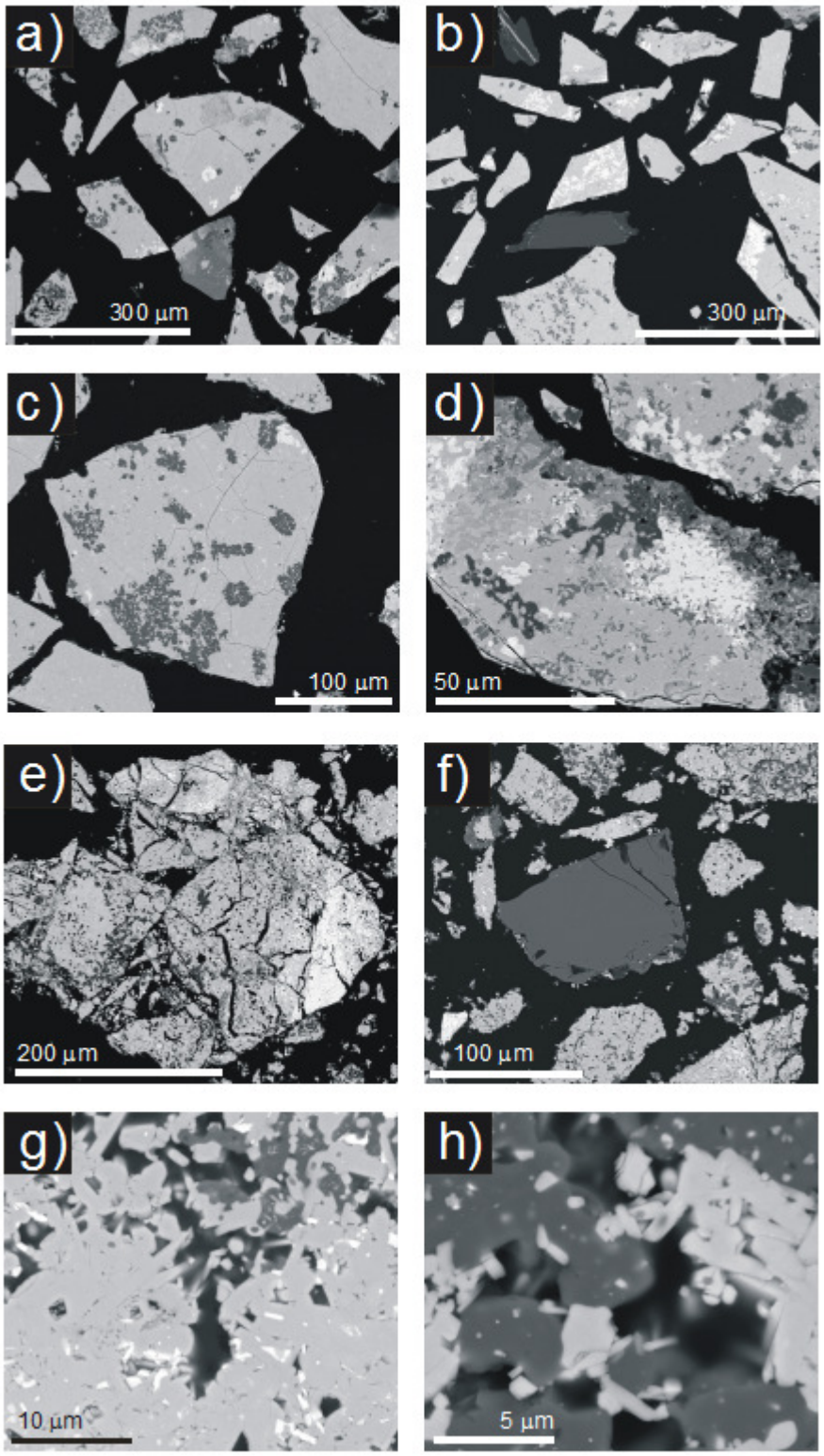

Figure 3.5: Representative back-scattered electron (BSE) images of brannerite samples from Crockers Well Images a-d are from the unheated sample showing Th-containing brannerite (medium grey) and recrystallisation to secondary phases including uranothorite (white) and rutile (small black patches). Additional dark phases in images b) and d) include

quartz and unidentified aluminosilicates. Images e-f are from the heated sample showing Th-containing brannerite (medium grey), uraninite (white) and rutile (small black patches). The large dark particle in f) is a rutile grain. Images g-h show magnified images of recrystallised areas. Note the recrystallisation of the brannerite to produce clusters of 2-3 µm sized, prismatic grains (medium grey phase in 3.5f) with uranothorite at grain boundaries (white phase in 3.5f) and small rutile crystals (dark phase in 3.5f and 3.5h). See text for further details.

EPMA mapping of the unheated Crockers Well samples (Figures 3.6a and 3.6b) confirmed the uranium-bearing mineralogy was made up mostly of Th-rich brannerite, uranothorite and a small amount (< 5 %) of an unidentified (U,Th,Ti,Si,Ca) oxide mineral – this was assumed to be an alteration product of the Th-rich brannerite. Minor gangue phases present in the unheated sample included (in approximate order of abundance) rutile, unidentified aluminosilicates, zircon and apatite. These additional gangue phases were not previously identified by the XRD analysis due to their relatively low abundance i.e. XRD is sensitive to mineral phases in abundances greater than about 1-2 wt %.

The heated Crockers Well sample had a grain population that exhibited less heterogeneous mineral and textural features than the unheated material (Figures 3.6c and 3.8d). The main mineral phase identified in the heated sample was Th-brannerite (over 70 %) although there was also uranothorite, a higher-Th brannerite, rutile and an unidentified (Th,Ca)-phosphate. Minor amounts of quartz, titanite and zircon were also identified in the heated sample.

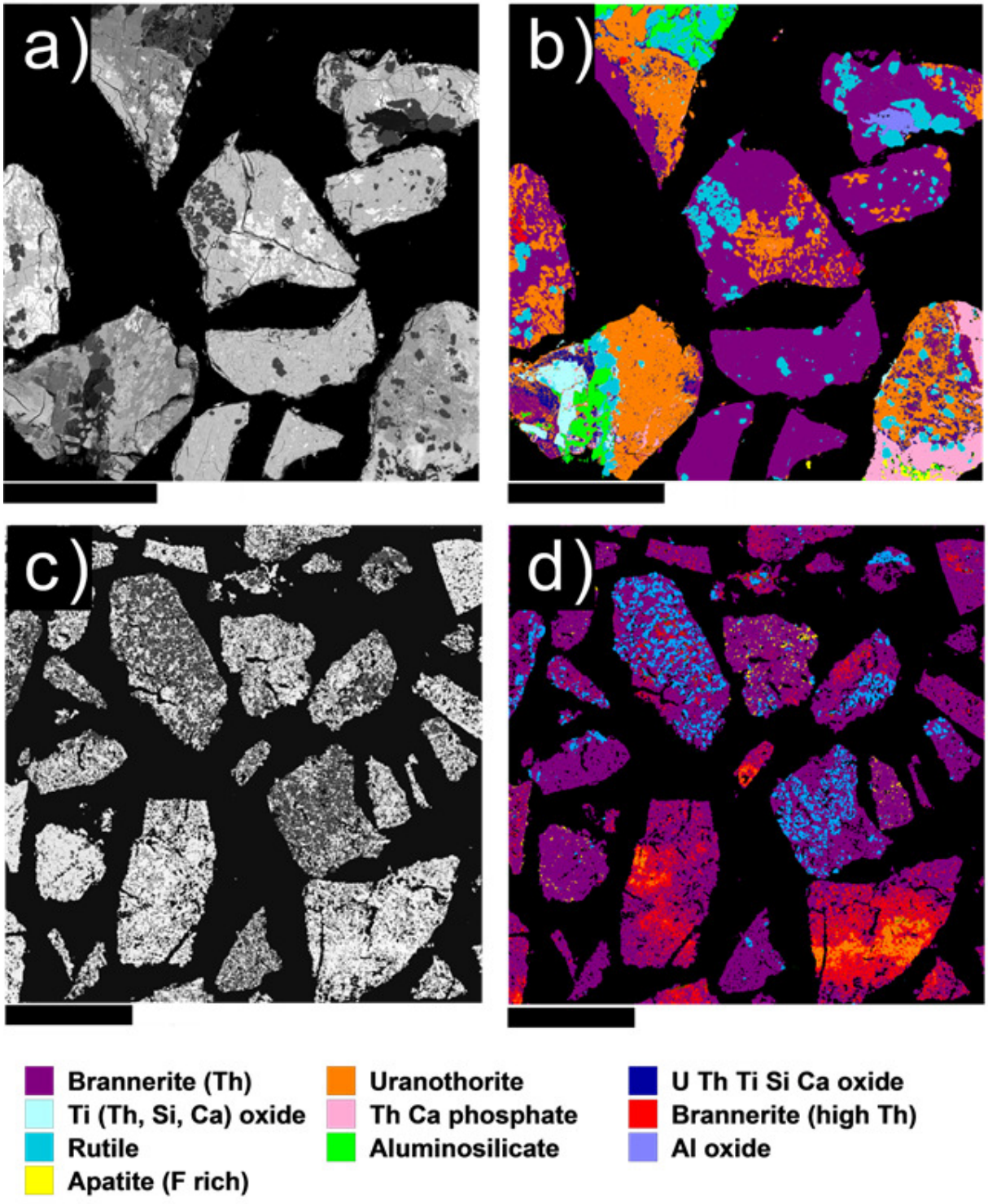

Figure 3.6: Back-scattered electron (BSE) image and corresponding classified mineral maps for the Crockers Well sample. Images a) and b) represent the natural, unheated sample (NBCW) while images c) and d) are from the sample calcined at 1200 ° C (HNBCW).

3.3.3.2. Roxby Downs (NBRD and HNBRD)

The natural sample from Roxby Downs consisted of a range of heterogeneous particles containing predominantly brannerite with smaller grains and inclusions of uranothorite, rutile, a thorianite-uraninite ([Th,U]O_2 phase and a Th-rich brannerite phase (Figure 3.7a-3.7c). Minor impurity phases included quartz, titanates and unidentified aluminosilicates. In general, impurity phases were much less common in the Roxby Downs brannerite sample compared to the one from Crockers Well. In patches, the brannerite showed evidence for extensive alteration (Figure 3.7d) and ED analysis of the altered material indicated that brannerite alteration was accompanied by a decrease in uranium and an increase in Si, Ca and Al.

Heating of the sample was associated with extensive recrystallisation (Figures 3.7e-3.7g) and segregation of phases. For example, Figure 3.7h shows a magnified view from a recrystallised brannerite particle – phases present include a Pb-silicate phase (dark grey) which appeared to have formed as a low melting point phase interstitial to prismatic brannerite grains (medium grey in Figure 3.7h) and uraninite (brightest phase). As with the Crockers Well sample, heating of the Roxby Downs sample appears to have broken down the thorianite-uraninite ([Th,U]O_2 into separate ThO_2 and UO_2 phases. The presence of uraninite and Pb-rich aluminosilicate glass films at grain boundaries is consistent with previous observations on brannerite heated up to 1000 °C made by Zhang et al. (2006).

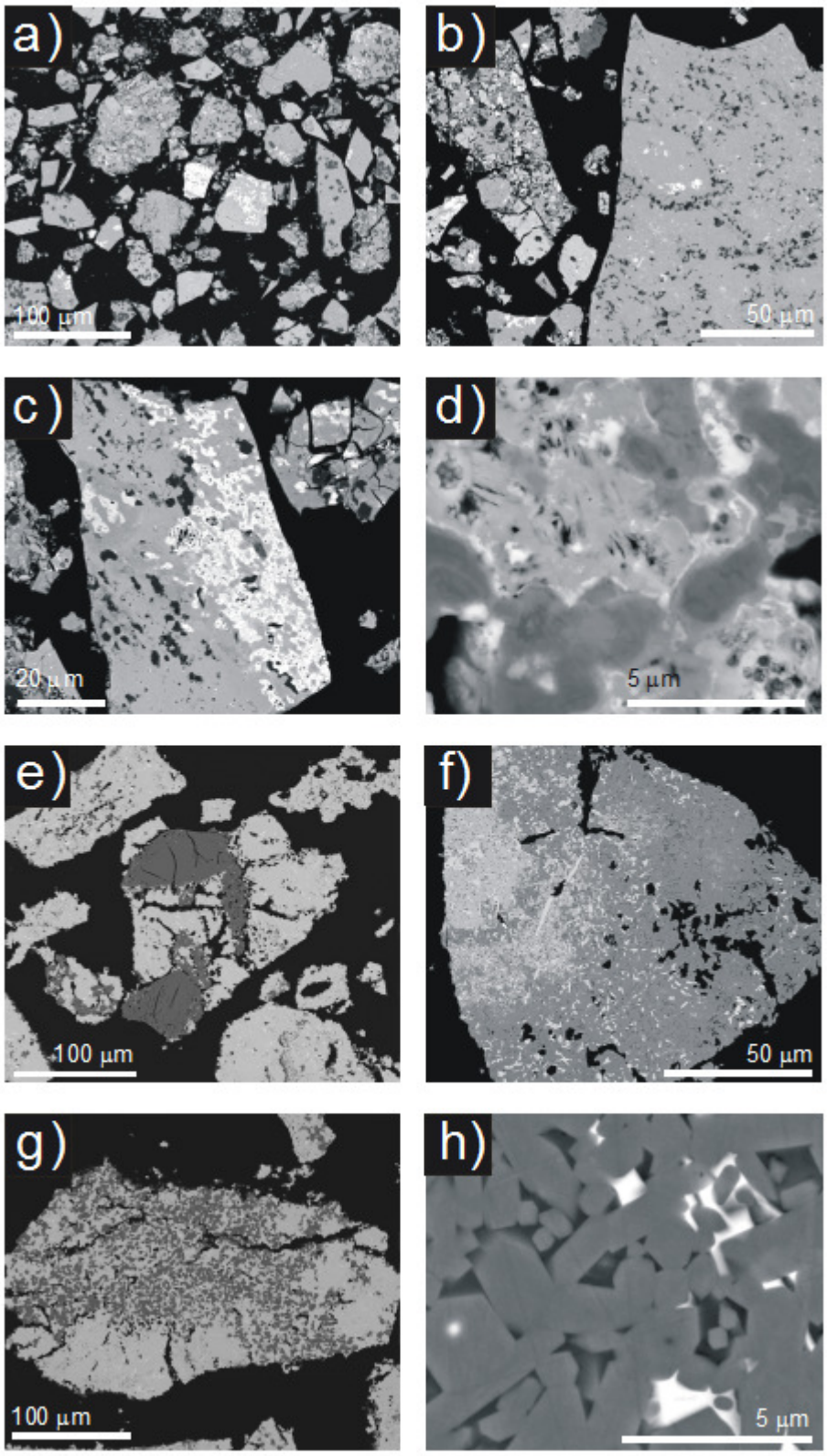

Figure 3.7: Representative back-scattered electron (BSE) images of brannerite samples from Roxby Downs Images a-d are from the unheated sample showing Th-rich brannerite (medium grey) and recrystallisation to secondary phases including uranothorite (white) and

rutile (small black patches). Image d) shows a hydrothermally altered section of a grain with uranothorite (white) at grains boundaries of Th-brannerite (medium and dark grey phases). Images e-f are from the heated sample showing Th-containing brannerite (medium grey), needle-like uraninite (white) and rutile (small black patches). The large dark particles in e) are rutile grains. Image h) shows a magnified view of the recrystallisation of the brannerite to produce clusters of < 5 μm sized, prismatic grains (grey) mixed with uraninite (white) and an interstitial Pb-silicate phase (dark). See text for further details.

EPMA map images showing mineral textures and phases present in the heated and unheated Roxby Downs sample are shown in Figure 3.8. The map for the unheated sample confirmed the lack of substantial amounts of impurities in the brannerite compared to the Crockers Well sample. After heating, the recrystallised sample exhibited a similar texture to that observed in the Crockers Well sample (c.f. Figures 3.8d and 3.6d).

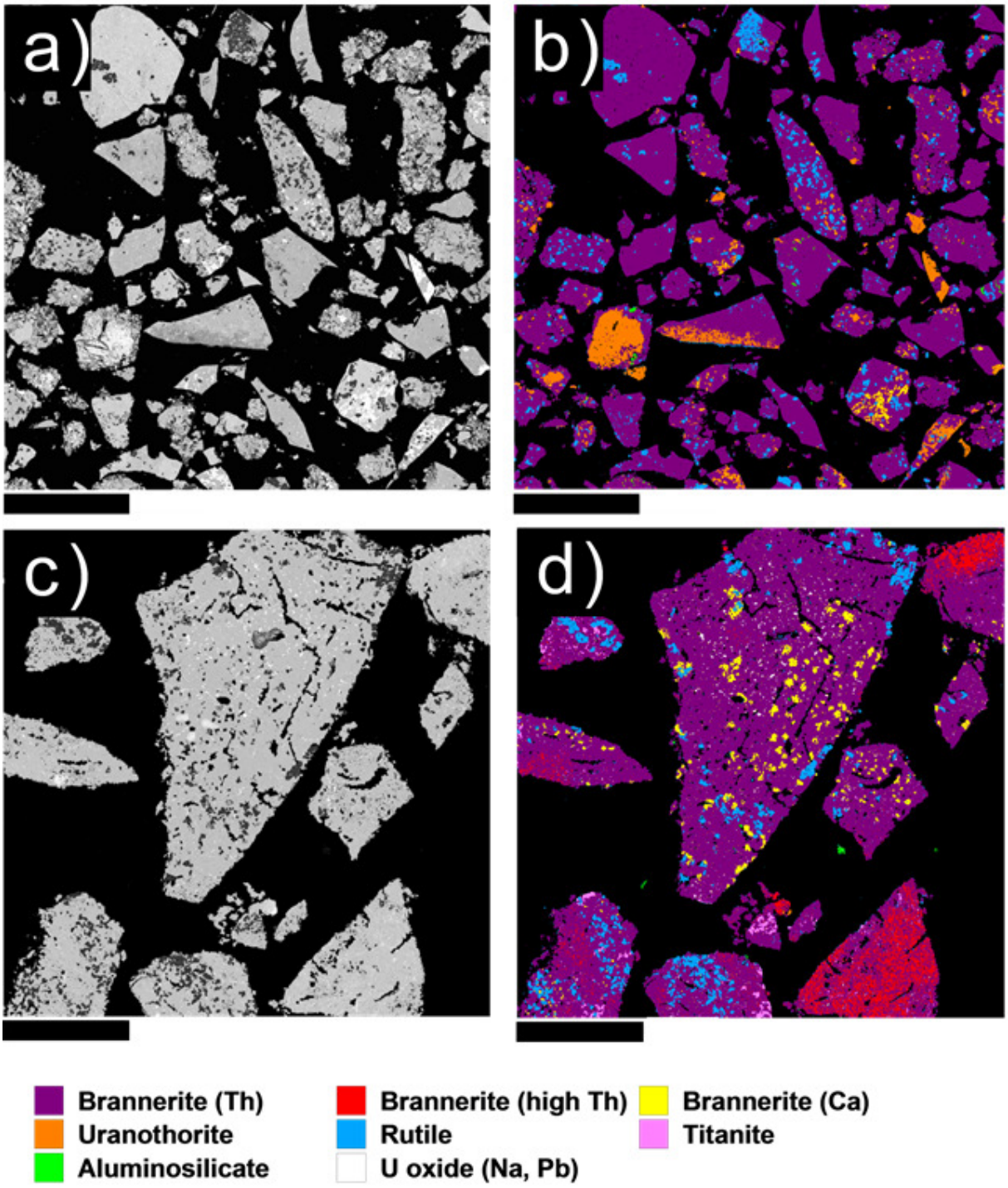

Figure 3.8: Back-scattered electron (BSE) image and corresponding classified mineral maps for the Roxby Downs sample. Images a) and b) represent the natural, unheated sample (NBRD) while images c) and d) are from the sample calcined at 1200 ° C (HNBRD).

3.3.4. Chemistry of Natural Brannerite - Quantitative EPMA

Average compositions for brannerite and associated uranium-containing mineral phases in the natural and recrystallised samples are provided in Table 3.2 and are described separately below.

3.4.1. Crockers Well (NBCW and HNBCW)

The brannerite in the unheated Crockers Well sample exhibited the following compositional ranges, based on fifteen analyses 7-10 wt % Th, 18-21 wt % Ti, 31-34 wt % U. Additional constituents include on average 0.9 wt % Fe, 0.4 wt % Si, 2.2 w t% Ca, < 0.1 wt % Al, 2.4 wt % Pb, 1.3 wt % Y, 0.1 wt % Zr and 0.7 wt % Ce. According to the analyses, the Crockers Well brannerite is thorium-rich, consistent with previous analyses from Whittle (1954) – included in Table 3.2 – and indicative of partial solid solution between brannerite and thorutite ($ThTi_2O_6$ – which has the brannerite structure). The data of Whittle (1954) also indicate the Crockers Well brannerite is hydrated, containing ~ 10 wt % H_2O. Total analysed contents of the brannerite measured via EPMA ranged from 88 to 93 %. These low totals are likely to reflect a combination of partially hydrated brannerite (c.f. Whittle, 1954), and metamict or slightly amorphous brannerite as described by Lumpkin et al. (2012). Assuming direct substitution of Th for U, the low combined U+Th compared to stoichiometric brannerite (41 wt % U+Th compared to 55 wt % U) indicates that up to 25 % (by weight) of the original amount of U+Th was lost as a result of alteration. As indicated by the extensive variation in BSE contrast in Figures 3.6a-3.6d, a large proportion of the sample is altered and fine-grained rutile and thorianite are present - presumably both formed as a result of alteration of the host natural brannerite.

For the heated sample, three uranium containing mineral phases were analysed. These included a brannerite of similar composition to the unheated sample, a high-Th brannerite and thorianite. Based on the SEM and EPMA results, uraninite was also present in the heated sample. However grainsizes of the uraninite were typically small and below the resolution of the EPMA's analytical capability. The brannerite exhibited the following compositional ranges, based on nine analyses, 9-11 wt % Th, 21-24 wt % Ti, 34-36 wt % U. Additional constituents included on average 1.1 wt % Fe, 0.1 wt % Si, 1.7 wt % Ca, < 0.1 wt % Al, 0.1 wt % Pb, 1.3 wt % Y, 0.1 wt % Zr and 1.0 wt % Ce. Total analysed contents of the brannerite measured via EPMA ranged from 97-100 % indicating that dehydration accompanied recrystallisation of the brannerite. Compared to the brannerite in the unheated sample, the heated brannerite contained less Si, less Ca and significantly less Pb. These elements appeared not to be stabilised in the high temperature brannerite with the Ca and Si being incorporated into a Ca silicate mineral phase (Figure 5) and the Pb and Si into a Pb-rich aluminosilicate film at grain boundaries. The heated sample also contained a high-Th brannerite (22 wt % Th, 25 wt % U) and a low uranium thorianite phase (1.8 wt % U, 61 wt % Th and 9.4 % Si).

Table 3.2: Average compositions of brannerite and other U-contaiing minerals in natural and heated samples from Crockers Well and Roxby Downs.

Element (wt %)	Brannerite (UTi_2O_6) Ideal	Brannerite-Crockers Well*	Brannerite NBCW	Brannerite HNBCW	High- Th Brannerite HNBCW	Thorite HNBCW	Brannerite NBRD	Med-Th Brannerite NBRD	High-Th Brannerite NBRD	Brannerite HNBRD	High- Th Brannerite HNBRD
Fe		0.96	0.90	1.07	1.06	0.05	1.07	1.64	0.47	1.07	1.05
Th		11.26	8.46	10.93	22.03	60.88	9.46	14.15	28.36	11.85	29.88
Si		-	0.40	0.12	1.57	9.40	0.31	0.19	2.77	0.91	1.61
Ti	22.29	22.29	20.01	23.41	21.99	0.74	19.69	21.05	10.81	22.49	18.00
Ca		-	2.19	1.68	1.18	0.32	2.03	1.93	0.87	1.77	1.96
Al		-	0.06	0.04	0.13	0.17	0.03	0.06	0.03	0.12	0.12
Pb		2.59	2.40	0.11	0.69	0.62	2.47	2.18	1.38	2.61	3.72
Y		2.92**	1.29	1.32	0.97	0.57	1.17	1.46	0.93	1.30	0.82
U	55.37	26.49	32.48	35.21	25.01	1.80	30.75	25.73	21.07	31.86	16.24
Zr		-	0.11	0.07	0.42	0.13	0.10	0.22	0.62	0.18	0.27
Ce		1.22	0.74	1.00	0.30	n.d.	0.85	1.48	0.71	0.49	0.31
O	22.33	-	21.67	23.84	24.55	20.77	21.22	22.46	21.58	23.23	23.31
Total	99.99	99.34	90.67	98.78	99.87	95.05	89.11	92.49	89.53	98.84	98.35
# Analyses			15	9	5	5	11	5	5	9	3

n.d. = below detection limit

* data from Whittle (1954). Sample includes ~10 wt % H_2O, 0.19 % Sc_2O_3 and 0.13 % P_2O_5

** including Er

3.4.2. Roxby Downs (NBRD and HNBRD)

Three distinct brannerite-like phases were observed in the unheated Roxby Downs sample (Table 3.2). The first, and most abundant type, contained significant thorium and had a similar composition (9-10 wt % Th, 19-20 % Ti, 28-33 wt % U from eleven analyses) to the brannerite from Crockers Well. There was also a medium-Th brannerite (14 wt % Th, 21 wt % Ti, 26 wt % U) and a high-Th (28 wt % Th, 11 wt % Ti, 21 wt % U) brannerite. For the latter phase it was not clear if this was a true brannerite phase (the average Ti was low compared to the typical Ti levels of ~19-21 wt % measured in all other brannerite phases). This composition may represent a mixture of fine-grained brannerite and thorianite phases.

In the heated Roxby Downs sample, two uranium containing mineral phases were analysed. These included a brannerite of similar composition to the unheated sample, plus a high-Th brannerite. The brannerite exhibited the following compositional ranges, based on nine analyses, 9-15 wt % Th, 22-23 wt % Ti, 29-35 wt % U. Additional constituents included on average 1.1 wt % Fe, 0.9 wt % Si, 1.8 wt % Ca, 0.1 wt % Al, 2.6 wt % Pb, 1.3 wt % Y, 0.2 wt % Zr and 0.5 wt % Ce. Total analysed contents of the brannerite measured via EPMA ranged from 96-101 %. The heated sample also contained a high-Th brannerite mineral phase (30 wt % Th, 18 wt % Ti, and 16 wt % U).

3.5. Examination of a brannerite ore (XRD / EPMA)

The mineralogy of a ‘high grade’ brannerite uranium leach feed sample (uranium bearing ore sample that had been through a flotation process) from the Roxby Downs region, South Australia was investigated.

The bulk mineralogy of the aforementioned sample was analysed by XRD and the pattern that was obtained is shown in Figure 3.9. The pattern was characterised by having three major phases of quartz (SiO_2) (ICDD pattern 01-085-1054), hematite (Fe_2O_3) (ICDD pattern 0-013-0534) and feldspar potassium ($K_{0.5}Na_{0.5}AlSi_3O_8$) (ICDD pattern 01-084-0710). A minor phase that was identified with this pattern was rutile (TiO_2) (ICDD pattern 00-004-0551). No brannerite matches were observed.

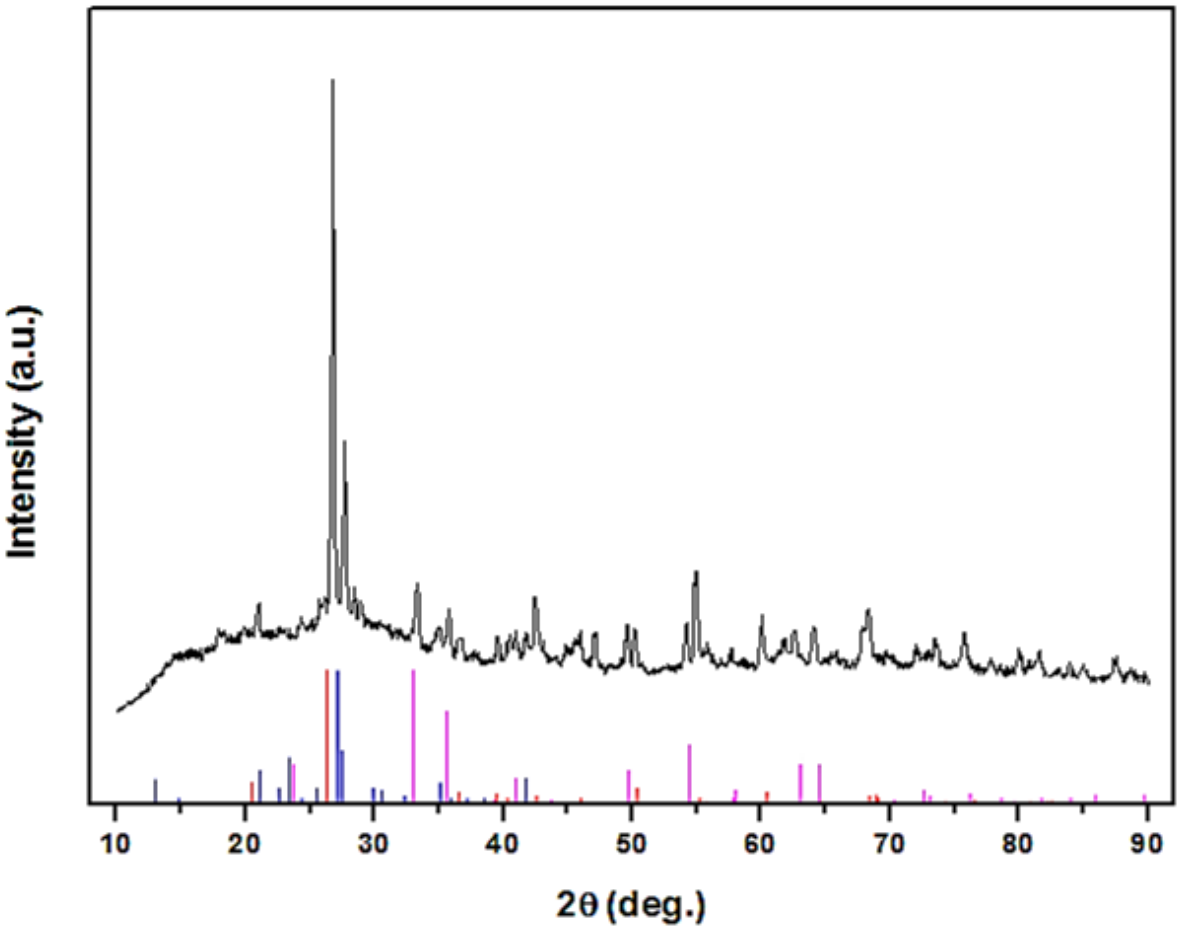

Figure 3.9: XRD pattern obtained for high grade brannerite uranium leach feed. Peak positions corresponding to quartz (SiO_2) (ICDD pattern 01-085-1054) (Red), hematite (Fe_2O_3) (ICDD pattern 0-013-0534) (Pink) and feldspar potassium ($K_{0.5}Na_{0.5}AlSi_3O_8$) (ICDD pattern 01-084-0710) (Blue) are shown as sharp lines along the x-axis.

Due to the lack of recognisable brannerite diffraction patterns EPMA analysis was used to locate the brannerite within this sample. Quantitative EPMA analysis was not performed on this sample as the map analysis gave an accurate representation of the types of minerals found within the sample.

The leach feed sample consisted of a range of heterogeneous particles containing predominantly quartz, iron oxides and feldspar potassium with smaller grains and inclusions of barite ((Ba, Pb)SiO_4), portlandite ($Ca(OH)_2$), bastnasite ((Ce, La)FCO_3), rutile and aluminosilicate phases (Figure 3.10).

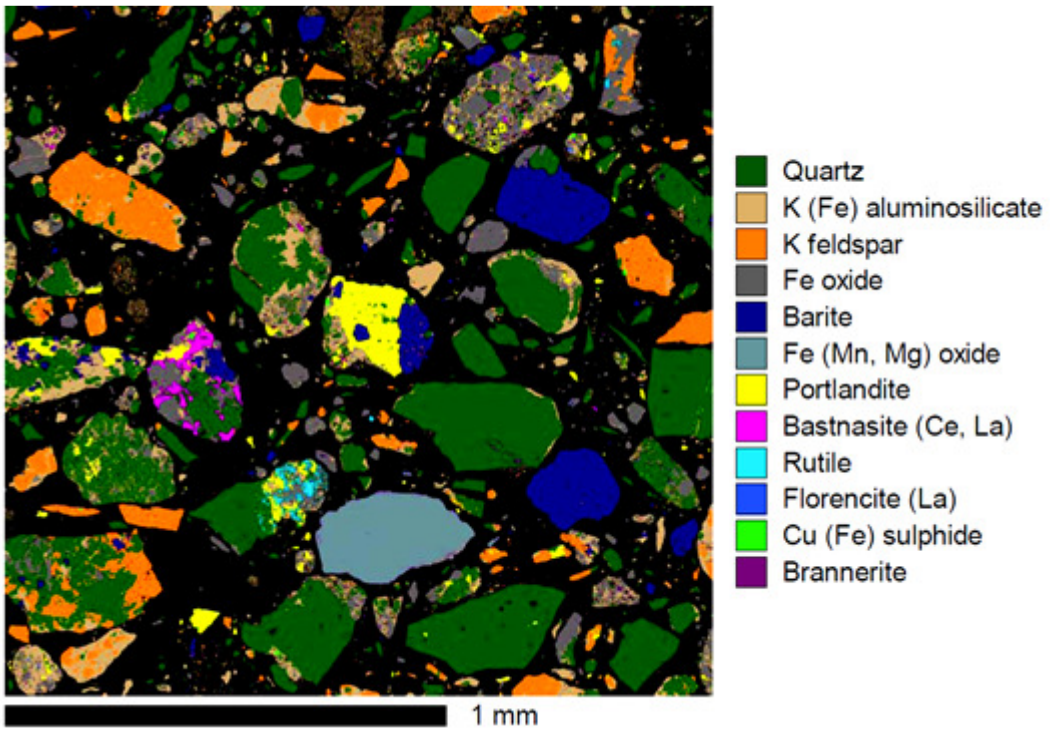

Figure 3.10: Mineral phase map for the Leach feed, Olympic Dam sample.

The brannerite (Figure 3.11) was found to be encapsulated within an aluminosilicate (high in potassium and iron) / quartz grain. The brannerite particles were also in close proximately to a portlandite inclusion with the aluminosilicate / quartz grain.

The map data obtained for the brannerite in the leach feed sample largely confirmed the XRD results as the sample is dominated by quartz, feldspar potassium and hematite. While other minerals are present, they are generally at low abundance and hence wouldn't be picked up by XRD. Even though this is presented as a 'high grade' brannerite sample, the actual amount of brannerite is very low. This conclusion is not surprising as the bulk sample contained very low total U and presumable most of the total U is present as uraninite.

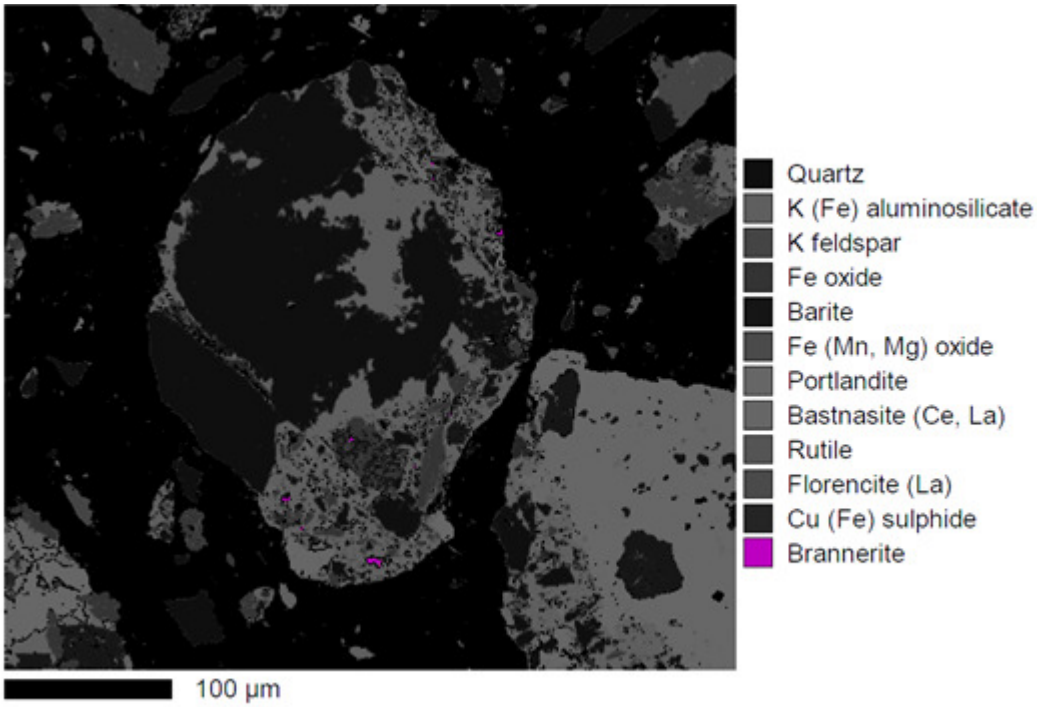

Figure 3.11: Mineral phase map magnified to 100 µm, showing brannerite inclusions.

3.4. Conclusions

Two natural brannerite samples from the Crockers Well and Roxby Downs deposits in South Australia were studied by XRD, Raman spectroscopy, SEM imaging and EPMA to determine their chemical, textural and structural properties. In addition the samples were heat treated to examine the effect of temperature on recrystallisation, mineral stability and deportment of impurities.

The XRD analysis of the unheated samples indicated both were amorphous having undergone radiation-induced metamictisation. The crystallinity of the brannerite was restored upon heating of the samples to 1200 °C for 24 hours in air. For the Crockers Well sample, radiation damage annealing began at temperatures as low as 800 °C while the Roxby Downs sample did not begin to show evidence of brannerite recrystallisation until an annealing temperature of 900 °C was reached.

Raman spectroscopy indicated that the effect of metamictisation was to make the peaks broad and of low intensity. The intensity of bands in the 50-900 cm^{-1} region for the Crockers Well sample were more reduced in intensity than for the Roxby Downs sample possibly indicating differences in the degree of metamictisation. After heating, the Raman peaks were sharpened and intensified due to the increased crystallinity.

SEM and EPMA investigations indicated that both samples exhibited complex, heterogeneous microstructural features including evidence for alteration, formation of secondary alteration products, and the presence of cracks and fractures within the brannerite grains and in adjacent minerals. In each sample, the brannerite was Th-rich (~ 8-10 wt % Th) indicating partial solid solution between brannerite and thorutite ($ThTi_2O_6$)

and was intimately mixed with uranothorite ([Th,U]SiO_4) and a solid solution of thorianite-uraninite ([Th,U]O_2). Typical gangue mineral phases included: rutile (distributed as fine-grained crystals throughout the Th-brannerite and uranothorite dominated particles), quartz, aluminosilicates, unidentified REE-containing phosphates, zircon, titanates and apatite.

In the heat treated natural brannerite samples (HNBCW and HNBRD), the recrystallisation of the brannerite caused a number of chemical changes. The heated brannerite generally contained less Si, less Ca and significantly less Pb. These elements appeared not to be stabilised in the high temperature brannerite with the Ca and Si being incorporated into a Ca silicate mineral phase and the Pb and Si into a Pb-rich aluminosilicate film at grain boundaries. In addition, both samples contained a high-Th brannerite (up to 22-30 wt % Th). The thorianite-uraninite phase in the unheated samples was decomposed into separate ThO_2 and UO_2 phases after heating.

A ‘high grade’ brannerite leach feed sample from the Olympic Dam deposit in South Australia was also studied by XRD and EPMA mapping analysis to determine the gangue mineralogy. XRD analysis of the ‘high grade’ ore samples indicated that the sample was high in quartz, iron oxides and feldspar potassium (no X-ray diffraction pattern for brannerite could be identified). EPMA mapping investigations determined very low quantities of brannerite within a quartz grain.

3.5. References

Adler, H.H. and Puig, J.A., 1961. Observations on the thermal behavior of brannerite, American Mineralogist, 46, 1086-1096.

Armstrong, J.T., 1995. CITZAF: a package of correction programs for the quantitative electron microbeam X-ray analysis of thick polished materials, thin films, and particles. Microbeam Analysis, 4, 177-200.

Ashley, P.M., 1984. Sodic granitoids and felsic gneisses associated with uranium-thorium mineralisation, Crockers Well, South Australia. Mineralium Deposita, 19, 7-18.

Balek, V., Zelenák, Z., Málek, Z., Vance, E.R. and Subrt, J., 2000. Emanation thermal analysis study of brannerite. MRS Proceedings, 663, 347.

Balek, V., Vance, E.R., Zelenák, Z., Málek, Z. and Subrt, J., 2007. Use of emanation thermal analysis to characterize thermal reactivity of brannerite mineral. Journal of Thermal Analysis and Calorimetry, 88, 93-98.

Campana, B. and King, D., 1958. Regional geology and mineral resources of the Olary Province. South Australian Geological Survey Bulletin 30, 70-50.

Colella, M., Lumpkin, G.R., Zhang, Z., Buck, E.C. and Smith, K.L., 2005. Determination of the uranium valence state in the brannerite structure using EELS. XPS, and EDX. Phys. Chem. Minerals, 32, 52-64.

Cross, K.C., Daly S.J. and Flint R.B., 1993. Olympic Dam deposit. In: Drexel, J.F. Press W.V. and Parker A.J. (Eds), The geology of South Australia. Geological Survey of South Australia, Bulletin 54, Vol. 1, pp. 132-138.

Fabris, A.J., Conor, C.H.H., Crooks, A.F. and Burrt, A.C., 2004. Uranium prospects of the southern Curnamona Province and cover sequences, South Australia. South Australia. Department of Primary Industries and Resources. Report Book 2004/22.

Finch, W.I., 1996. Uranium Provinces of North America, Their Definition, Distribution, and Models, U.S. Geological Survey Bulletin 2141, U.S. Department of the Interior, pp. 76.

Finch, R.J. and Murakami, T., 1999. Systematics and paragenesis of uranium minerals. In: Burns, P.C., Finch, R.J. (Eds), Uranium: Mineralogy, Geochemistry and the Environment. Reviews in Mineralogy, vol. 38, pp. 91–180.

Fleischer, M. and Mandarino, J.A., 1995. Glossary of mineral species. Mineralogical Record Inc., Tucson, Arizona, pp. 280.

Frost, R.L., 2011 Raman spectroscopic study of the uranyl titanate mineral holfertite $Ca_xU_{2-x}Ti(O_{8-x}OH_{4x}).3H_2O$ and the lack of metamictization. Radiation Effects and Defects in Solids, 166**,** 24-29.

Frost, R.L., Cejka, J. and Dickfos, M.J., 2009. Raman spectroscopic study of the uranyl minerals vanmeersscheite $U(OH)_4[(UO_2)_3(PO_4)_2(OH)_2].4H_2O$ and arsenouranylite

$Ca(UO_2)[(UO_2)_3(AsO_4)_2(OH)_2].(OH)_2.6H_2O$. Spectrochimica Acta Part A: Molecular and Biomolecular Spectroscopy, 71, 1799-1803.

Frost, R.L. and Reddy, B.J., 2010. Raman spectroscopic study of the uranyl titanate mineral betafite $(Ca,U)_2(Ti,Nb)_2O_6(OH)$: effect of metamictization. Radiation Effects and Defects in Solids: Incorporation Plasma Science and Plasma Technology, 165, 868-875.

Frost, R.L. and Reddy, B.J., 2011. Raman spectroscopic study of the uranyl titanate mineral brannerite $(U,Ca,Y,Ce)_2(Ti,Fe)_2O_6$: effect of metamictisation. Journal of Raman Spectroscopy, 42, 691-695.

Goldney, L.H., Canning, R.G. and Gooden, J.E.A., 1972. Extraction investigations with some Australian uranium ores. AAEC Symposium on Uranium Processing, Paper V, V1-V18.

Harrowfield, I.R., MacRae, C.M. and Wilson, N.C., 1993. Chemical imaging in electron microprobes. In Proceedings of the 27th Annual MAS Meeting, Microbeam Analysis Society, New York, 547-548.

Hess, F.L. and Wells, R.C., 1920. Brannerite, a new uranium mineral. Journal of the Franklin Institute, 189, 225-237.

Hewett, D.F., Stone, J. And Levine, H., 1957. Brannerite from San Bernardino County, California. American Mineralogist 42, 30-38.

Lian, J., Wang, L., Lumpkin, G.R. and Ewing, R.C., 2002. Heavy ion irradiation effects of brannerite-type ceramics. Nuclear Instruments and Methods in Physics Research B, 191, 565-570

Liu, J.-H., Van den Berghe, S. and Konstantinovic, M.J., 2009. XPS spectra of the $U5^{+}$ compounds KUO_3, $NaUO_3$ and $Ba_2U_2O_7$. Journal of Solid State Chemistry 182, 1105-1108.

Ludwig, K.R. and Cooper, J.A., 1984. Geochronology of Precambrian granites and associated U-Ti-Th mineralization, northern Olary province South Australia. Contributions to Mineralogy and Petrology, 86, 298-308.

Lumpkin, G.R., Leung, S.H.F., Colella, M., 2000. Composition, geochemical alteration, and alpha-decay damage effects of natural brannerites. In: Smith, R.W. and Shoesmith, D.W. (Eds) Scientific basis for nuclear waste management XXIII. Mat. Res. Symp. Proc., 608, 359-368.

Lumpkin, G.R., Leung, S.H.F. and Ferenczy, J., 2012. Chemistry, microstructure, and alpha decay damage of natural brannerite. Chemical Geology, 291, 55-68.

Merritt, R.C., 1971. The Extractive Metallurgy of Uranium. Colorado School of Mines Research Institute, Colorado. 576.

Macnaughton, S.J., Ring, R.J., Day, A., Collier, D.E. and Tan, L.K.P., 1999. Optimisation of the leach conditions for a copper/uranium ore. In: EPD Congress 1999. San Diego, California, The Minerals, Metals and Materials Society, 509-522.

McCready, A.J. and Parnell, E.J., 1998. A Phanerozoic analogue for Witwatersrand-type uranium mineralization: uranium-titanium-bitumen nodules in Devonian conglomerate/sandstone, Orkney, Scotland. Trans Inst. Min. Metal. B, 107, 89-97.

Muralikrishna, N., Mohanty, K.B. and Viswamohan, K., 1991. Extraction of uranium from refractory type of ores - a case study of brannerite from Ramsingpura, Sikar District, Rajasthan, India. Exploration and Research for Atomic Minerals, 4, 203-208.

Pabst, A., 1954. Brannerite from California, American Mineralogist, 39, 109-117.

Patchett, J.E. and Nuffield, E.W., 1960. Studies of radioactive compounds X- the synthesis and crystallography of brannerite. The Canadian Mineralogist, 6, 483-490.

Polito, P.A., Kyser, T.K. and Stanley, C., 2009. The Proterozoic, albitite-hosted, Valhalla uranium deposit, Queensland, Australia: a description of the alteration assemblage associated with uranium mineralisation in diamond drill hole V39. Mineralium Deposita, 44, 11-40.

Pouchou, J.L. and Pichoir, F., 1985. "PAP", Procedure for improved quantitative microanalysis, Microbeam Analysis Proc., Armstrong, J.T. (Ed.), San Francisco Press, pp. 104-106.

Pouchou, J.L. and Pichoir, F., 1991. Quantitative analysis of homogeneous or stratified microvolumes applying the model "PAP". In: Electron Probe Quantitation, Heinrich, K.F.J. and Newbury, D.E. (Eds), Plenum Press, New York, pp. 31-75.

Reeve, J.S., Cross, K.C., Smith, R.N., Oreskes, N., 1990. Olympic Dam copper–uranium–gold–silver deposit. In: Hughes, F.E. (Ed.), Geology of the Mineral Deposits of Australia and Papua New Guinea. Australasian Institute of Mining and Metallurgy, Melbourne, pp. 1009-1035.

Reynolds, L., 2000. Geology of the Olympic Dam Cu-U-Au-Ag-REE deposit.In: Porter, T.M. (Ed), Hydrothermal Iron Oxide Copper-Gold and Related Deposits: A Global Perspective, PGC Publishing, Adelaide, 1, pp. 93-104.

Roberts, D.E., Hudson, G.R.T., 1983. The Olympic Dam copper-uranium-gold deposit, Roxby Downs, South Australia., Economic Geology, 78(5), 799-822.

Ruzicka, V., 1989. Conceptual models for important types of uranium deposits and areas favourable for their occurrence in Canada. In: IAEA, Proc. Tech. Comm. Meet. Uranium Res. Geol. North America, IAEA Vienna, TECDOC-500, 49-80.

Skirrow, R.G., Bastrakov, E.N., Barovich, K., Fraser, G.L., Creaser, R.A., Fanning, C.M., Raymond, O.L., and Davidson, G.J., 2007. Timing of iron oxide Cu-Au-(U) hydrothermal activity and Nd isotope constraints on metal sources in the Gawler Craton, South Australia. Economic Geology, 102, 1441-1470.

Smith, D.K.Jr, 1984 Uranium mineralogy. In: deViv, B., Ippolito F., Capaldi, G. and Simpson, P.R. (Eds), Uranium Geochemistry, Mineralogy, Geology, Exploration and Resources. The Institution of Mining and Metallurgy, London, pp. 43-88.

Szymanski, J.T. and Scott, J.D., 1982. A crystal-structure refinement of synthetic brannerite, UTi_2O_6, and its bearing on rate of alkaline-carbonate leaching of brannerite in ore. The Canadian Mineralogist, 20, 271-279.

Tonkin, D.G., 1992. Previous investigation of the Crocker Well uranium prospects, EL 1748 Crocker Well, South Australia. Department of Primary Industries and Resources. Open File Envelope 8531.

Vance, E.R., Watson, J.N., Carter, M.L., Day, R.A., Lumpkin, G.R., Hart, K.P., Zhang, Y., McGlinn, P.J., Stewart, M.W.A. and Cassidy, D.J., 2000. Crystal chemistry, radiation effects and aqueous leaching of brannerite, UTi_2O_6. Ceramic Transactions, 107, 561-568.

Whittle, A.W.G., 1954. Petrology of the Crockers Well uranium deposit. In: Dickinson, S.B. et al. Uranium deposits in South Australia. South Australian Geological Survey Bulletin, 30, 79-83.

Wilson, N.C. & MacRae, C.M., 2005. An automated hybrid clustering technique applied to spectral data sets. Microscopy and Microanalysis, 11, Suppl. 2, 434CD.

Zhang, Y., Lumpkin, G.R., Li, H., Blackford, M.G., Colella, M., Carter, M.L. and Vance E.R., 2006. Recrystallisation of amorphous natural brannerite through annealing: the effect

of radiation damage on the chemical durability of brannerite. Journal of Nuclear Materials, 350, 293-300.

Chapter 4

Synthesis, characterisation, dissolution and electrochemical behaviour of synthetic brannerite (UTi_2O_6)

This chapter includes results on the synthesis and dissolution of synthetic brannerite (UTi_2O_6). Results on the influence of the start U : Ti ratio used to prepare synthetic brannerite on the purity of synthetic brannerite produced are presented along with results on the influence of the following parameters on synthetic brannerite dissolution: Temperature, [Fe(III)] and [H_2SO_4]. This chapter also includes studies on the dissolution of brannerite using an electrochemistry technique.

4.1. Introduction

The synthesis of synthetic brannerite has been of interest due to its potential as a storage material for radioactive waste generated from nuclear fuel and secondly due to the potential of this material for use in gaining an improved understanding of the dissolution of brannerite found in commercially important uranium ore bodies. As mentioned previously a greater understanding of the chemistry of brannerite leaching is important for the development of improved processes for the production of uranium for use in nuclear fuel.

As mentioned earlier (Chapter 1), there are many ways to synthesise synthetic brannerite (UTi_2O_6), from wet grinding to mechano-chemical methods. Synthesis of brannerite using the wet grinding method involves the following: stoichiometric oxide mixtures are cautiously mixed and calcined to 1100 °C for 5 hours in air; wet ground for 1 hour; andpressed into pellets under pressure and calcined at 1480 °C for 24 hours in air (Lu et al., 2006). The mechano-chemical method of synthesising brannerite involves the use of high purity uranium oxide and anatase (TiO_2) which is dry mixed, followed by ball-milling and pressed into a pellet and calcined in a mixture of CO (5 %) and CO_2 for 300 hours at a temperature of 1350 °C (Donaldson et al, 2005). The most common technique to synthesise UTi_2O_6 is using the alkoxide/nitrate route under low-oxygen conditions (Ringwood et al., 1988 and Szymanski and Scott, 1982). The alkoxide/nitrate route involves the following five reaction steps for the synthesis to take place, they include; preparation of an aqueous solution containing stoichiometric amounts of U and Ti, co-precipitating as U and Ti hydroxides, calcining the hydroxides to remove water, nitrate and alcohol, wet milling and drying and finally hot-pressing the milled product at 1260 °C for 2 hours under 21 MPa in graphite dies.

As mentioned previously in Chapter 1 the main reasons that brannerite has not been extensively exploited as a source of uranium is due to the uranium in this mineral generally has been found to be difficult to leach under mild conditions (such as those used to leach uraninite). The dissolution of the non-substituted form of brannerite, UTi_2O_6, has been proposed by Gogoleva to occur via reactions 1 and 2 in acidic media containing ferric ion (Gogoleva, 2012).

$$UTi_2O_6 + Fe_2(SO_4)_3 = 2FeSO_4 + UO_2SO_4 + 2TiO_2 \quad \text{(Equation 4.1)}$$

$$TiO_2 + H_2SO_4 = TiOSO_4 + H_2O \quad \text{(Equation 4.2)}$$

Thomas and Zhang have also proposed a reaction sequence for brannerite dissolution (reactions 3 and 4) that involves the oxidation of U^{4+} to U^{6+} on the brannerite surface followed by a second reaction that involves surface complexation of the U^{6+} from the lattice (Thomas and Zhang, 2003).

$$S - U^{4+}O_2 + \frac{1}{2}O_2 \rightarrow S - U^{5+}O_3 \quad \text{(Equation 4.3)}$$

$$S - U^{5+}O_3 + nL \rightarrow "UL_n"_{(aq)} + S - U^{4+}O_2 \quad \text{(Equation 4.4)}$$

Where '*S*' represents the surface of the brannerite, '*L*' represents a single complexing / coordinating species such as H^+, '*n*' represents the reaction order and "UL_n" represents all uranium solution species that are unknown.

As previously mentioned in *1.5.2*, there have been several studies conducted on the rate and / or extent of dissolution of both natural and synthetic brannerites over a range of conditions using various processes. Muralikrishna et al (1991) used a combination of

gravity concentration and wet high intensity magnetic separation to obtain 93% uranium extraction from a natural brannerite containing ore from Ramsingpura, India, under the following conditions: 1224 kg H_2SO_4 / t, 80 °C, 6 hours (Muralikrishna et al., 1991). They concluded that concentrated acid leaching is required to extract uranium from the pre-concentrate. Ifll et al determined that natural brannerite ($(U_{0.629}Th_{0.039}Ca_{0.20})(Ti_{2.199}Fe_{0.13})O_{69}$) from the New Quirke and Panel mines at Elliot Lake, Ontario, was not readily leachable in sulphuric or hydrochloric acid solutions under the following conditions: 75 g/L H_2SO_4, 5 g/L $NaClO_3$, 4 g/L Fe^{3+} as $Fe_2(SO_4)_3$, 60 °C, 8 hours. Ifill et al (1996) reported that the resistance of brannerite to leaching was not improved by textural and morphological variations nor by crystallite size (Ifill et al., 1996). Studies by Macnaughton et al (1999) showed that natural brannerite ($U(Ti, Fe)_2O_6$) from the Olympic Dam deposit in South Australia was found to be entirely unaffected by leaching under the conditions used (20 g/L H_2SO_4, 55 °C, 1 g/L of Fe (Fe^{2+}:Fe^{3+} = 1:1, 12 hours) (Macnaughton et al., 1999)), where no visible effects on either morphology or composition were observed. Lottering et al investigated natural brannerite dissolution from Vaal river ore bodies from South Africa (bulk mineralogy of brannerite was found to be $(U, Th, Ca)(Ti, Fe)_2O_6$) and found that under the conditions studied (temperature of 40 °C, 50 °C and 60 °C, 36.5 % Fe as a solid oxidant, 647 g/L H_2SO_4). Lottering et al reported that since the total uranium dissolution obtained (90 %) could not be accounted for by uraninite alone (composition of ore was Uraninite 85 %, Brannerite 12 %) that some of the brannerite must have dissolved (Lottering et al., 2008). Gogoleva et al, 2012 also found that natural brannerite (from a uranium deposit at Jakutia in Russia) dissolution rates were significantly influenced by temperature and acid concentration under the conditions studied (10-200 g/L H_2SO_4, 0.0025-0.010 M Fe^{3+} as $Fe_2(SO_4)_3$ and 70 °C for 8 hours).

The majority of studies that have been published in the open literature on the dissolution of synthetic brannerites have been focussed on determination of the stability of this mineral when used as a storage material for radioactive waste (where it is commonly referred to as synroc) (Zhang et al., 2001). The conditions used in these studies (simulated environmental conditions) are however significantly different to those used in uranium minerals processing. Shatalov et al investigated the dissolution of synthetic brannerite under conditions relevant to minerals processing. They reported that synthetic brannerite can be completely dissolved in solution containing 10-15 g/L H_2SO_4 at 140 ^oC in an oxidative autoclave leaching process (Shatalov et al., 2007).

Although there have been several studies that have reported on the dissolution of brannerite published in the literature there have been no detailed studies conducted on the dissolution of this mineral under conditions similar to those used in uranium minerals processing. There is also very little information on the mechanism of dissolution of this mineral under these conditions.

As mentioned in Chapter 1, there have been no specific studies to investigating the electrochemical behaviour of brannerite. As previously discussed in section 1.4.2.3 in Chapter 1, studies on minerals such as chalcopyrite in carbon paste electrodes have been shown it to be a reliable way to observe the leaching behaviour, particularly in regards to the effects of electrolyte and temperature on dissolution processes surface passivation, and the study of possible leaching mechanisms. The use of carbon paste electrodes (CPE) to measure minerals by electrochemically means have been previously applied predominantly to sulphide minerals. Studies included; similar conditions under which industrial leaching of sulphide minerals had taken place (Cruz et al., 2005), and for chalcopyrite to determine

the differences in the kinetics of the leaching process in different acidic media (Lazaro et al., 1995). The electrochemical activity of galena in CPE was studied and is directly proportional to the amount of galena present at the electrode surface and therefore minerals in powder form and flotation concentrates can be used directly as electrode material, which implies the optimisation of individual leaching processes (Ahlbery and Asbjornsson, 1993). Studies of voltammetric in carbon paste are thus able to give a preliminary screen for the conditions under which a mineral will effectively leach, and enable convenient iteration to leaching parameters that are likely to be effective in a metallurgical process.

The main aim of the research presented in this chapter were (1) To synthesise and characterise UTi_2O_6 that has as little impurities such as rutile (TiO_2) and uraninite (UO_2); (2) To investigate the rate of dissolution of synthetic brannerite over a range of conditions including conditions similar to those used in tank based leaching of uranium minerals. The conditions investigated included temperature, [Fe(III)] and [H_2SO_4], (3) To investigate the mechanism of brannerite dissolution and (4) To investigate and probe the electrochemical behaviour of synthetic brannerite using a carbon paste electrode, under a range of varying [H_2SO_4] solutions and at differing temperatures which were relevant to commercial leaching

4.2. Materials and Methods

4.2.1. Materials

Uranyl acetate ($UO_2(CH_3COO)_2.2H_2O$) (97.5 %) and titanyl sulphate dihydrate ($TiOSO_4.2H_2O$) (97 %) were used as received. Sulphuric acid (H_2SO_4) (Aldrich Chemical), iron sulphate ($Fe_2(SO_4)_3$) (Aldrich Chemical), nitric acid (HNO_3) (70 % AR grade) (Merck Led) and 1000 ppm uranium ICP-MS standard (AccuStandard). Carbon Paste (CP) was used as received from Bioanalytical Systems (West Lafayette, USA). Milli-Q water (H_2O) (18 MΩ cm) was used for material synthesis, dissolution and electrochemical experiments.

4.2.2. Methods

The details of the methods used to conduct the research presented in this chapter for characterisation studies (XRD, SEM/EDX Mapping, XPS and ICP-MS analysis) and dissolution test procedures are given in Chapter 2.

4.2.2.1. Electrochemical methods

To prepare the working formula, a 1:1 ratio of Carbon Paste: Synthetic Brannerite (by weight) was freshly prepared by grinding in a mortar and pestle, to obtain a homogeneous paste. This paste was placed in a working electrode with a diameter of approximately 0.3 cm, levelled with a spatula and polished on low roughness paper to obtain a flat, reproducible surface. Based on amounts of brannerite used, and SEM mapping studies of carbon paste/synthetic brannerite surfaces after preparation, the estimated area of exposed brannerite in all voltammetric and scanning experiments were 0.7 cm^2. All experiments were undertaken under a nitrogen atmosphere in a 100 mL temperature controlled glass reactor with a Pt wire as a counter electrode, an Ag/Ag/Cl reference electrode held at

ambient (220 °C) temperature by separation from the reaction vessel with a salt bridge, and a compressed and polished Carbon Paste-brannerite mixture as the working electrode. The reactor was maintained at the desired temperature with a circulating hot water bath. Electrochemical experiments were undertaken with a CH Instruments CH920D potentiostat. Solutions of varying concentrations of H_2SO_4 were prepared with Milli-Q water (H_2O) (18 MΩ cm). For potential scanning experiments in H_2SO_4 the Carbon Paste-brannerite working electrode was initially rested in the electrolyte solution for 10 min before scanning as practice showed that this resulted in the most reproducible results.

4.3. Results and Discussion

4.3.1 Synthesis and Characterisation of Synthetic Brannerite

Synthetic brannerite (UTi_2O_6) was prepared using a method similar to that reported by Hussein et al (2008). This method involved the following: Oxalic acid (12.607 g in 100 mL), uranyl acetate (0.0557 g) and titanyl sulphate dihydrate (0.1345 g) were added to Milli-Q water (50 mL) and the resulting mixture was agitated until clear to confirm dissolution of all components; the resulting solution was then heated (200 °C) to dryness and the solids collected; the solids obtained were then calcined at 600 °C for 5 hours in Ar/H_2 (95 %/ 5 %) and then ground with a mortar and pestle before being calcined in Ar/H_2 at 1200 °C for 96 hours.

An XRD pattern of synthetic brannerite prepared using the aforementioned quantities of oxalic acid, uranyl acetate and titanyl sulphate dihydrate is presented in Figure 4.1. The pattern displays all of the diffraction lines associated with the mineral brannerite. In addition a low intensity diffraction line not due to brannerite is present at ~ 28.5 °. This

diffraction line is most likely due to the presence of uraninite in the prepared material. The intensity of this line which is the main diffraction line for uraninite is low however compared to those obtained for brannerite, and hence indicative of the sample containing only a low amount of uraninite. Based on the results presented in Figure 4.1 it was decided to investigate the influence of the U : Ti ratio to determine the purity of synthesis UTi_2O_6.

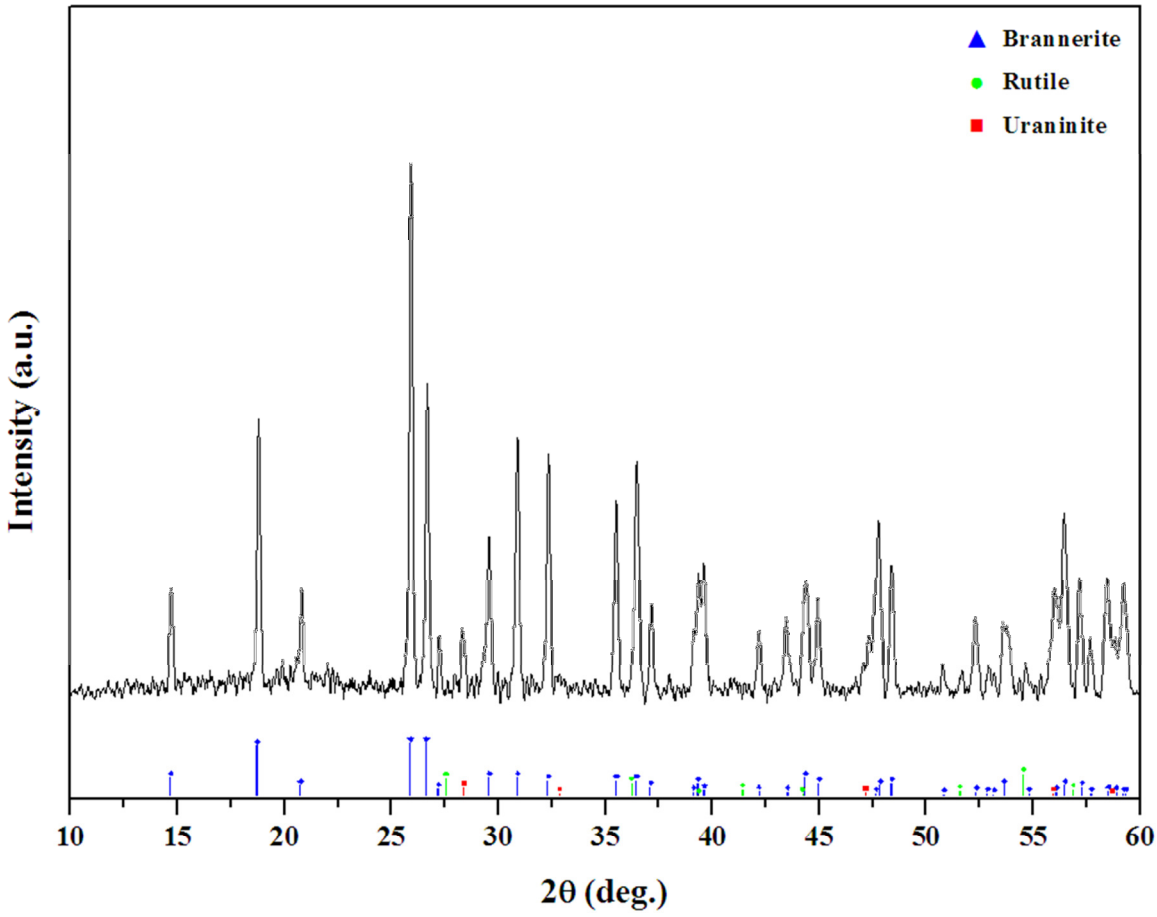

Figure 4.1: XRD pattern of prepared brannerite (▲ brannerite, ● rutile and ■ uraninite patterns).

4.3.1.1. Investigations on the influence U : Ti ratios on preparation of synthetic brannerite

The influence of the initial U:Ti ratio on the purity of synthetic brannerite produced using the method discussed in the previous section was investigated. Six synthesis experiments were conducted with varying Ti molar concentrations, (Table 4.1) while the concentration of U was kept constant. The XRD patterns of the materials prepared using the varying U:Ti ratios are shown in Figure 4.2. All materials clearly contained brannerite based on the XRD results obtained. The U:Ti ratio used however did influence the extent of uraninite and rutile impurity (based on the intensity of the diffraction lines observed for these compounds in prepared brannerites). If there were less than 5.23 mols of Ti in the system, the formation of uraninite (ICDD 01-075-0421) is prominent. If there were more than 5.23 of Ti in the system, the formation of uraninite (ICDD 01-075-0421) and rutile (001-1292) is observed. It was seen that the composition of experiment A is the optimum Ti/U ratio to synthesise brannerite.

Table 4.1: Varying Ratios of U vs. Ti for the synthesis of undoped brannerite.

Experiment	Uranium (mols)	Titanium (mols)	U : Ti Molar Ratio
A	0.525	2.745	1 : 5.23
B	0.525	2.725	1 : 5.19
C	0.525	2.735	1 : 5.21
D	0.525	2.752	1 : 5.24
E	0.525	2.755	1 : 5.25
F	0.525	2.900	1 : 5.52

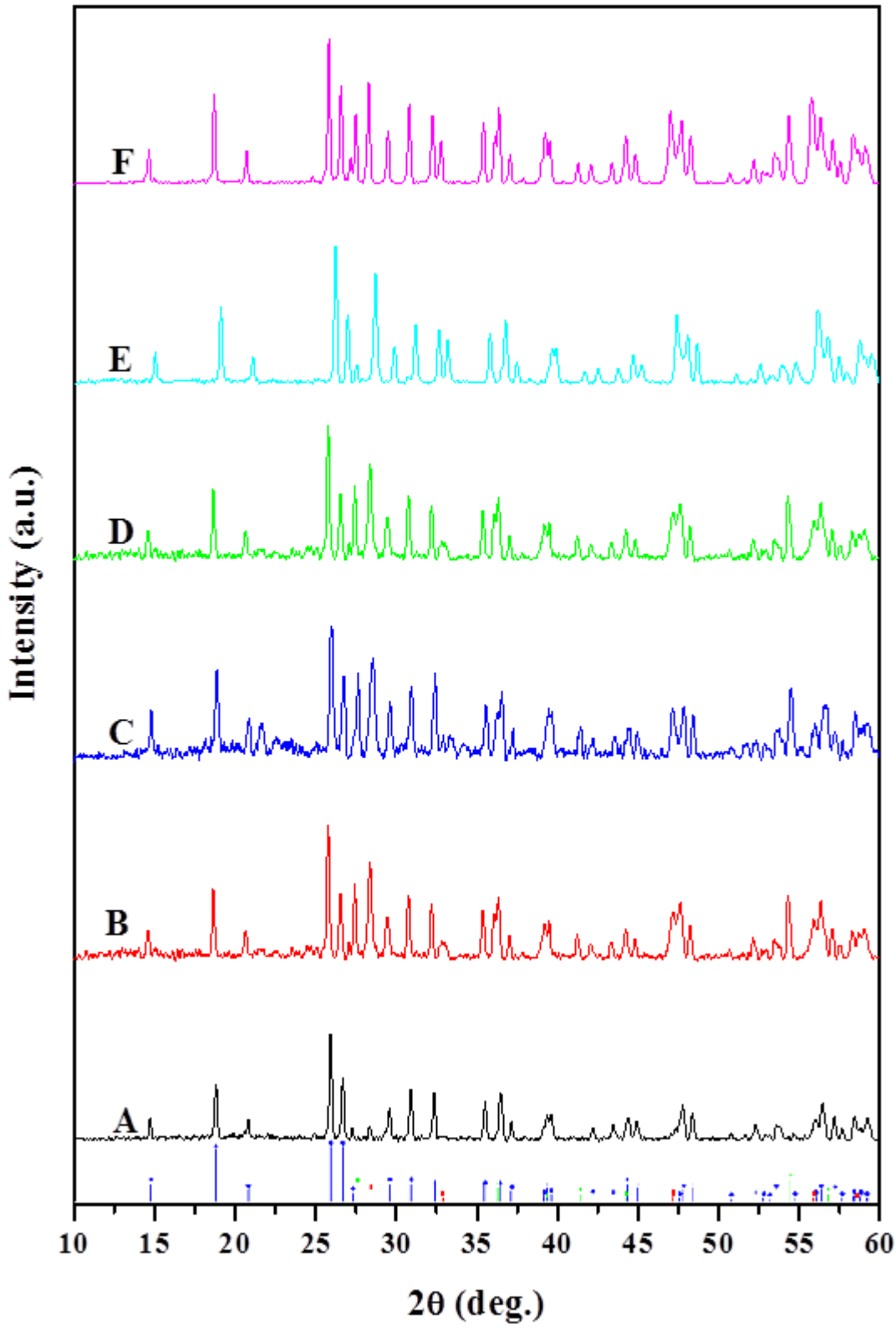

Figure 4.2: XRD patterns of products obtained using differing ratios of U:Ti to synthesise undoped brannerite (♦ brannerite, ▲ rutile and ■ uraninite patterns).

4.3.1.2. SEM/EDX Mapping Analysis

SEM/EDX mapping analysis was used to investigate the homogeneity of the prepared brannerite and the degree of uraninite impurity. The results obtained from SEM / EDX mapping analyses are presented in Figure 4.3. Figure 4.3 shows the homogeneity of the synthesised brannerite, where no significant clusters of titanium or uranium can be observed. The lack of significant clusters of uranium in the mapping image indicated that the prepared brannerite contained only minor amounts of uraninite.

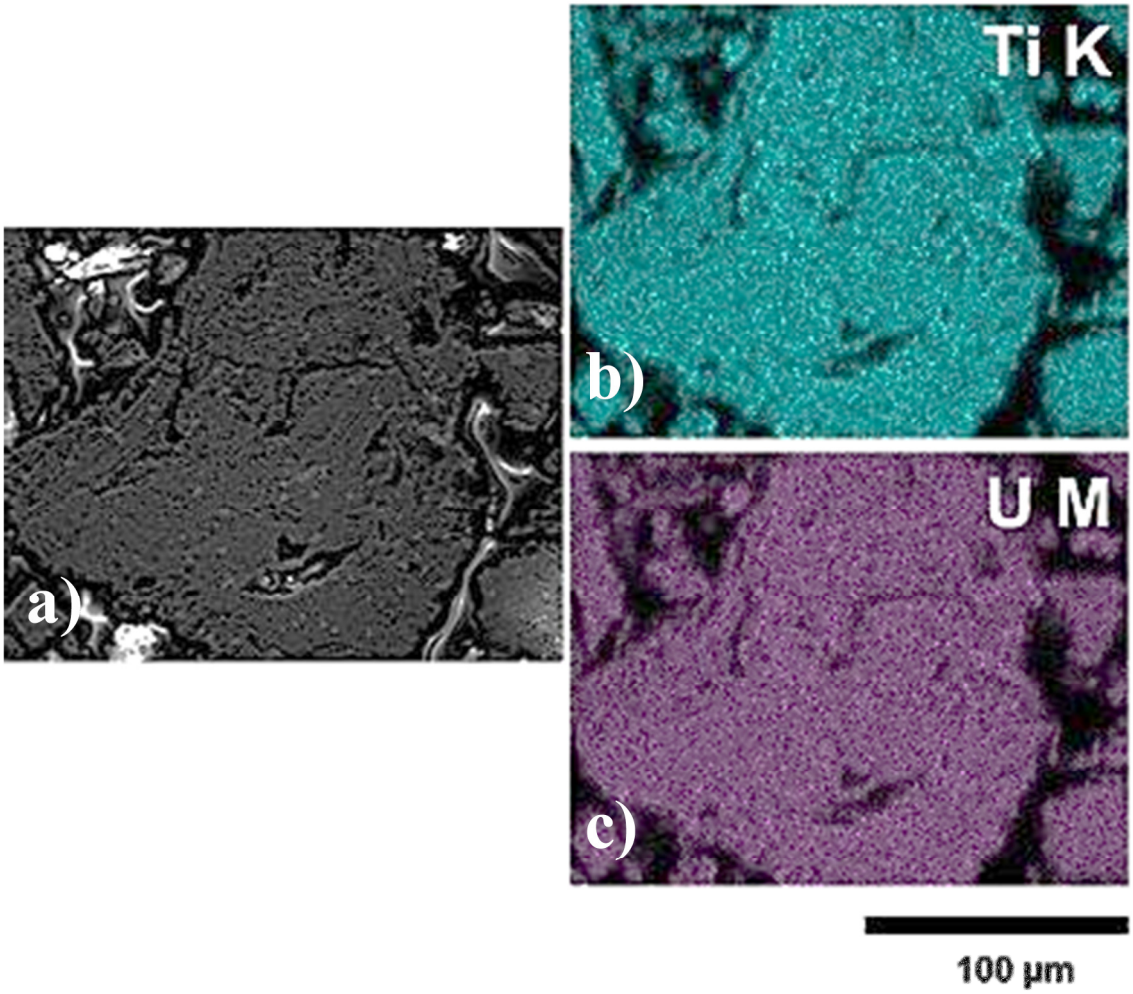

Figure 4.3: SEM/EDX mapping analysis of prepared synthetic brannerite a) SEM image of UTi_2O_6, b) and c) SEM/EDX maps showing the distribution of titanium (b) and uranium (c).

4.3.1.3. XPS Analysis

An XPS spectra obtained for a sample of the prepared synthetic brannerite is shown in Figure 4.4. The spectrum contains two main peaks U $4f_{7/2}$ (380.12 eV) and $4f_{5/2}$ (391.63 eV), around 10.78 eV apart due to the spin-orbit splitting, as well as their corresponding satellite peaks (marked sat $4f_{7/2}$ and $4f_{5/2}$). The two main peaks at 380.12 and 381.68 eV are due to U^{4+} and U^{6+}, respectively. The main satellite peak for U^{4+} was observed at 7.15 eV from the U^{4+} $4f_{7/2}$ peak and U^{6+} was located 6.88 and 7.9 eV above the U^{6+} $4f_{5/2}$ peak. The presence of U^{6+} at the surface, which based on the intensity of the peaks obtained is less than the amount of U^{4+} present, is most likely due to oxidation of surface U^{4+} from exposure of the sample to air. Oxidation of surface U^{4+} has been previously reported to occur in synthetic brannerite (Colella et al., 2005). Based on the lack of any pattern for a U^{6+} bearing compound in the XRD pattern obtained the total amount of U^{6+} present in the prepared synthetic brannerite was most likely low and most likely restricted to the surface of the sample.

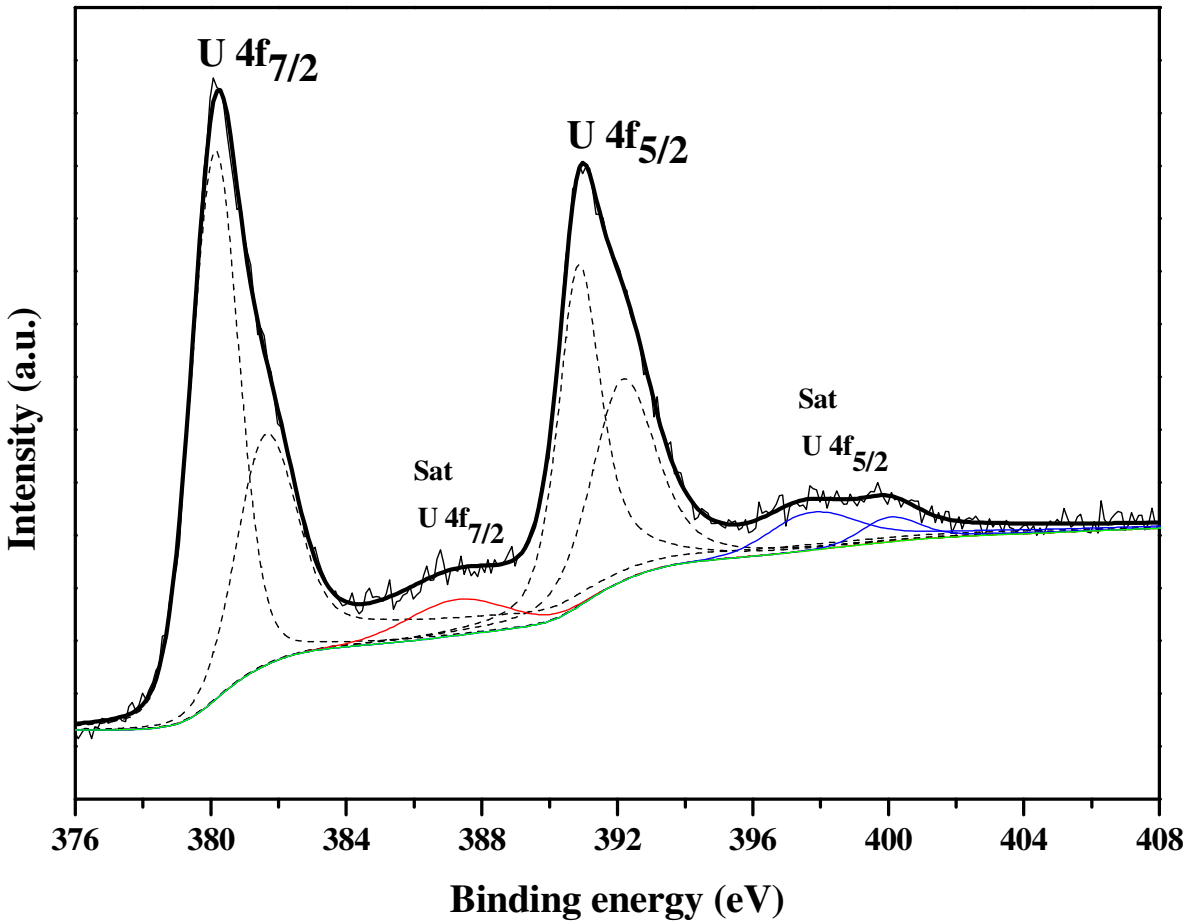

Figure 4.4: XPS U 4f spectra of synthetic UTi_2O_6 showing curve fitting using Gaussian/Lorentzian peaks. Dashed lines are shown for the fitted peaks, solid black lines are shown for the satellite peaks and the thick black line represents the envelope of the fit. All energies are shifted by 0.71 eV as their calibration was based on fixing the C 1s peak at 285 eV.

4.3.2. Dissolution Studies using a standard reaction vessel

The influence of temperature, [Fe(III)] and [H_2SO_4] on synthetic brannerite dissolution was investigated. These studies ecompassed testing under some conditions very similar to those used in large scale tank based uranium minerals leaching processes.

4.3.2.1. Synthetic brannerite dissolution under conditions similar to those used in large scale tank based uranium minerals leaching processes

Four dissolution experiments were conducted to investigate the dissolution of synthetic brannerite under temperature and [H_2SO_4] conditions similar to those used in large scale tank based leaching of uranium minerals (T ~ 50 °C, [H_2SO_4] ~ 15 g/L (Macnaughton et al., 1999). The influence of [Fe(III)] under the aforementioned conditions was also investigated. The conditions used in these tests and the results obtained are given in Table 4.2 and Figure 4.5 respectively. From the results presented in Figure 4.5 it can be seen that only a very small amount of dissolution of synthetic brannerite occurred (as a percentage of the initial slurry concentration), under the conditions used, within 6 hours. Increasing [Fe(III)] clearly had no influence on brannerite dissolution under the conditions used.

Table 4.2: Conditions for tests conducted on influence of [Fe(III)].

Test condition	Value
Initial brannerite slurry concentration	100 mg/L as U
Temperature	50 °C
[H_2SO_4]	15 g/L
[$Fe_2(SO_4)_3$]	3, 6, 9 and 12 g/L (as [Fe(III)])
Solution ORP	650-700 mV

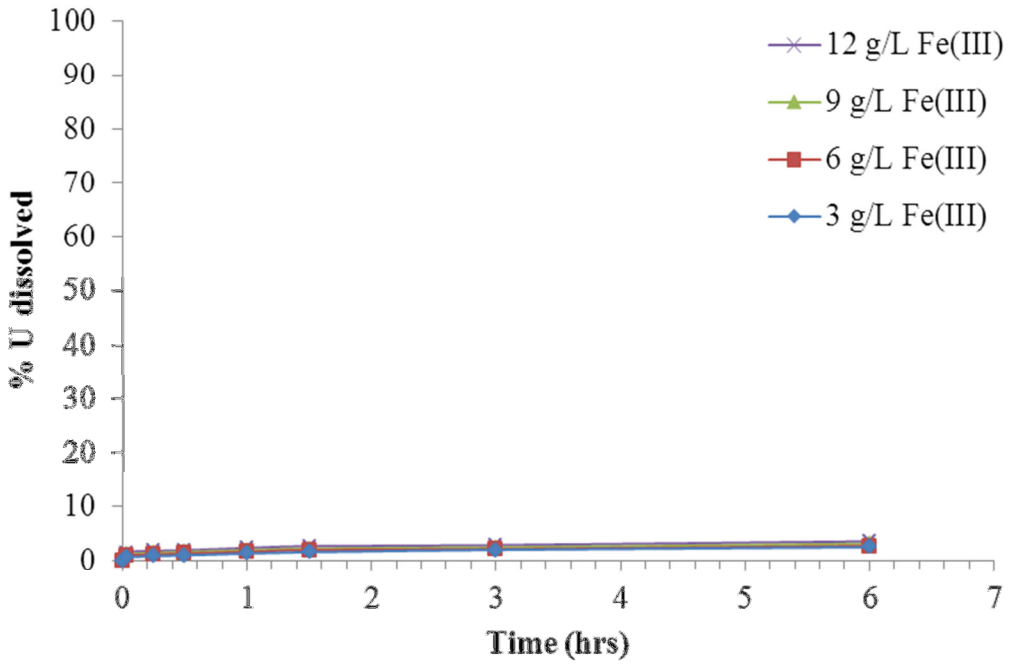

Figure 4.5: % Uranium (brannerite) dissolved as a function of time for solutions containing various [Fe(III)]. Refer to Table 1 for reaction conditions.

4.3.2.2 Effect of temperature

The effect of temperature on the dissolution of synthetic brannerite was investigated over the temperature range 50 – 95 °C. Other conditions used in these tests are given in Table 4.3. The results showed that an increase in temperature from 50 °C to 95 °C increased the dissolution of UTi_2O_6 in 1 hour from ~ 1 % to ~ 8 %. At 95 °C, ~ 16 % uranium was dissolved from UTi_2O_6 after 6 hours (Figure 4.6).

Table 4.3: Conditions for tests conducted on influence of temperature.

Test condition	Value
Initial brannerite slurry concentration	100 mg/L as U
Temperature	50, 65, 80, 95 °C
$[H_2SO_4]$	15 g/L
$[Fe_2(SO_4)_3]$	3 g/L (as [Fe(III)])
Solution ORP	600-700 mV

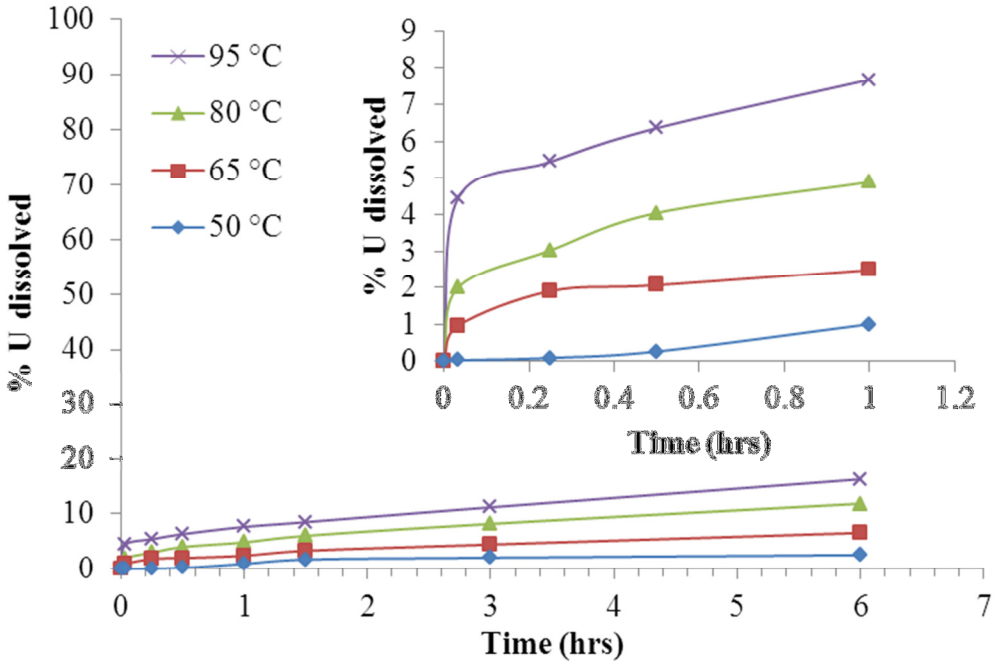

Figure 4.6: % Uranium dissolved as a function of time at various temperatures. Refer to Table 4.2 for test conditions.

The brannerite dissolution / uranium leaching from brannerite kinetics obtained from the tests conducted were analysed to investigate the order of the dissolution. The results of this analysis showed that the kinetics' of dissolution of uranium from synthetic brannerite were most closely fitted by first order kinetics under the conditions studied (Figure 4.7). When synthetic brannerite initial rates are compared to synthetic uraninite studies (Ram, et al., 2011) the initial rate of synthetic uraninite is significantly lower than the observed synthetic brannerite rates.

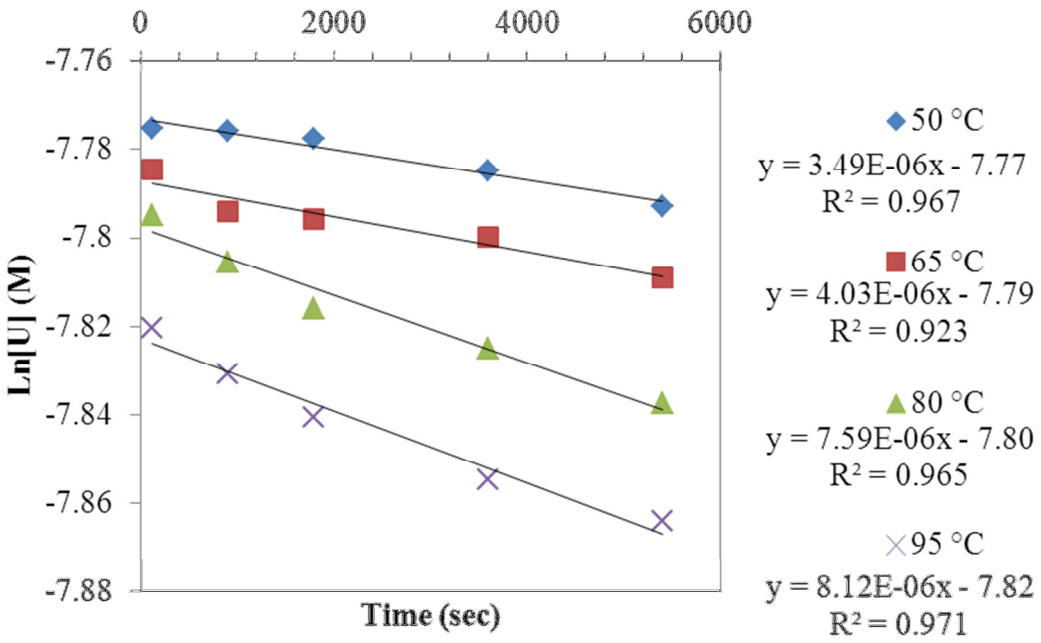

Figure 4.7: Plot of Ln [U] (M) versus time for dissolution of synthetic brannerite at various temperatures.

4.3.2.3. Effect of [H_2SO_4]

The effect of [H_2SO_4] on brannerite dissolution was investigated by conducting dissolution tests at five different [H_2SO_4]: 15 g/L, 50 g/L, 100 g/L, 150 g/L and 200 g/L. The other reaction conditions that were used in these tests are given in Table 4.4. From the results presented in Figure 4.8 it can be seen that synthetic brannerite dissolution increased with increasing [H_2SO_4] over the concentration range investigated (at a reaction temperature of 50 °C). The results show a ~ 8 % increase in uranium dissolution over the initial hour when 200 g/L H_2SO_4 was used compared to 15 g/L H_2SO_4. This increase in U dissolution rate was shown to continue for the duration of the 6 hour experiment with ~ 15 % more uranium liberated out of brannerite using 200 g/L H_2SO_4. This was shown to be a significant increase in uranium dissolution with respect to the 150 g/L of H_2SO_4 where by ~ 10 % of uranium was leached after 6 hours.

Table 4.4: Conditions for tests conducted on influence of [H_2SO_4].

Test condition	Value
Initial brannerite slurry concentration	100 mg/L as U
Temperature	50 °C
[H_2SO_4]	15, 50, 100, 150 and 200 g/L
[$Fe_2(SO_4)_3$]	3 g/L (as [Fe(III)])
Solution ORP	600-700 mV

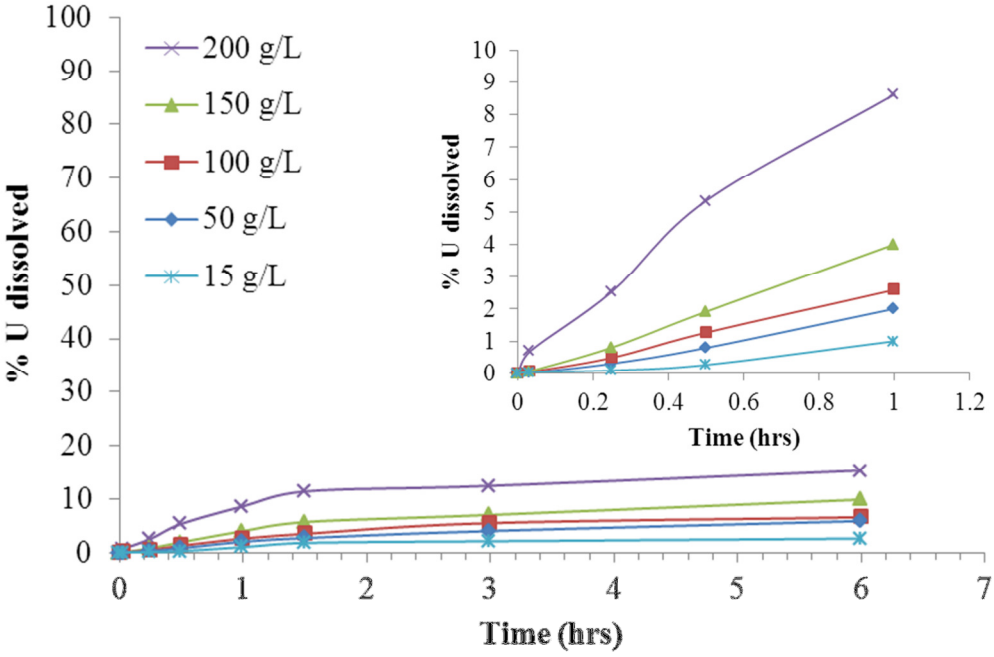

Figure 4.8: % Uranium dissolved as a function of time for solutions containing various [H_2SO_4]. For conditions refer to Table 4.3.

The brannerite dissolution / uranium leaching from brannerite kinetics for the tests conducted using varying [H_2SO_4] were analysed to investigate the order of the dissolution under these conditions. The results of this analysis showed that the kinetics' of dissolution of uranium from synthetic brannerite were most closely fitted by first order kinetics for over the range of [H_2SO_4] investigated (Figure 4.9).

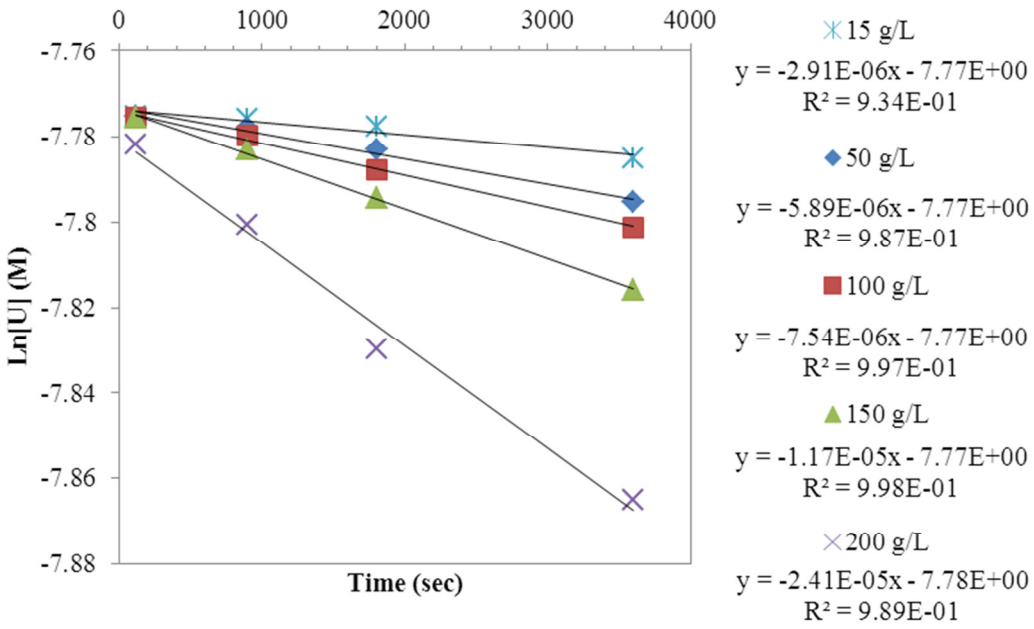

Figure 4.9: Plot of Ln [U] (M) versus time for dissolution of synthetic brannerite in different concentrations of [H_2SO_4].

4.3.2.4. Studies on the effect of [Fe(III)] and [H_2SO_4] using a high reaction temperature (95 °C).

The effect of [Fe(III)] on the dissolution of synthetic brannerite was investigated using a higher reaction temperature then that used for the initial tests reported in section 4.3.2.1, where [Fe(III)] was shown to have no significant effect on brannerite dissolution when a reaction temperature of 50 °C was used. The conditions used in the tests to investigate the effect of [Fe(III)] at a higher temperature are given in Table 4.5. As can be seen in Figure 4.10, the dissolution rate of uranium increased with increasing [Fe(III)] over the range investigated. Between 3 g/L and 6 g/L of Fe(III) a significant increase in the rate of dissolution can be seen in the first hour of leaching where ~ 7 % of uranium is released for the system containing 3 g/L Fe(III) compared to ~ 14% for the system containing 6 g/L Fe(III). It can also be seen that for the system containing 12 g/L Fe(III) ~ 35 % of the

uranium in the synthetic brannerite was dissolved after 6 hours. The results obtained on the influence of [Fe(III)] at 50 °C (Figure 4) and 95 °C clearly show that [Fe(III)] only influenced the dissolution of synthetic brannerite when a higher reaction temperature is used (for systems having an [H_2SO_4] of 15 g/L). Interestingly [H_2SO_4] however had a significant influence on the dissolution of brannerite at a lower reaction temperature (50 °C) (for systems containing 3 g/L [Fe(III)]) (Figure 4.8).

Table 4.5: Conditions for tests conducted on influence of [Fe(III)].

Test condition	Value
Initial brannerite slurry concentration	100 mg/L as U
Temperature	95 °C
[H_2SO_4]	15 g/L
[$Fe_2(SO_4)_3$]	3, 6, 9 and 12 g/L (as [Fe(III)])
Solution ORP	600-650 mV

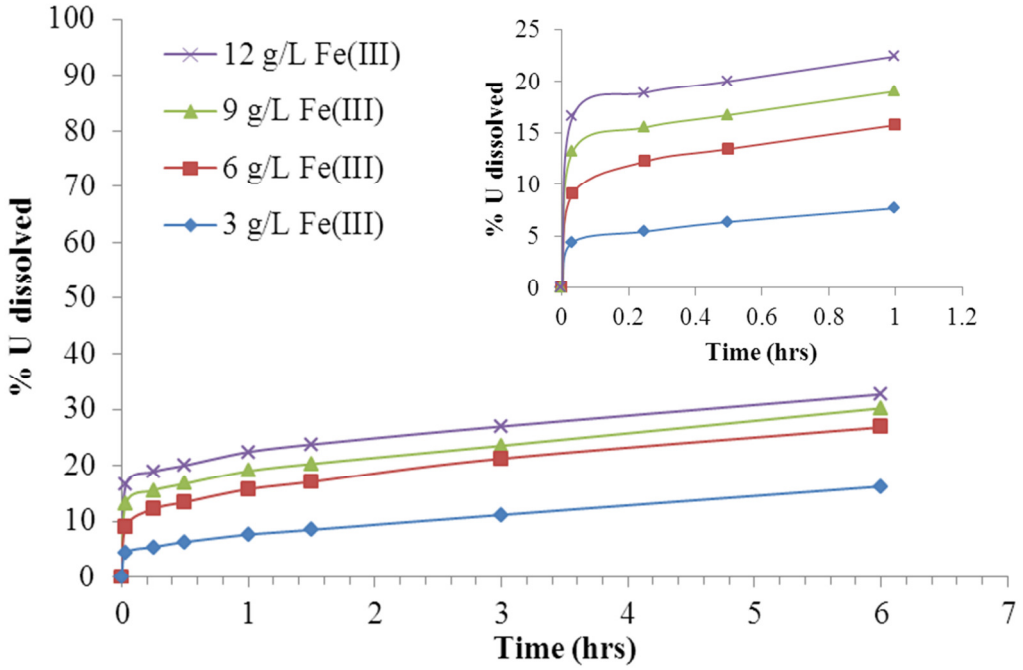

Figure 4.10: % U dissolved versus time for systems containing varying [Fe(III)] at 95 °C. For reaction conditions refer to Table 4.4.

The effect of [H_2SO_4] was also investigated at a higher reaction temperature (95 °C). The conditions used in these tests and the results obtained are given in Table 4.6 and Figure 4.11 respectively. From the results presented in Figure 4.11 it can be seen that increasing [H_2SO_4] led to significant increases in brannerite dissolution at the higher reaction temperature used (95 °C).

Table 4.6: Conditions for tests conducted on influence of [H_2SO_4].

Test condition	Value
Initial brannerite slurry concentration	100 mg/L as U
Temperature	95 °C
[H_2SO_4]	15, 50, 100, 150 and 200 g/L
[$Fe_2(SO_4)_3$]	3 g/L (as [Fe(III)])
Solution ORP	600-610 mV

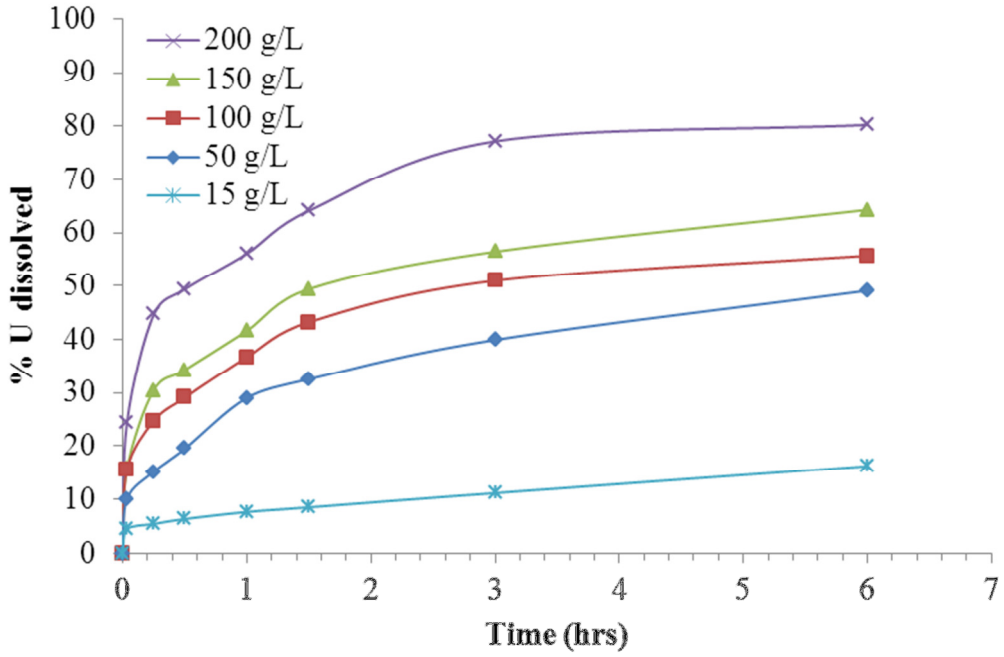

Figure 4.11: % U dissolved versus time for systems containing varying [H_2SO_4]. For reaction conditions refer to Table 4.6.

From the results obtained on the influence of [H_2SO_4] at 50 and 95 °C respectively (Figures 4.8 and 4.11) it can be seen that the influence of [H_2SO_4] on brannerite dissolution is clearly higher when a higher reaction temperature is used. For example at a reaction temperature of 50 °C increasing [H_2SO_4] from 15 g/L to 50 g/L led to an increase in dissolution from 2.59 % to 5.87 %, whereas at a temperature of 95 °C increasing [H_2SO_4] from 15 to 50 g/L led to an increase in dissolution from 16.23 % to 49.11 %. Furthermore at 95 °C, increasing the [H_2SO_4] from 15 to 200 g/L led to a significant increase in dissolution from 16.23 % to of 80.23 %. These results clearly show that temperature has an influence on the role(s) that H_2SO_4 has in the mechanism of synthetic brannerite dissolution.

Based on the results observed on the influence of [Fe(III)] and [H_2SO_4] on brannerite dissolution at 95 °C (Figures 4.10 and 4.11) it was decided to investigate the influence of [Fe(III)] under conditions of moderate [H_2SO_4] (50 g/L) at high temperature (95 °C). The results from the aforementioned tests are presented in Figure 4.12. As can be seen in Figure 4.12 the dissolution rate increased with increasing [Fe(III)] over the range tested (3 g/L to 12 g/L). It was observed that ~ 37 % of uranium dissolved from synthetic brannerite when 3 g/L of [Fe(III)] was present, whereas at 12 g/L Fe(III) ~ 65 % of the uranium dissolved. The dissolution of brannerite in the test containing 12 g/L Fe(III) also most likely reached equilibrium at a value of ~ 65% as there was no significant change in the extent of dissolution after 3 hours. The extent of dissolution that occurred after 6 hours in the test using 50 g/L H_2SO_4 and 12 g/L [Fe(III)] (~ 65%) was significantly lower than that obtained for the system containing 3 g/L Fe(III) and 200 g/L H_2SO_4 (Figure 4.11) and hence indicates that [H_2SO_4] has a significant influence on the equilibrium solubility of synthetic brannerite.

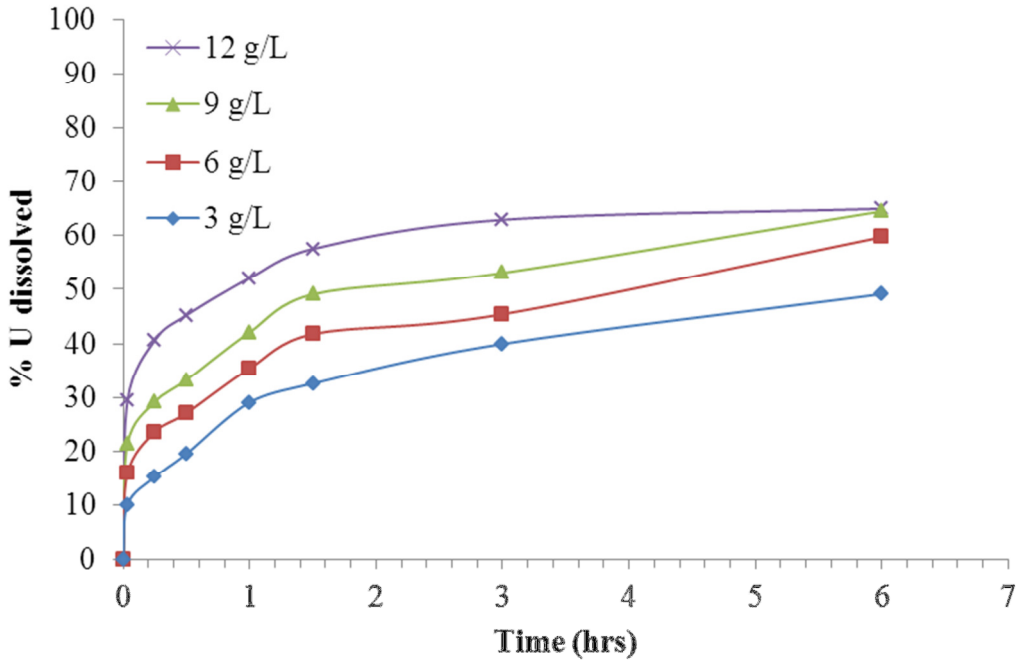

Figure 4.12: % Uranium (brannerite) dissolved as a function of time for solutions containing various [FeIII] at an [H_2SO_4] of 50 g/L and a temperature of 95 °C.

Comparison of the data obtained on the influence of [Fe(III)] at 15 and 50 g/L H_2SO_4, for a reaction temperature of 95 °C, showed that the influence of [Fe(III)] on the extent of brannerite dissolution after 6 hours for these systems containing differing [H_2SO_4] was very similar. Hence the role of Fe(III) in the dissolution of brannerite was not significantly impacted by [H_2SO_4] under the conditions investigated.

The influence of H_2SO_4 alone at 95 °C (in the absence of any Fe(III)) was investigated to determine if dissolution of brannerite could be achieved without any Fe(III) present (and hence to determine if the significant influences of [H_2SO_4] identified may have been due to a dissolution mechanism that did not involve Fe(III)). The results of this test, conducted using a [H_2SO_4] of 150 g/L, are shown in Figure 4.13. From the results presented in Figure 4.13 it is clear that no significant dissolution of brannerite occurred under these conditions.

Hence the significant influence of [H_2SO_4] on brannerite dissolution clearly relies on the presence of Fe(III). The influence of [H_2SO_4] on brannerite dissolution therefore is most likely due to one or more of the following:

- H_2SO_4 initiates dissolution of brannerite through reacting with surface functional groups which leads to the formation of surface species that can react with Fe(III) species (with this latter reaction resulting in subsequent uranium dissolution)
- H_2SO_4 influences the species of Fe(III) present, leading to the formation of species that react with brannerite surface functional groups leading to subsequent uranium dissolution

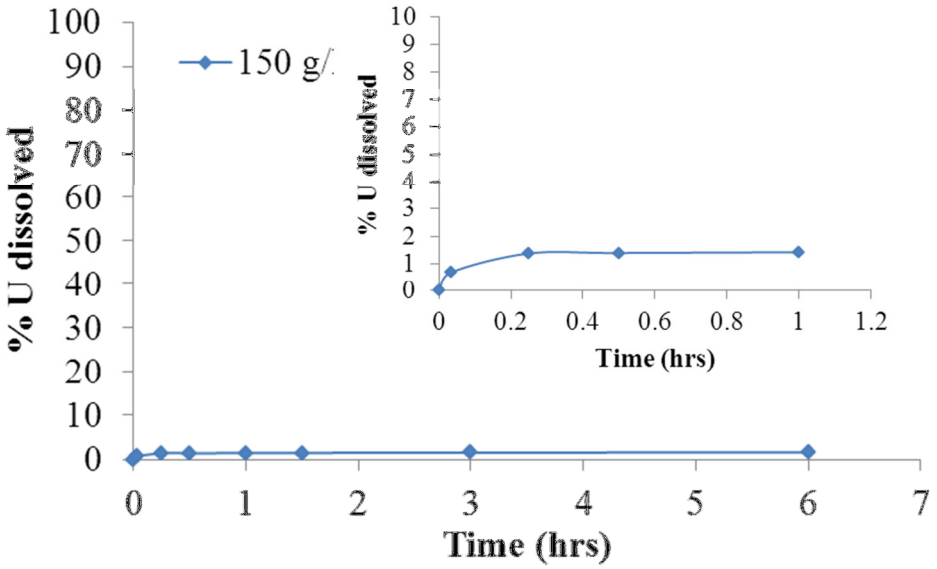

Figure 4.13: % Uranium (brannerite) dissolved as a function of time in a solution containing no [Fe(III)] at a temperature of 95 °C and [H_2SO_4] of 150 g/L.

In aqueous H_2SO_4 solutions Fe distributes as dissolved Fe(II) and Fe(III) species , as free ions (Fe^{3+}, Fe^{2+}) or complex compounds [$FeSO_4$, $FeSO_4^+$, $Fe(SO_4)^{2-}$] (Casas et al., 2005). The concentration of these species is strongly dependent on solution composition

and temperature (Figure 4.14). Previous results that have indicated Fe speciation influencing uranium mineral dissolution (uraninite) via an electron-transfer reaction have been published by Laxen (1971) (Laxen, 1971). Laxen (1971) reported that Fe^{3+} in the presence of SO_4^{2-} increases the rate of dissolution. An increase in rate is thought to be recognized as an increase in active ferric sulphate complexes and free hydroxyl complexes which either do or do not contain SO_4^{2-} species.

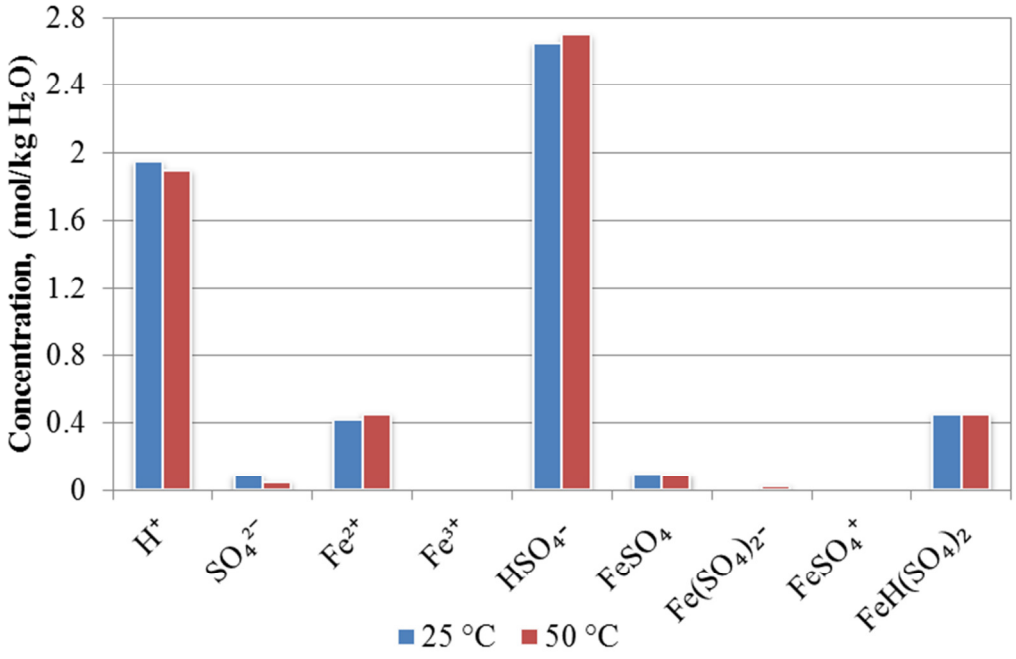

Figure 4.14: Calculated speciation at 25 and 50 °C for an aqueous solution containing: [H_2SO_4] = 2.22 m (200 g/L); [Fe(II)] = 0.543 m (27 g/L); [Fe(III)] = 0.437 m (23 g/L) (Casas et al., 2005).

4.3.2.5. Investigation of decrease in rate of synthetic brannerite dissolution

The decreases in rate of synthetic brannerite dissolution that were observed in a number of tests were investigated to determine if this was predominantly due to decreasing brannerite slurry concentration. This involved combining brannerite remaining from tests

that had been conducted under the following conditions ([Fe(III)] = 3 g/L, temperature = 95 °C, [H_2SO_4] = 100 and 150 g/L), t = 3 hours) with fresh brannerite (to give the same total intial brannerite slurry concentration as used in all prevous tests) and studying the overall rate of dissolution of the combined used and fresh brannerite. The results of these tests are shown in Figure 4.15. From the results presented in Figure 4.15 it is clear that the dissolution rate of the pre leached brannerite / fresh brannerite combinations were significantly lower than those obtained with fresh brannerite, and hence show that the decreases in brannerite dissolution rate observed in previous tests under the same test conditions were not predominantly due to the decreasing brannerite slurry concentrations that occur during testing, but due to a change in the rate of dissolution from the undissolved brannerite particles remaining in solution. The rate of dissolution of the brannerite particles present in solution could change (decrease) over time due to one or more of the following:

- Surface compositional changes / surface passivation
- Surface morphology changes (decrease in surface roughness / surface area)
- Change in particle size distribution (change in overall surface area)

Based on Ifill et al's finding discussed earlier that the resistance of brannerite to leaching is not improved by textural and morphological variations, nor by crystallite size, it was decided to investigate if there were any significant differences between the surfaces of the pre leached brannerite and fresh brannerite particles. This was done by conducting XPS analyses of the pre-leached brannerite particles (Figure 4.16) and comparing these results with those obtained for fresh brannerite particles. The results of these analyses showed that there were no significant differences in the ratio of surface U^{4+} to U^{6+} between the pre-leached brannerite particles and the fresh brannerite particles (Figure 4.4). Therefore the

significantly slower dissolution observed for the pre-leached brannerite particles was most likely not due to any changes in the uranium speciation. Semi quantitative data obtained using XPS on the composition of the surfaces of the pre-leached and fresh particles also showed no significant differences in surface composition between these. Hence based on the aforementioned data obtained the significantly lower dissolution rates observed for pre-leached particles was most likely due to changes in surface morphology and / or particle size. It is important to note however that the aforementioned XPS surface composition data was semi-quantitative and hence could not be used to determine subtle differences in surface composition that may have led to significant differences in dissolution from the surface.

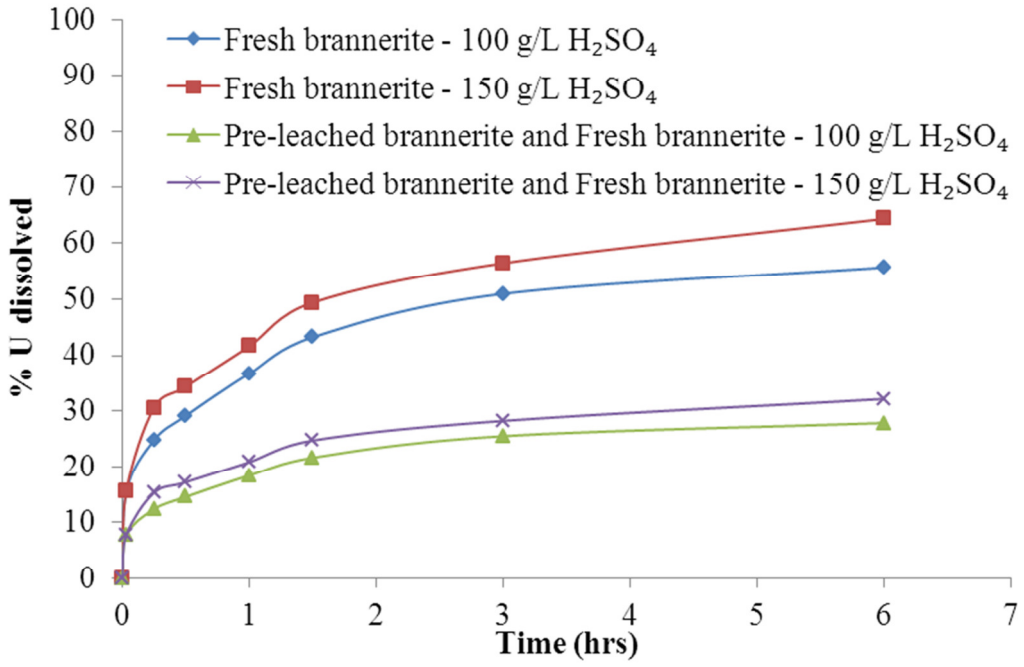

Figure 4.15: % Uranium (brannerite) dissolved as a function of time for solutions containing various [H_2SO_4] and at constant [Fe(III)] of 3 g/L and temperature of 95 °C. The amount of pre-leached brannerite and Fresh brannerite added for 100 g/L H_2SO_4 were 0.0458 g and 0.04442 g respectively. The total amount of pre-leached brannerite and fresh brannerite added for 150 g/L H_2SO_4 were 0.0476 g and 0.0427 g respectively.

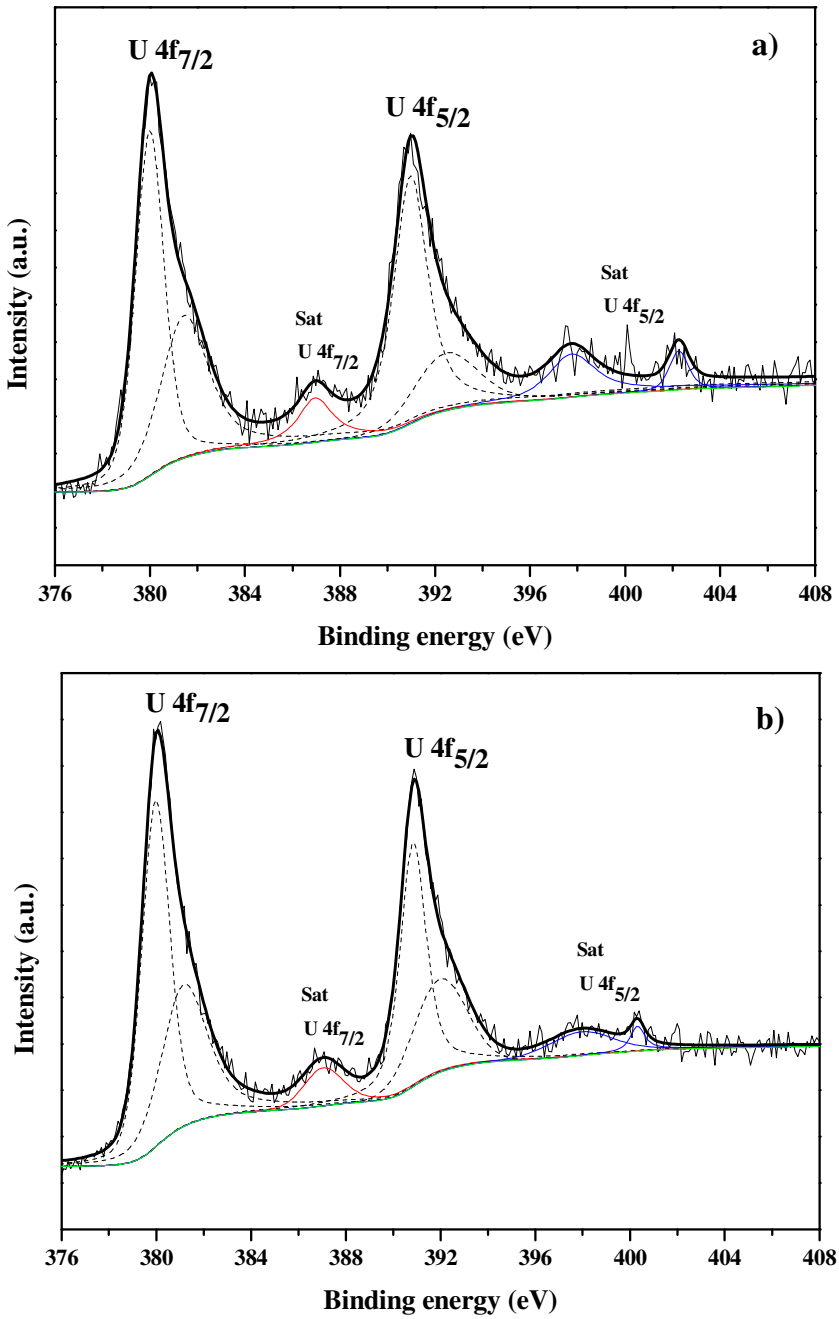

Figure 4.16: XPS U 4f spectra of a) Pre-leached brannerite and Fresh brannerite – 100 g/L H_2SO_4 and b) Pre-leached brannerite and Fresh brannerite – 150 g/L H_2SO_4 residue samples showing curve fitting using Gaussian/Lorentzian peaks. Dashed lines are shown for the fitted peaks, solid black lines are shown for the satellite peaks and the thick black line represents the envelope of the fit. All energies are shifted by 0.71 eV as their calibration was based on fixing the C 1s peak at 285 eV.

4.3.3. Dissolution studies using an electrochemical method

Electrochemical studies were used to determine if synthetic brannerite under high [H_2SO_4] conditions from previous experiments in section *4.3.2.3* could lead to understanding the mechanism of brannerite leaching under these conditions.

As discussed in *4.2.2.2*, the working formula of 1:1 ratio of Carbon Paste: Synthetic Brannerite (by weight) was freshly prepared by grinding in a mortar and pestle, to obtain a homogeneous paste. This paste was placed in a working electrode where upon it was analysed using SEM mapping studies to determine if the surface after preparation of the carbon paste/synthetic brannerite electrode was homogenous.

The results obtained from SEM / EDX mapping analyses are presented in Figure 4.17, showing the homogeneity of the synthetic brannerite in the CPE, where concentration of the titanium, uranium and carbon are well dispersed. This indicates that the crushed synthetic brannerite / carbon paste samples were homogeneously mixed, with adequate dispersion of the brannerite throughout the carbon paste mixture.

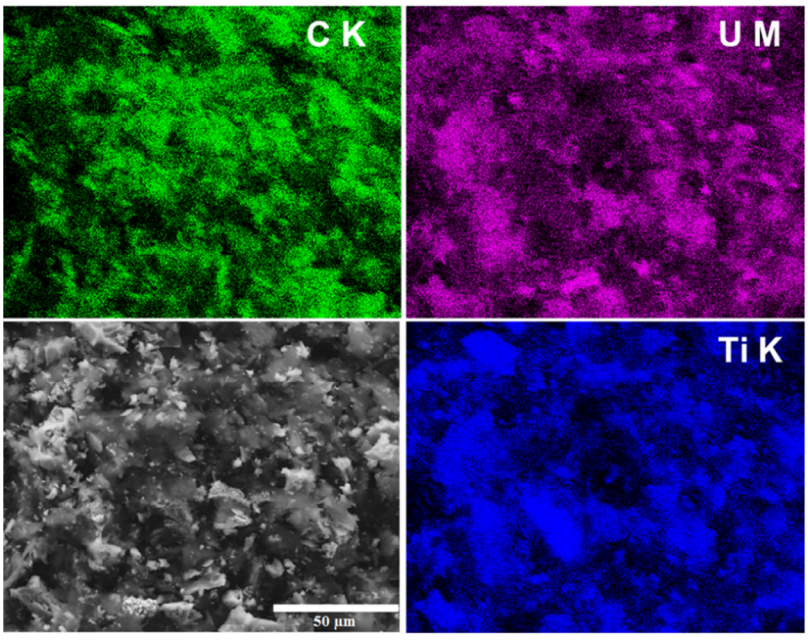

Figure 4.17: SEM/EDX mapping analysis of synthetic brannerite/CPE. Colour maps are based upon the Kα C, Mα U and Kα Ti line intensities.

4.3.3.1 Electrochemical Studies

Electrochemical experiments were conducted over a range of conditions to investigate the influence of temperature and sulphuric acid concentration on synthetic brannerite dissolution. These studies also were conducted under some conditions very similar to those used in uranium minerals leaching processes (large scale tank based procedures).

The following conditions were set in the electrochemical leaching tests of synthetic brannerite: constant temperature of 50 °C and differing concentrations of H_2SO_4 15, 50, 100 and 150 g/L. No Fe was added to the solutions as the main focus of these experiments was to apply a potential across the synthetic brannerite/CPE surface and determine the electrochemical behaviour of the sample.

Figure 4.18 shows a scan from the open circuit potential (OCP) to anodic potentials resulting in dissolution of the brannerite. Figure 4.18 shows that there are two distinct regions: 1) active- where the current rises quickly with respect to the potential and 2) passive- where the current flattens out with respect to the potential.

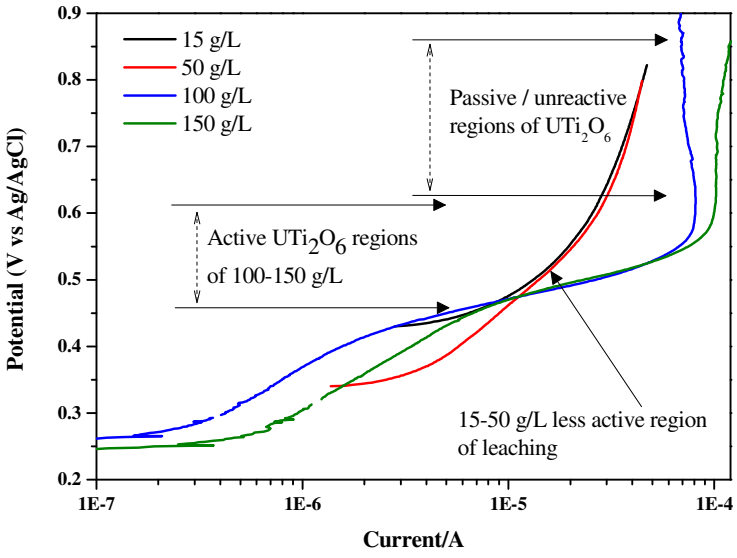

Figure 4.18: Open circuit potential in the anodic direction for four different [H_2SO_4] of 15, 50, 100 and 150 g/L at 50 °C of synthetic brannerite.

A clear observation between the different in behaviour seen for 15-50 g/L [H_2SO_4] and the 100-150 g/L [H_2SO], where 15-50 g/L shows modest reactivity on increasing the potential, current gains (which is due to dissolution) are modest. Compared to 100-150 g/L, where there is a very 'active' region, which is seen between potentials of 0.44-0.60 V. This gives way to an area where there is surface passivation, a decrease in current, and this is presumably due to blocking / coating the surface of the brannerite with the purpose of inhibiting dissolution. In the active regions, it can still be assume that passivation will occur, nonetheless the passive layer takes time to form, it is not instantaneous, and thus as scanning continues, the potential may takes a few hundred mV until the passive region has been reached.

It is therefore concluded that the ideal region for leaching brannerite would take place is between 0.4-0.6 V and similarly an ORP that places the potential of the brannerite in this region of activity. The potential of the brannerite in a leaching solution would be situated somewhere between the open circuit potential (where we start the scan), and the ORP of the leaching solution (600 mV).

4.3.3.1.1 Investigation of the residue of electrochemical leaching via SEM/EDX mapping analysis

Scanning electron microscopy and energy dispersive X-ray analysis were used to investigate further the leaching of synthetic brannerite/CPE sample. Figure 4.17 shows an SEM/EDX image of the synthetic brannerite/CPE pre leaching. Figure 4.20 shows an SEM/EDX image of post leaching at conditions of 15 g/L H_2SO_4 at 25 °C, after a series of voltammograms (Figure 4.19). The successive scans in this voltammogram show that the height of the anodic peak is successively decreased on repeat scans, indicating dissolution of the surface, and possible passivation. SEM/EDX mapping confirmed compositional

changes across the surface of the brannerite sample. Figure 4.21 illustrates this by determining a decrease in U post leaching by EDX analysis.

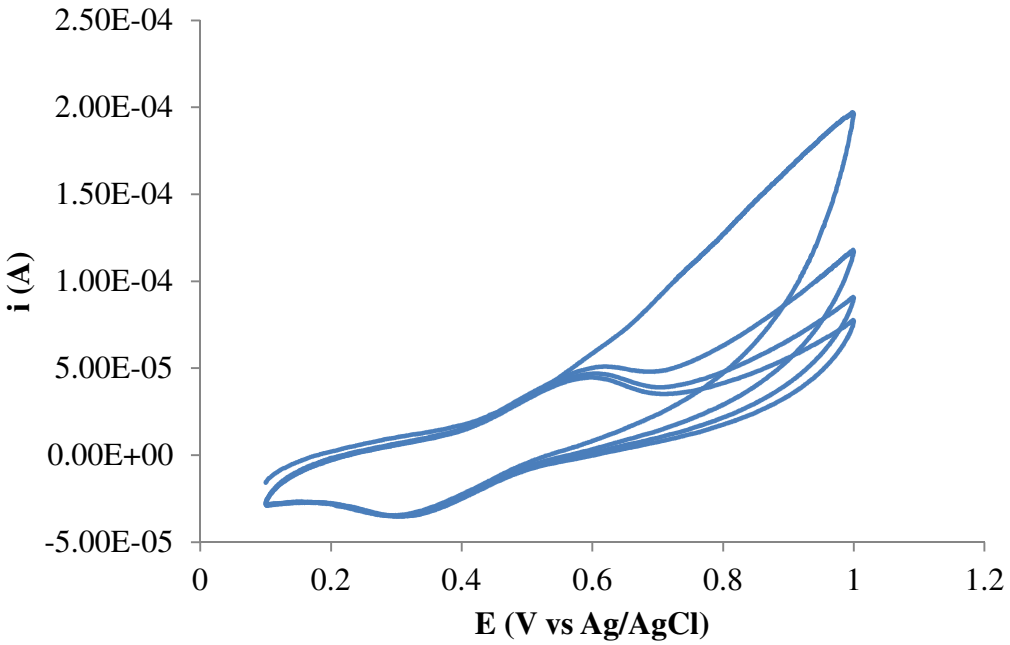

Figure 4.19: Cyclic voltammograms of synthetic brannerite/CPE, [H_2SO_4] = 15 g/L, temperature = 25 °C, scan rate = 0.05 V/s and segments = 8.

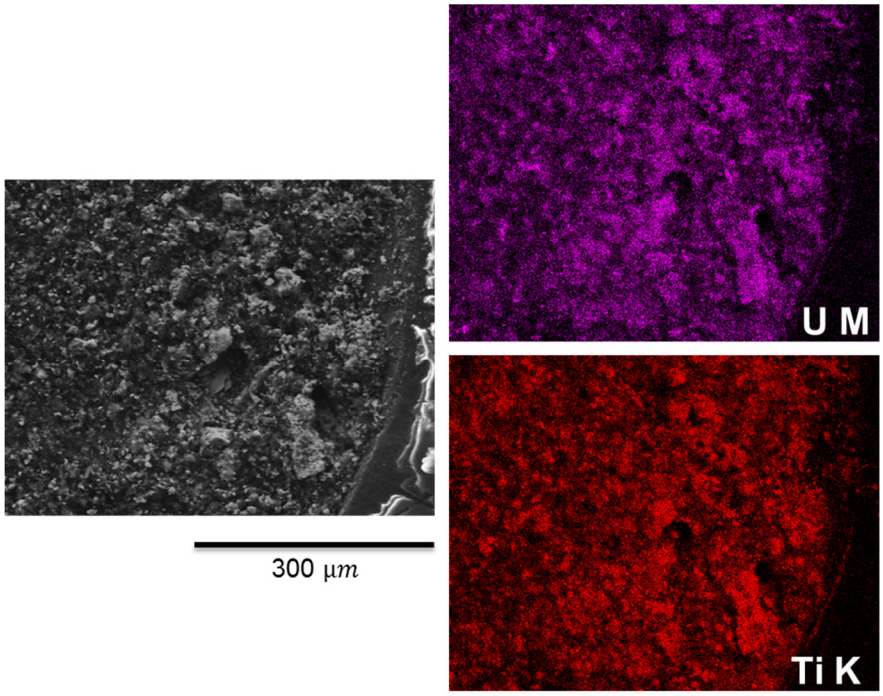

Figure 4.20: SEM/EDX mapping analysis of synthetic brannerite/CPE post leaching. Colour maps are based upon the Mα U and Kα Ti line intensities.

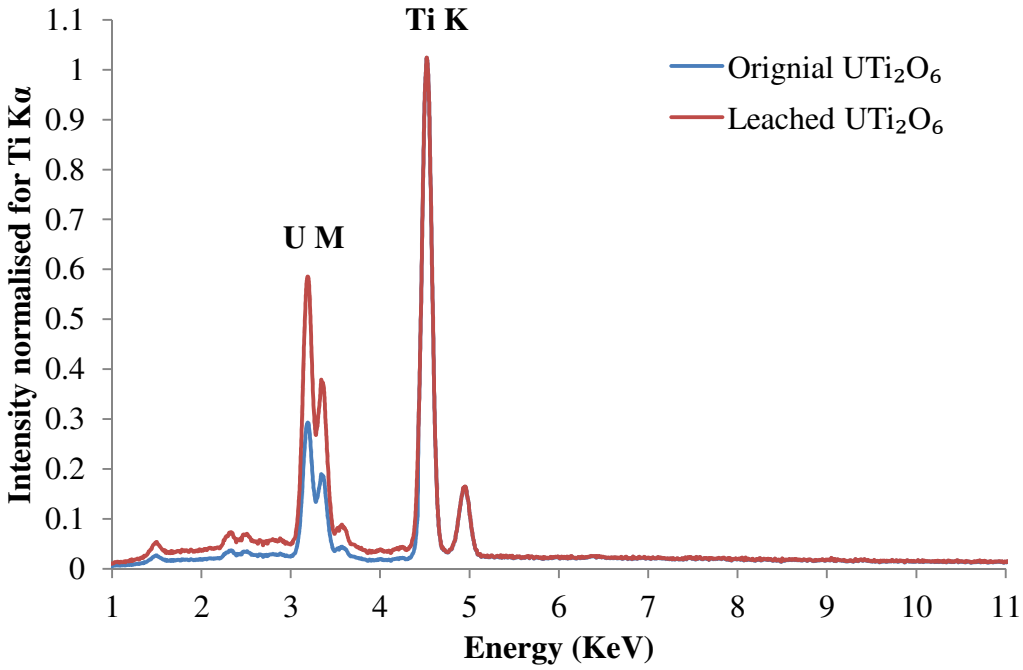

Figure 4.21: EDX analysis un-leaching of CPE-brannerite and leached CPE-brannerite ([H_2SO_4] = 15 g/L at 25 °C).

ICP-MS analysis of the solution was taken and analysed to determine the amount of U and Ti in solution. The ICP-MS results showed that amount of U in solution was 0.00478 % and Ti in solution was 0.00049 %. Analysis showed that U leached out of the brannerite structure 10 times more than Ti. Considering again equations (4.1) and (4.2) in section 4.1 of this chapter we can conclude that predominate reaction is the dissolution of U(IV) species, solubilised by the electrode potentials positive of approximately 0.4 Vs vs Ag/AgCl and also that due to the surface decrease in uranium concentration with respect to titanium concentration, thus indicating that a TiO_x passivation layer is responsible for this limited leaching of synthetic brannerite.

4.3.3.1.2 Activation Energies

Apparent activation energy values were determined by studying the oxidation of synthetic brannerite/CPE at varies temperatures (25 – 80 °C), which can be seen in Figure 4.22. Determination of activation energies will thus provide evidence to how much temperature affects dissolution in each region – and will be indicative of a possible mechanism.

The following CV shows that the rate of dissolution is dependent upon the temperature. A significant elevation of leaching is observed when temperature is increased from 25 to 50 °C. A further increase in leaching is also observed between 50 and 65 °C, suggesting that (dissolution noticeably increases) temperature affects the dissolution reaction as expect.

The activation energies were determined from the slopes of plots at two differing potentials of 0.51 V (Figure 4.23) and 0.61 V (Figure 4.24). From these potentials, it was observed that an active region was present at the potential of 0.51 V and a passivated region at the 0.61 V potential.

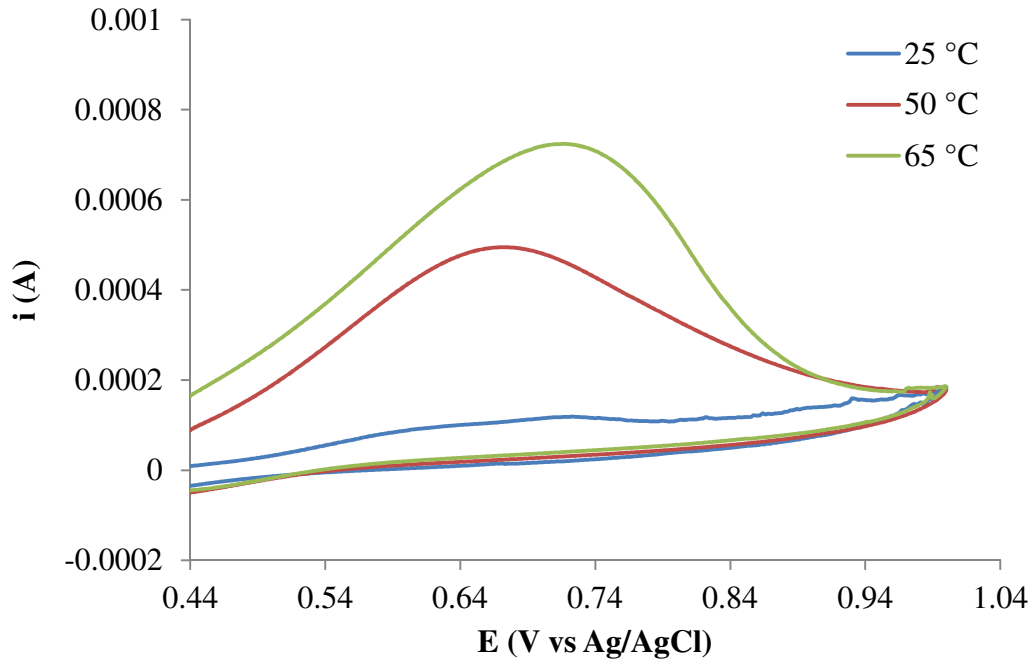

Figure 4.22: Cyclic voltammograms obtained for CPE in synthetic brannerite with different temperature conditions and [H_2SO_4] = 15 g/L.

The initial dissolution of synthetic brannerite will always be rapid as seen in Figure 4.19, where at low or high [H_2SO_4] a rapid increase is observed. Passivation will eventually follow as seen in vessel dissolution tests in Figure 4.8 at high [H_2SO_4] (100 g/L and above) if held in the potential of the active region.

In order to quantify as well as possible the increase in the anodic dissolution with temperature, linear scans were undertaken at a slower scan rate (5 mV/s) to extract apparent activation energies. The current under these conditions can be regarded as quasi stationary, approaching steady state within the practical limits of the system under study. Figure 4.23 shows the plot of ln i vs 1/T, where the higher slopes of 100 g/L and 150 g/L is visible here, indicating a different reaction mechanism. Calculated activation energies are in the Table 4.7 below.

Table 4.7: Calculated activation energies at potentials of 0.51 and 0.61 V vs Ag/AgCl.

Potential at 0.51 V				
[H_2SO_4]	15 g/L	50 g/L	100 g/L	150 g/L
Slope (K, Ea/R)	-4396	-5185	-6012	-6067
Ea (kJ/mol)	36.5	43.1	50.0	50.4
Potential at 0.61 V				
[H_2SO_4]	15 g/L	50 g/L	100 g/L	150 g/L
Slope (K, Ea/R)	-3689	-3752	-3202	-3780
Ea (kJ/mol)	30.7	31.2	26.6	31.4

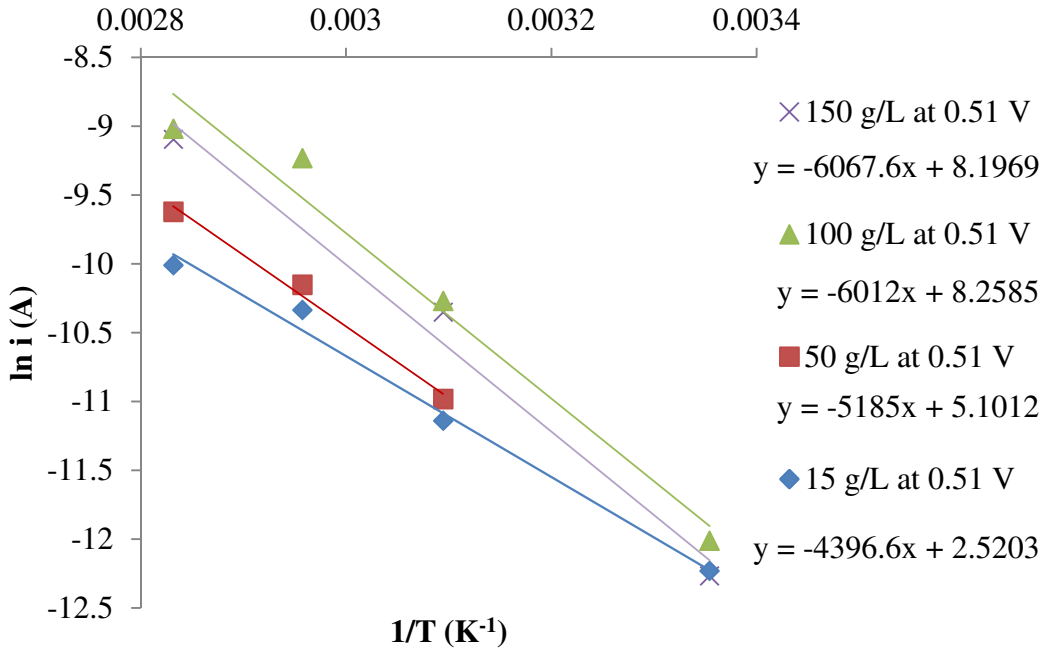

Figure 4.23: The determination of activation energy at 0.51 V.

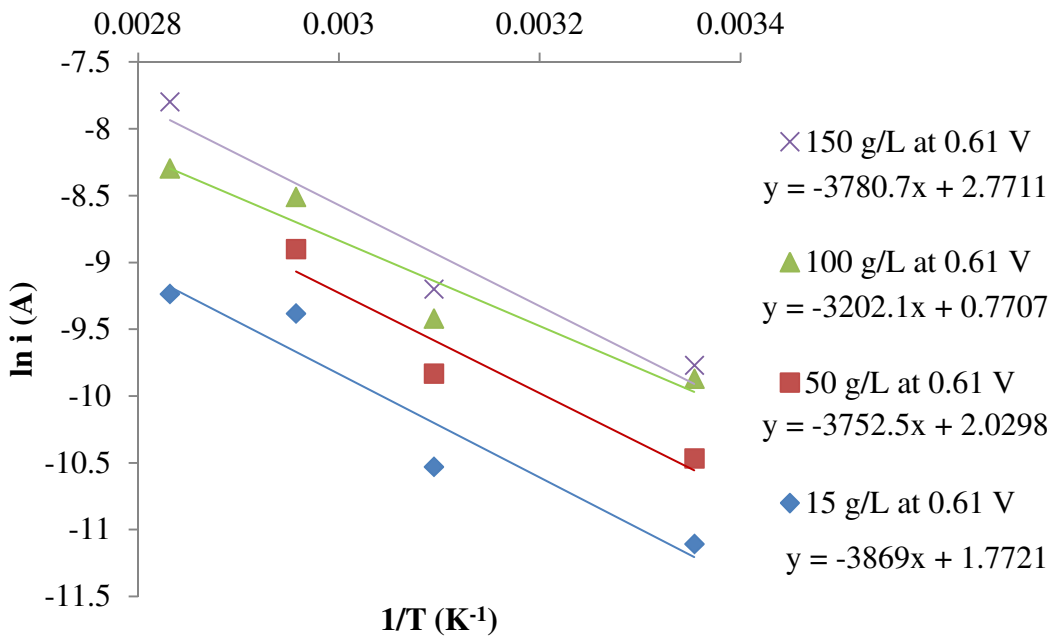

Figure 4.24: The determination of activation energy at 0.61 V.

From the activation results from Figures 4.23 and 4.24 the following information can be extracted:

- At a potential of 0.51 V in the active region, an activation energy of ~ 50 kJ/mol, typical for an active dissolution, and also quite similar to the work published of Gogoleva (2012).
- When slower leaching can be observed or passivation, the activation energy is much lower – from approximately mid 20 kJ/mol ~ 40 kJ/mol. This due to the activation energy being a measurement of the effect of temperature on the process and therefore the dissolution process is most affected by the change in temperature than a surface process such as passivation.
- As can be seen in Figure 4.11, an increase in temperature with differing [H_2SO_4] leads to differing mechanisms for leaching synthetic brannerite, which can be seen in smaller electrochemical leaching solutions such as Figure 4.18 and 4.22.

4.4. Conclusions

UTi_2O_6 was successfully synthesised and extensively characterised. The X-ray diffraction pattern confirmed the formation of UTi_2O_6 with impurities from uraninite (UO_2). The SEM/EDX analysis showed homogenous distribution between the U and the Ti and therefore the impurity of uraninite was found to be minimal. The oxidation state of U in the UTi_2O_6 structure was determined to be majority U^{4+}.

Based on the results obtained from synthetic brannerite dissolution studies the following conclusions can be made:

- [Fe(III)] (over the range 3 – 12 g/L) does not have a significant influence on dissolution at a reaction temperature of 50 °C (in 15 g/L H_2SO_4). However at 95° C in 15 g/L H_2SO_4, increasing [Fe(III)] (over the range 3 – 12 g/L) leads to significant increases in the dissolution rate.

- [H_2SO_4] has a significant influence on dissolution at 50 °C and 95° C in solutions containing 3 g/L Fe(III). This influence is however significantly higher at a reaction temperature of 95° C, and is consistent with a combined effect of acid and temperature.

- No significant dissolution occurs at 95° C at high acid concentration ([H_2SO_4] = 150 g/L) in solution containing no Fe(III).

- Synthetic brannerite dissolution most closely follows first order kinetics under the following conditions (T = 95° C, [H_2SO_4] = 15 – 200 g/L), [Fe(III)] = 3 g/L).

- Tests conducted on synthetic brannerite residues combined with fresh synthetic brannerite showed that decreases in dissolution rates observed during the dissolution of synthetic brannerite were predominantly not due to decreasing brannerite slurry concentration and were most likely due to one or more of the following:

  - Changes in surface composition / surface passivation
  - Changes in surface morphology

- Changes in particle size

Synthetic brannerite electrochemical properties in [H_2SO_4] were studied in a carbon paste electrode. The results are as follows:

- It is shown that H_2SO_4 concentration has a predominate effect on the anodic dissolution rate of brannerite, confirming the importance of acid concentration in dissolution studies of naturally occurring ores containing brannerite.
- Voltametric scans at a range of temperatures have shown that the surface of the brannerite is liable to passivate, with the solution temperature and acid concentration key players in the behaviour of the surface. Acid concentrations of above 100 g/L are required to prevent the onset of a passive region at moderate over-potentials, and promote facile dissolution.
- Tafel curves reveal that acid concentrations from 15 to 50 g/l H_2SO_4 show limited leaching, with only a modestly active region corresponding to dissolution. H_2SO_4 concentrations of 100 to 150 g/L show a well-defined active region, ranging from approximately 0.45 to 0.55 V vs Ag/AgCl, where dissolution proceeds readily, but further scanning in the anodic direction leads to surface passivation, and a rapid drop off of the dissolution current.
- EDX analysis after scanning for several minutes shows that the surface concentration of U relative to Ti is significantly decreased, indicating that a TiO_x passivating layer is responsible for the limited leaching of brannerite in commonly employed leaching conditions. Analysis of the electrolyte solution after electrochemical leaching revealed that approximately 10 times the concentration of U dissolved when compared to Ti.

- Apparent activation energies for the brannerite leaching in this active area was calculated to be around 50 kJ/mol when the concentration of the acid was above 100 g/L, and this drops to around 30 kJ/mol for regions where passivation is seen in the polarisation curves.

- Electrochemistry of synthetic brannerite in a carbon paste is thus revealed as a highly useful tool to screen and better understand the leaching behaviour of synthetic ores of uranium that have been empirically shown to display refractory behaviour.

4.5. References

Ahlberg, E. and Asbjornsson, J., 1993. Carbon paste electrodes in mineral processing: an electrochemical study of galena. Hydrometallurgy, 34: 171-185.

Casas, J.M., Crisostomo, G. and Cifuentes, L., 2005. Speciation of the Fe (II)-Fe (III)-H2SO4-H2O system at 25 and 50 °C. Hydrometallurgy 80(4): 254-264.

Colella, M., Lumpkin, G.R., Zhang, Z., Buck, E.C. and Smith, K.L., 2005. Determination of the uranium valence state in the brannerite structure using EELS, XPS, and EDX. Physics and Chemistry of Minerals, 32(1): 52-64.

Cruz, R., Luna-Sanchez, R.M., Lapidus, G.T., Gonzalez, I. and Monroy, M., 2005. An experimental strategy tp determine galvanic interactions affecting the reactivity of sulphide mineral concentrates. Hydrometallurgy, 78 (3-4): 198-208.

Donaldson, M., Stevens, R., Lang, B.E., Boerio-Goates, J., Woodfielda, B.F., Putnam, R.L. and Navrotsky, A., 2005. Heat capacities and absolute entropies of UTi2O6 and CeTi2O6. Journal of Thermal Analysis and Calorimetry, 81(3): p. 617-625.

Finch, R.J. and Murakami, T., 1999. Systematics and paragenesis of uranium minerals. Uranium: Mineralogy, Geochemistry and the Environment. Reviews in Mineralogy. , 38, 91-180 pp.

Gogoleva, E.M., 2012. The leaching kinetics of brannerite ore in sulfate solutions with iron(III). Journal of Radioanalytical and Nuclear Chemistry, 293(1): 185-191.

Hussein, A., Tardio, J. and Bhargava, S., 2008. Synthesis and dissolution studies of brannerite, a uranium containing mineral. Proceedings of CHEMECA 2008, Australia, 28-01/09-10/2008.

Ifill, R.O., Cooper, W.C. and Clark, A.H., 1996. Mineralogical and process controls on the oxidative acid-leaching of radioactive phases in Elliot Lake, Ontario, uranium ores: II-Brannerite and allied titaniferous assemblages. Canadian Institute of Mining Bulletin 89(1001): 93-103.

Laxen, P.A., 1971. Dissolution of Uranium Dioxide as an Electron Transfer Reaction, The Recovery of Uranium: Proceedings of a symposium, International Atomic Energy Agency, Vienna

Lazaro, I., Martinez-Medina, N., Rodriguez, I., Arce, E. and Gonzalez, I., 1995. The use of carbon paste electrodes with non-conducting binder for the study of minerals: Chalcopyrite. Hydrometallurgy, 38: 277-287.

Lottering, M.J., Lorenzen, L., Phala, N.S., Smit, J.T. and Schalkwyk, G.A.C., 2008. Mineralogy and uranium leaching response of low grade South African ores. Minerals Engineering, 21(1): 16-22.

Lu, D., Toda, M. and Sugano, M., 2006. High-Permittivity double rare-earth-doped barium titanate ceramics with diffuse phase transition. Journal of the American Ceramic Society, 89(10): p. 3112-3123.

Macnaughton, S.J., Ring, R.J., Day, A., Collier, D.E. and Tan, L.K.P., 1999. Optimisation of the leach conditions for a copper/uranium ore. In: B. Mishra (Ed.), EPD Congress, Proceeding of Sessions and Symposia Minerals, Metals and Materials Society. The Minerals, Metals and Materials Society, 1999, San Diego, California.

Muralikrishna, N., Mohanty, K.B. and Viswamohan, K., 1991. Extraction of uranium from refractory type of ores- A case study of brannerite from Ramsingpura, Sikar District, Rajasthan, India. Exploration and Research for Atomic Minerals, 4: 203-208.

Ram, R., Charalambous, F., Tardio, T. and Bhargava, S.K., 2011. An investigation on the effects of Fe (Fe^{II} & Fe^{III}) and oxidation reduction potential on the dissolution of synthetic uraninite (UO_2). Hydrometallurgy, 109 (12).

Shatalov, V.V., Pirkovskii, S.A. and Smirnov, K.M., 2007. Oxidation of pyrite by oxygen and concurrent leaching of uranium from ore under the conditions of an autogenous autoclave process. Atomic Energy, 102(2): 146-150.

Thomas, B.S. and Zhang, Y., 2003. A kinetic model of the oxidative dissolution of brannerite, UTi_2O_6. Radiochimica Acta, 91: 463-472.

Zhang, Y., Hart, K.P., Bourcier, W.L., Day, R.A., Thomas, B., Aly, Z. and Jostsons, A., 2001. Kinetics of uranium release from Synroc phases. Journal of Nuclear Materials, 289(3): 254-262.

Chapter 5

Dissolution of natural brannerite ores

In this chapter, two natural brannerites and two calcined natural brannerites were investigated to obtain information on the influences of the effect of temperature, [H_2SO_4] and [Fe(III)] on the dissolution of these natural minerals. A greater understanding of the influence of the aforementioned on the dissolution of these minerals will assist in the development of improved processes for extracting uranium from these minerals.

5.1. Introduction

As discussed in Chapter 3, natural brannerites have been found to contain a number of substituent elements. Pb, Ca, Th, Y and rare earth elements are commonly found to substitute for U and Si, whilst Al and Fe have been found to substitute for Ti (Lian et al., 2002). The influence of the aforementioned substitutions on the structure and properties of brannerite are of significant interest to the nuclear waste industry due to the potential of brannerite to be used as a repository for radioactive isotopes present in nuclear waste. The influence of substitution is also of significant interest to the uranium minerals processing industry as it most likely influences the processing of brannerite bearing ores.

As mentioned previous in Chapter 1, natural brannerite is also partly oxidised and hydrated (Finch and Murakami, 1999) and shows extensive evidence for metamictisation as a result of α-decay event damage. The formula for brannerite is considerably more complex than the ideal UTi_2O_6 and is therefore more accurately reported as $(U,Ca,Th,Y,REE)(Ti,Si,Fe,Al)_2O_{6-8}(OH)_x$, which is also mention in Chapter 4, in addition, an examination of the valence state of uranium in a range of natural brannerite samples by Colella et al (2005) indicated the presence of minor U^{5+} and/or U^{6+} (in addition to U^{4+}) suggesting partial solid solution with orthobrannerite, $(U^{6+},U^{4+})Ti_2O_6(OH)$ is common.

From previously reviewed literature in Chapter 1, there have been numerous studies on the rate and/or extent of dissolution of both natural and synthetic brannerites over a range of conditions. Brannerite ores are known to require stronger leaching conditions than ores containing uraninite or secondary uranium minerals, and this was confirmed by Goldney et al (1972). They showed, using a brannerite-rich ore from the Valhalla prospect (Queensland, Australia), that over 80 % extraction of uranium could be obtained with

sulphuric acid leaching at 50 °C with continuous agitation over a period of 50 hours, provided the ore was finely ground to ~ 63 microns and the free acidity of the leach liquor was maintained at 0.5 N or higher throughout the leaching period. Similar results could be achieved in shorter times using higher free acidity levels and/or higher temperatures. The addition of oxidant, either as a soluble ferric salt or as MnO_2 increased the rate of leaching significantly under most conditions and also increased the final leaching efficiency. The effect of the addition of oxidant was more significant at the lower free acidity levels. Finer grinding of the ore to ~ 45 microns resulted in a small improvement in leaching rate and in final extraction in tests at 50 °C, but had no effect in tests at 70 °C. Goldney et al (1972) therefore concluded that finer grinding would not be worthwhile. The effectiveness of an alternative alkaline leach option was also briefly investigated by Goldney et al (1972). This resulted in a uranium extraction of only 24 % on a composite sample ground to -45 microns and leached at 50 ºC for 50 h using 50 g Na_2CO_3 and 50 g $NaHCO_3$. A similar leach at 20 ºC resulted in 18 % extraction of uranium while an alkaline leach at 100 ºC on a random Valhalla sample was ineffective (Goldney et al., 1972).

Ring (1979) conducted sulphuric acid leaching studies of uraninite-brannerite containing ores from a number of Australian deposits (Ranger, Nabarlek and Koongarra all within the Alligator Rivers region) as well as a uranium-rich copper tailings concentrate from the Roxby Downs (Olympic Dam) deposit. The three ores from the Alligator Rivers region all had uraninite or pitchblende as the primary uranium mineral although some uranium was present as brannerite, and unidentified uranium-titanium, -phosphate and -silicate minerals. All three ores were readily amenable to conventional sulphuric acid leaching (T = 35-40 °C, time = 16-24 h, pH = 1.5-2.0, redox potential of ~ 475 mV and acid addition 37-55 kg/t^{-1} ore) with variations in temperature and pH had the most

influence in determining the most suitable leaching conditions. The presence of minor refractory brannerite, which was not affected by the leach conditions, limited uranium extraction to 90-96 %. In comparison, the leaching characteristics of the Roxby Downs copper tailings residue differed considerably from the Alligator Rivers ores because of the different gangue composition and uranium mineralogy. The Roxby Downs ore had both uraninite and brannerite as the primary uranium minerals while the gangue was made up of quartz, sericite, hematite and minor barite and fluorite. The extraction of uranium from the refractory uranium minerals in this ore required stringent oxidising conditions with leaching at 55 °C and a redox potential of ~ 650 mV. Under these conditions however, the initial rate and overall extraction of uranium were reduced to below 90 %.

MacNaughton et al (1999) followed up the study by Ring (1979) and also examined the leaching behaviour of brannerite present in three uranium-rich copper tailings (1600 ppm U_3O_8) from the Olympic Dam deposit. In the samples tested, brannerite occurred as a minor uranium-bearing component (10-11 %) in association with uraninite (80-82 %) and some coffinite (8-9 %). Uranium leaching behaviour was found to be characterised by a very rapid initial dissolution (> 60 % dissolution after ~ 15 mins) that slowed down significantly after ~ 80 % dissolution. The slow uranium leaching rate above ~ 80 % extraction was attributed to the presence of additional uranium-bearing minerals including coffinite and brannerite as well as poorly liberated uraninite. In all cases, uranium extraction increased with acidity and temperature and had a complex co-dependence on Fe^{3+} and redox potential. They also observed that the amount of acid consumed under standard leach conditions (pH 1.5, 55 °C, 55 wt % solids and 1.5 kg/t^{-1} $NaClO_3$) significantly varied across the three samples due to changes in gangue mineral (mainly chlorite and fluorite) abundances.

As previously discussed in Chapter 1 and 4, Muralikrishna et al (1991) used a combination of gravity concentration and wet high intensity magnetic separation to produce 93 % uranium containing brannerite concentrate from Rajasthan India. Eighty percent uranium extraction was achieved under the following conditions; 1224 kg H_2SO_4/t, 80 °C, 6 hours leach time. They concluded that concentrated acid leaching conducted at elevated temperatures was required to maximise the extraction of uranium from the brannerite pre-concentrate.

Ifill et al (1996) conducted laboratory leach tests on single specimens of natural brannerite of composition $(U_{0.629}Th_{0.039}Ca_{0.20})(Ti_{2.199}Fe_{0.13})O_{69}$ from the Elliot Lake uranium district, Ontario, Canada. They concluded that brannerite was not readily leachable in sulphuric or hydrochloric acid solutions. Furthermore, the resistance of brannerite to leaching was not significantly improved by using samples with different textural and morphological variations, nor by grinding and decreasing the overall crystallite size. Results were consistent with previous work on Elliot Lake brannerite ores which demonstrated that lengthy retention times (36 h to 48 h), high temperatures (75 ºC) and high initial acid concentrations (75 g/L H_2SO_4) were required (LaRocque and Pakkala, 1979; Hester, 1979).

Previously discussed in Chapter 1, Lottering et al (2008) investigated uranium dissolution on three low grade uranium ores from the Vaal River region in South Africa. Characterisation of the ores showed that uraninite as well as brannerite were jointly responsible for the uranium carrier minerals in the ores with 80-90 % of the uranium present in uraninite, 8-19 % as brannerite, and the balance as traces of coffinite and uranium phosphates. Results showed it was difficult to achieve uranium dissolutions higher

than 90 % under conventional uranium leaching conditions. This was attributed to the presence of refractory brannerite in the ores. If ~ 100 % uranium extraction was desired, more extreme conditions (probably pressure leaching) would be required.

Previously reviewed in Chapter 4, Gogoleva (2012) conducted a leaching study on a powdered brannerite ore (Jakutia, Russia) and determined that dissolution rates were significantly influenced by temperature and acid concentration. Maximum uranium extraction (~ 99 % U) was achieved using T = 90 ºC, 0.5 M H_2SO_4 and $[Fe(III)]_{initial}$ = 0.01 M. Analysis of samples led Gogoleva (2012) to conclude that low extraction rates were due to the development of an amorphous film on the surface of the brannerite. X-ray diffraction analysis indicated the amorphous layer was TiO_2 which was presumed to inhibit uranium extraction kinetics and is the rate controlling mechanism of the dissolution reaction.

In this Chapter, the uranium extraction results from already well-characterised (Chapter 3), naturally-occurring high-grade brannerite samples that were subject to variations in standard brannerite leach parameters including [Fe(III)], [H_2SO_4] and temperature. As well, heat treated samples were examined to characterise the effect of recrystallisation on the extent of uranium dissolution. Leached residues were analysed using scanning electron microscopy (SEM) and electron probe microanalysis (EPMA) techniques to scrutinise the distribution of any remaining uranium.

5.2. Materials and Methods

5.2.1 Materials

Details of the two naturally occurring brannerite samples that were used to obtain the results presented in this chapter, NBCW (Natural Brannerite Crockers Well) and NBRD (Natural Brannerite Roxby Downs) are given in Chapter 3.

Sulphuric acid (H_2SO_4) (Aldrich Chemical), iron sulphate ($Fe_2(SO_4)_3$) (Aldrich Chemical), nitric acid (HNO_3) (70 % AR grade) (Merck Led) and a 1000 ppm uranium ICP-MS standard (AccuStandard) were used as received. Milli-Q water (H_2O) (18 MΩ cm) was used to prepare all solutions.

5.2.2. Methods

The following methods that were used to conduct the research presented in this chapter; dissolution test procedure, acid digestion test procedure, XRD analysis, EPMA analysis and ICP-MS analysis are given in Chapter 2. During all dissolution experiments within this chapter, the ORP of the reaction solution varied by ± 10 mV.

5.2.1. Electron Probe Microanalysis (EPMA) analysis

Residues **-** Selected residues were prepared as polished mounts and examined using a high resolution Field Emission Gun (FEG) equipped EPMA (JEOL 8500F Hyperprobe). This was done in order to: 1) locate residual brannerite grains and examine their distribution, 2) to examine the chemical homogeneity of the brannerite grains, and, 3) to determine if any other mineralogical changes had occurred (e.g. dissolution/removal of

some gangue components). The sample preparations of polished samples are discussed in greater detail in Chapter 2.

5.3. Results and Discussion

5.3.1. Characterisation of samples containing natural brannerite

Characterisation results obtained for the samples containing natural brannerite that were used to conduct dissolution tests are given in Chapter 3. Briefly, these results showed the following:

Composition

Brannerite was the main component in the samples based on XRD analysis. EPMA analysis indicated that in each sample, the brannerite was Th-rich (8-10 wt % Th) indicating partial solid solution between brannerite and thorutite ($ThTi_2O_6$) and was intimately mixed with uranothorite ($[Th,U]SiO_4$) and a solid solution of thorianite-uraninite ($[Th,U]O_2$). Typical gangue mineral phases included: rutile (distributed as fine-grained crystals throughout the Th-brannerite and uranothorite dominated particles), quartz, aluminosilicates, unidentified REE-containing phosphates, zircon, titanates and apatite.

Brannerite structure

XRD analysis of the samples indicated both were amorphous having undergone radiation-induced metamictisation. It was found that the crystallinity of the brannerite in these samples was restored upon heating the samples to 1200 ºC for 24 h in air (Figure 5.1). The recrystallisation of the brannerite resulted in a number of chemical changes.

Microstructure

Both samples exhibited complex, heterogeneous microstructural features including evidence for alteration, formation of secondary alteration products, and the presence of cracks and fractures within the brannerite grains and in adjacent minerals.

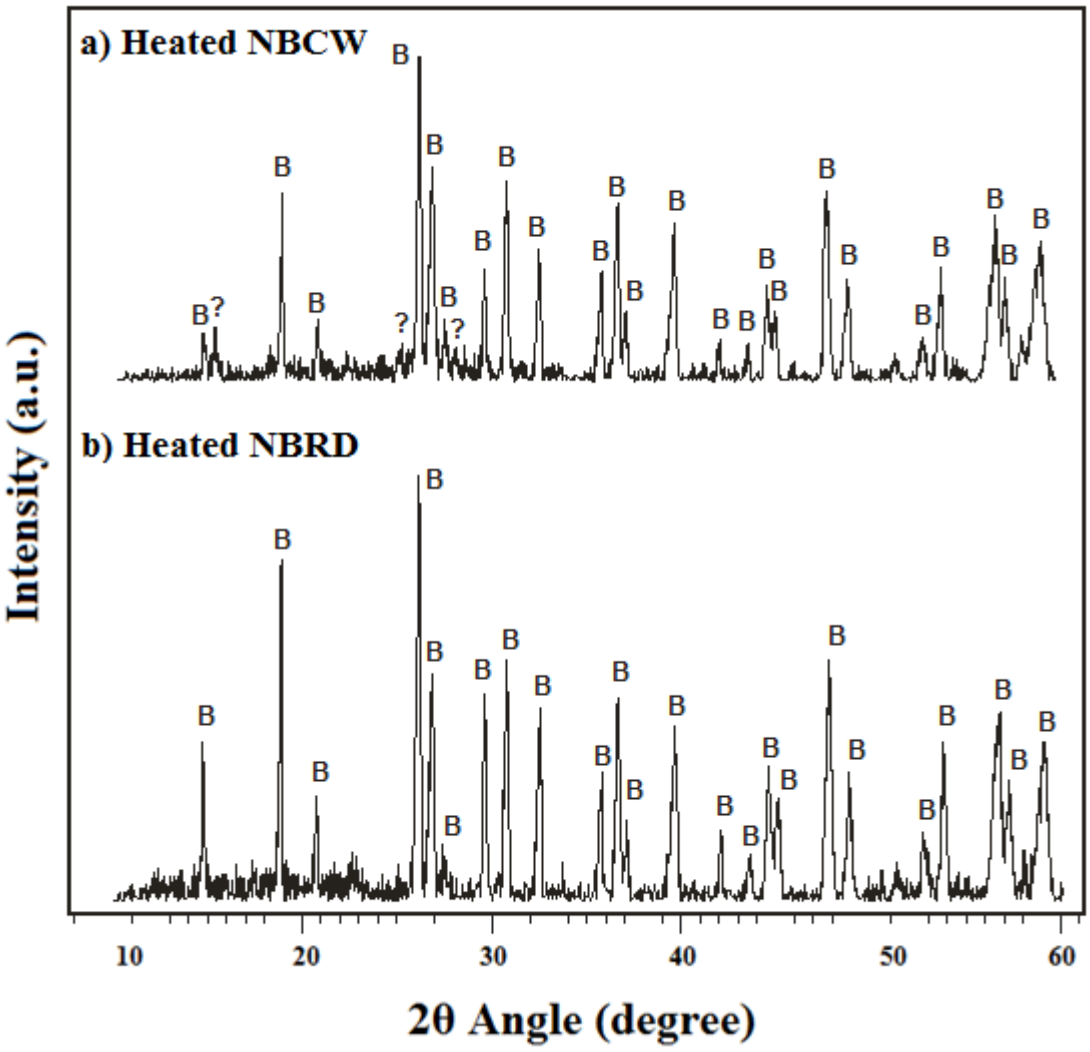

Figure 5.1: X-ray diffraction patterns comparing data obtained from the calcined brannerite samples. 'B' indicates brannerite peaks whereas peaks labelled '?' are unknown (see Chapter 3, section 3.3.1).

In the heated samples, crystalline heated brannerite (Database of the International Centre for Diffraction Data (ICDD) pattern 12-0477) was the major mineral found in the

XRD patterns for both samples. For HNBCW sample, the diffraction line at ~ 27.5 ° 2θ was most likely due to the presence of rutile/anatase (TiO_2), whereas sample HNBRD appeared to consist almost exclusively of recrystallised brannerite plus a minor amount of rutile/anatase.

5.3.2 Dissolution studies

It is important to note that as the samples obtained for investigating the dissolution of natural brannerite contained other uranium bearing minerals (see Chapter 3) the amount of uranium that was leached from these samples that was solely due to brannerite dissolution in dissolution tests could not be determined. Hence the amount of uranium dissolved from these samples that is reported hereafter in this chapter refers to the amount of uranium dissolved from all uranium bearing minerals in the samples tested and not solely due to brannerite. For ease of discussion however, and due to brannerite clearly being the predominant uranium mineral present in the samples tested, hereafter the uranium dissolved from the samples tested is described as uranium dissolved from natural brannerite. The amount of sample containing natural brannerite used in the dissolution tests conducted was determined based on the total amount of uranium in the respective samples (elemental composition data for the samples investigated is given in Table 5.1).

Table 5.1: Summary of bulk chemical analysis data determined by ICP-MS for the natural brannerite samples NBCW and NBRD (in average weight % concentrations).

Elements	NBCW	NBRD
Na	0.00	0.47
Al	1.70	2.63
K	0.00	10.20
Ca	1.36	2.23
Ti	19.30	21.04
V	0.05	0.05
Mn	0.04	0.15
Fe	0.00	0.00
Cu	2.41	0.00
Zn	1.13	0.17
Nb	0.31	0.77
Mo	0.02	0.02
Ag	0.01	0.02
Sb	0.06	0.06
Ba	0.01	0.00
Ta	0.04	0.07
Tl	0.02	0.02
Pb	0.49	0.57
Th	6.85	6.68
U	24.16	26.45

The initial slurry concentration of the samples that contained natural brannerite that was used in dissolution tests was the same as that used in the dissolution tests conducted on synthetic brannerite in terms of initial uranium concentration (100 mg/L U). The initial sample slurry concentration used in tests conducted with NBCW was 0.4139 g /L. The initial sample slurry concentration used in tests conducted with NBRD was 0.3781 g /L.

An initial series of dissolution tests were conducted in order to determine the dissolution of NBCW and NBRD under conditions typically used at mining operations (e.g. Merritt, 1971; Ring, 1979; MacNaughton et al., 1999). The dissolution conditions used are given in Table 5.2 while results showing the percentage dissolution of uranium

versus time are shown in Figure 5.2. The influence of varying the oxidant concentration, [Fe(III)], under the aforementioned conditions was also studied.

Table 5.2: Standard parameters used for brannerite dissolution tests using standard leach parameters and also using variable [Fe(III)].

Parameter	Value
$[H_2SO_4]$	15 g/L
Temperature	50 °C
Initial U slurry concentration	100 mg/L as U
$[Fe_2(SO_4)_3]$	3, 6, 9 and 12 g/L (as [Fe(III)]
Initial ORP	650-700 mV

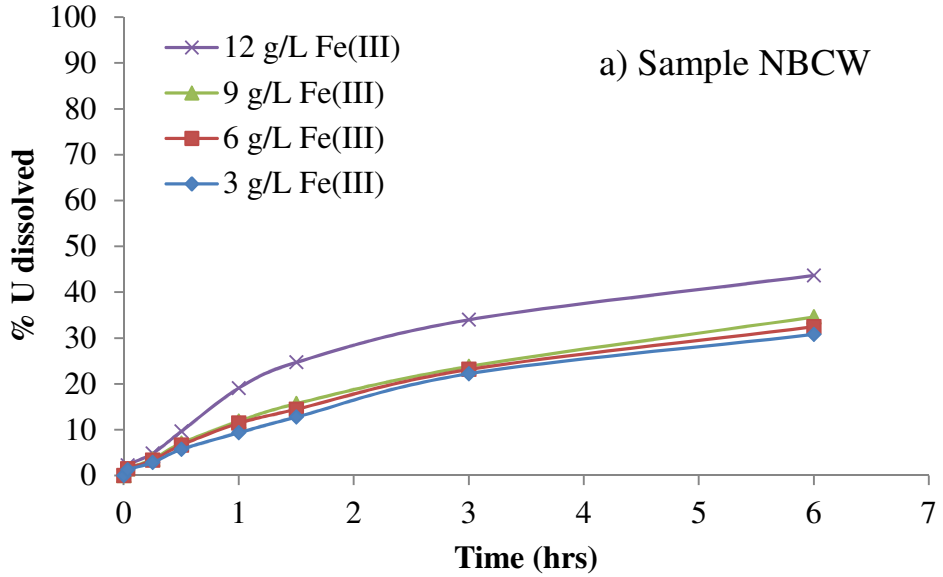

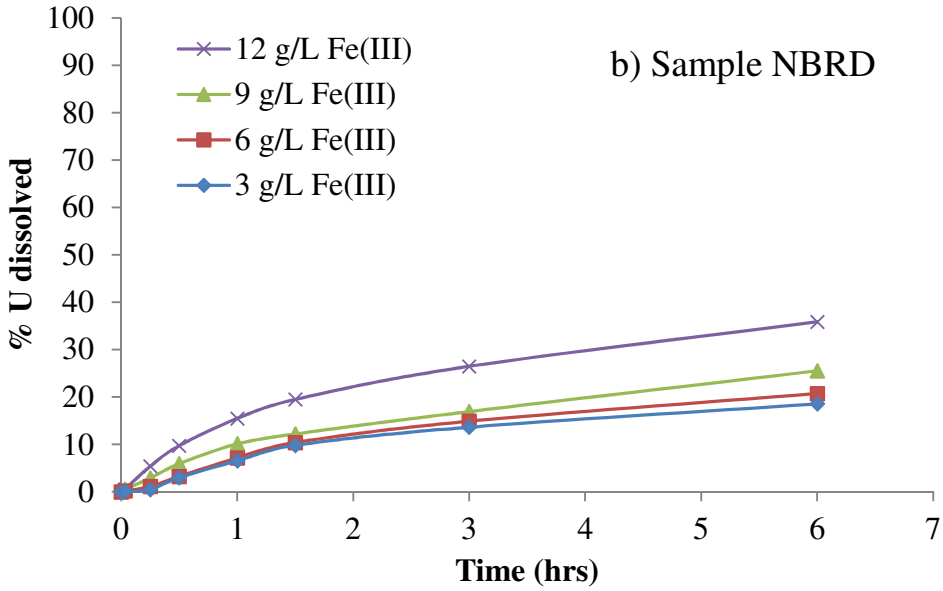

Figure 5.2: % U dissolved *vs.* time for tests conducted using standard leach parameters (T = 50°C, ([H_2SO_4] = 0.15M, initial slurry concentration of 100 mg/L as U), and with variable oxidant concentration ([Fe(III)]). Plot a) shows the data for sample NBCW, plot b) the data for sample NBRD.

Results in leach tests conducted up to 6 hours in duration showed that increasing [Fe(III)] had a significant effect on brannerite dissolution results under the conditions used. For both samples, the initial total uranium dissolved (as a percentage of the initial slurry concentration), was low but underwent a rapid increase after 0.5 h leach time. Overall, sample NBCW proved easier to extract uranium from, with a final U extraction percentage after 6 hours that was ~ 8 % U greater than measured for sample NBRD (i.e. 43 % U dissolution for sample NBCW compared to only 35 % U for sample NBRD).

The dissolution rates observed for the two natural brannerite samples were significantly higher than those observed for synthetic brannerite under identical conditions (where ~ 5 % of uranium was dissolved from synthetic brannerite after 6 hours under the following conditions T = 50 °C, [H_2SO_4] = 15 g/L, [Fe(III)] = 12 g/L, ORP = 650-700 mV, see section 4.3.2 Chapter 4).It is also interesting to note the difference in the influence of [Fe(III)] on the dissolution of natural brannerite versus synthetic brannerite where [Fe(III)] was found to have no influence on the dissolution of synthetic brannerite. The aforementioned differences in dissolution between the natural brannerite samples and synthetic brannerite are discussed in detail in section 5.3.1.4.

The difference in the dissolution rates observed for the natural brannerite samples was most likely due to one or more of the following: Differences in the extent of crystallinity of the samples (Based on the textural observations of the two samples presented in Chapter 3 the only difference between the samples was that NBCW appeared (based on Raman

spectroscopic measurements) to be slightly more metamict than sample NBRD and had some evidence for the Th-brannerite having undergone more pervasive alteration. As well, additional U-bearing phases such as uranothorite, uraninite and thorianite-uraninite were more abundant than in the Roxby Downs sample.

Differences in the composition of the brannerite grains present in the respective samples may either decrease or increase the dissolution of brannerite leaching. For example Ifill et al (1996) concluded that natural brannerite of composition $(U_{0.629}Th_{0.039}Ca_{0.20})(Ti_{2.199}Fe_{0.13})O_{69}$) did not increase the extraction of uranium and the overall leaching.

These observations, together with the dissolution test results, suggest either; a) uranium may be more easily extracted from less crystalline brannerite ores, or; b) the uranium solubility of the other U-bearing phases present in sample NBCW (uranothorite, uraninite and thorianite-uraninite) may be higher than that of brannerite.

5.3.1.1. Effect of Temperature

The effect of temperature on the dissolution of natural brannerite in samples NBCW and NBRD was investigated over the temperature range 50-95 °C with an initial slurry concentration of 100 mg/L (as U), the acid concentration kept constant at 15 g/L, an [Fe(III)] of 3 g/L, and a solution ORP of between 600-700 mV.

Results are shown in Figure 5.3 and these indicate that for both samples, there was a systematic increase in the amount of uranium dissolved as the temperature was increased from 50 to 95 °C. As for the tests conducted under standard leach conditions, the effect of temperature was much greater for sample NBCW compared to sample NBRD. It is also of note that the effect of increasing the temperature of dissolution is similar to the effect of

increasing the overall Fe(III) concentration. For both samples, the % U dissolved at 95 °C is almost identical to the % U dissolved at the highest Fe(III) concentrations tested under standard leach conditions (c.f. the results at 12 g/L Fe(III) in Figure 5.2 with the results at 95 °C in Figure 5.3).

The dissolution rates observed for synthetic brannerite under identical conditions (see section 4.3.2.2 in Chapter 4) where ~ 16 % of uranium was dissolved from synthetic brannerite after 6 hours. The two natural brannerite samples were significantly higher in uranium extraction than those observed for synthetic brannerite.

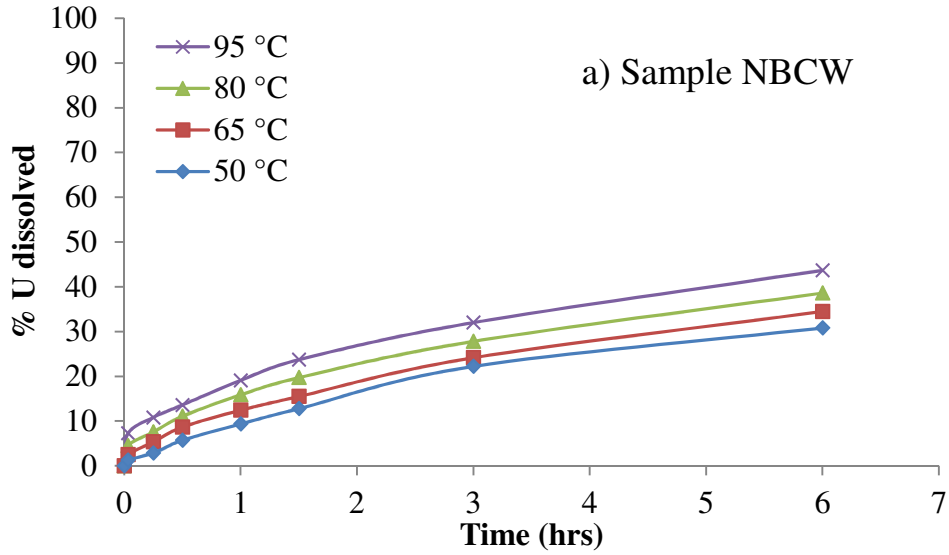

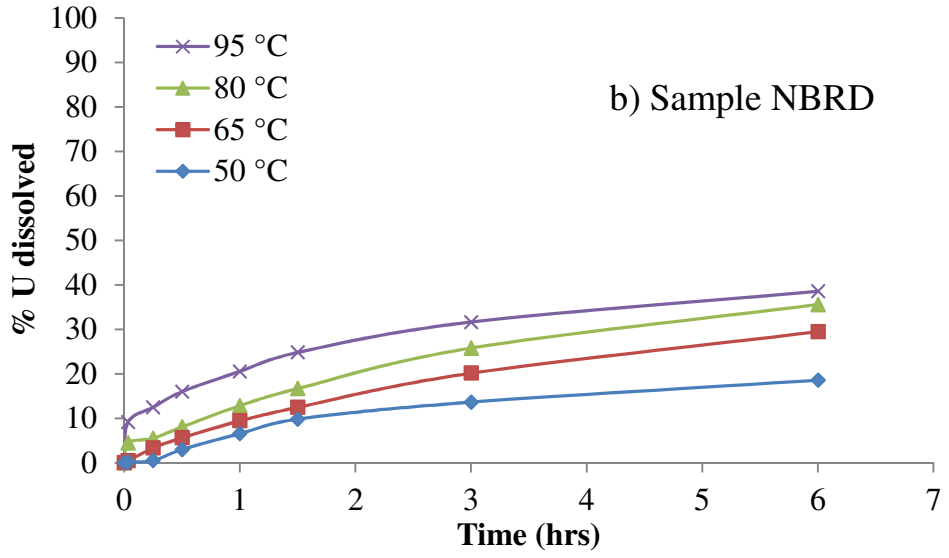

Figure 5.3: % U dissolved *vs.* time for tests conducted at different temperatures between 50-95 °C with an initial slurry concentration of 100 mg/L (as U), the acid concentration kept constant at 15 g/L, an Fe(III) concentration of 3 g/L, and a solution ORP of between 600-700 mV. Plot a) shows the data for sample NBCW, plot b) the data for sample NBRD.

Plots of the dissolution kinetics obtained from the temperature dissolution tests conducted for the two samples are shown in Figure 5.4. The results of this analysis showed that for both samples, the kinetics of uranium dissolution were closely fitted by first order kinetic equations. When these results are compared to the dissolution kinetics of synthetic brannerite (section 4.3.2.2 in Chapter 4), the initial rate is marginally higher for synthetic brannerite with respect to the two natural brannerite initial rates seen in Figure 5.4. When synthetic brannerite and the two natural brannerite initial rates are compared to synthetic uraninite studies (Ram, et al., 2011) it is obvious that the initial rate of synthetic uraninite is significantly lower than the observed synthetic and natural brannerite rates.

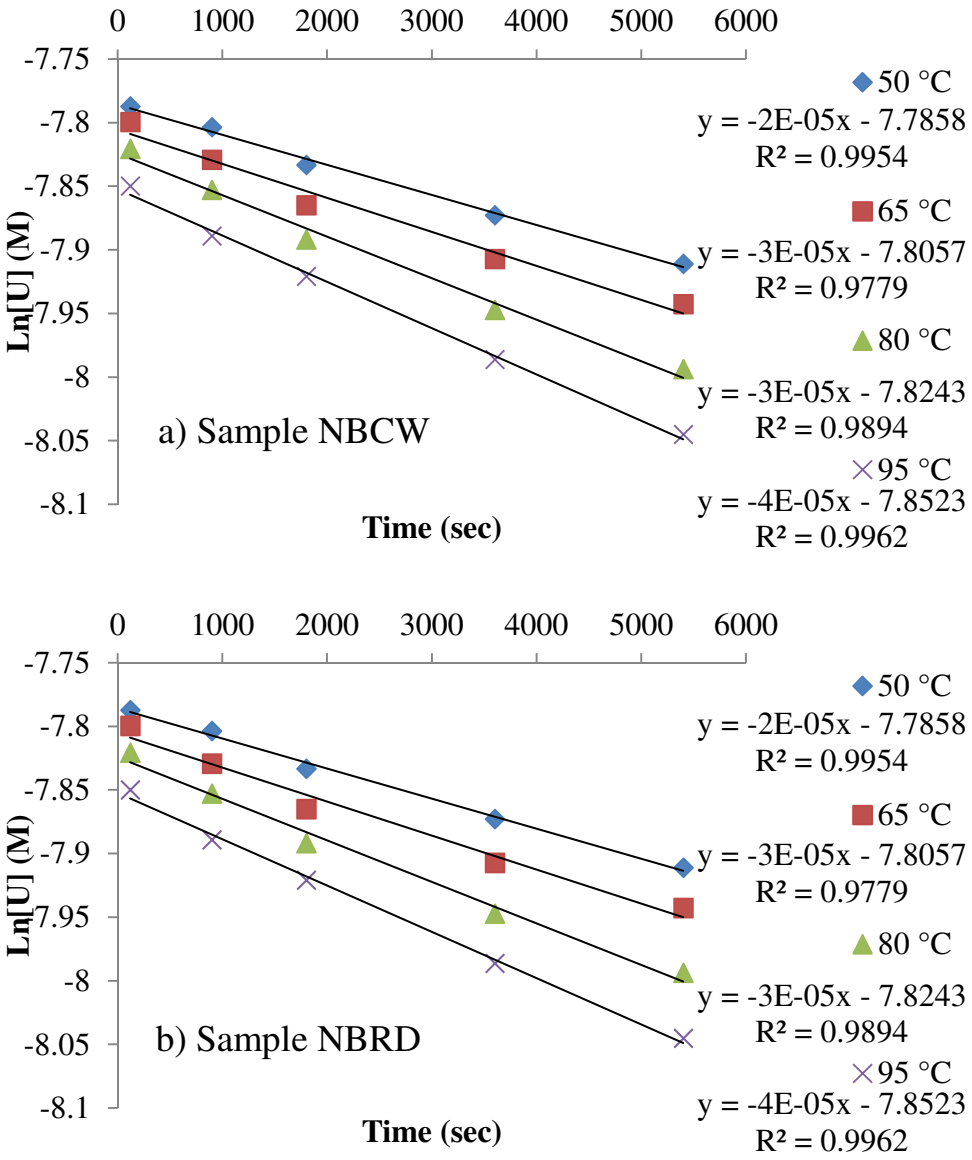

Figure 5.4: Plot of Ln [U] *vs.* time for the dissolution of uranium at various temperatures. Plot a) shows the data for sample NBCW, plot b) the data for sample NBRD.

5.3.1.2. Effect of [H_2SO_4]

The effect of H_2SO_4concentration was investigated to determine if an increase in concentration would increase uranium extraction rates. The H_2SO_4 concentrations tested were 15 g/L, 25 g/L, 50 g/L, 100 g/L and 150 g/L with all other experimental parameters (temperature, initial ORP, Fe(III) concentration) the same as used for the effect of temperature measurements. Results, shown in Figure 5.5 indicate that H_2SO_4 concentration had a significant effect on the rate and % U dissolution for both samples with uranium dissolution percentages increasing to over 50 % after 6 hours at the highest acid concentration of 150 g/L.

When these results are compared with synthetic brannerite (studies in section 4.3.2.3 in Chapter 4) where ~ 10 % of uranium was dissolved from synthetic brannerite after 6 hours under the following conditions T = 50 °C, [H_2SO_4] = 150 g/L, [Fe(III)] = 3 g/L, ORP = 600-700 mV. This result, while confirming previous experimental work on natural brannerite-containing ores (Gogoleva, 2012) is in contrast to leaching studies on uraninite ores which showed that uranium solubility was largely independent of high acid concentrations, all other parameters remaining constant (e.g. Ring, 1979). The data provide further proof that compared to the easily leached uraninite phase, brannerite ores require significantly higher acid strengths in order to dissolve uranium.

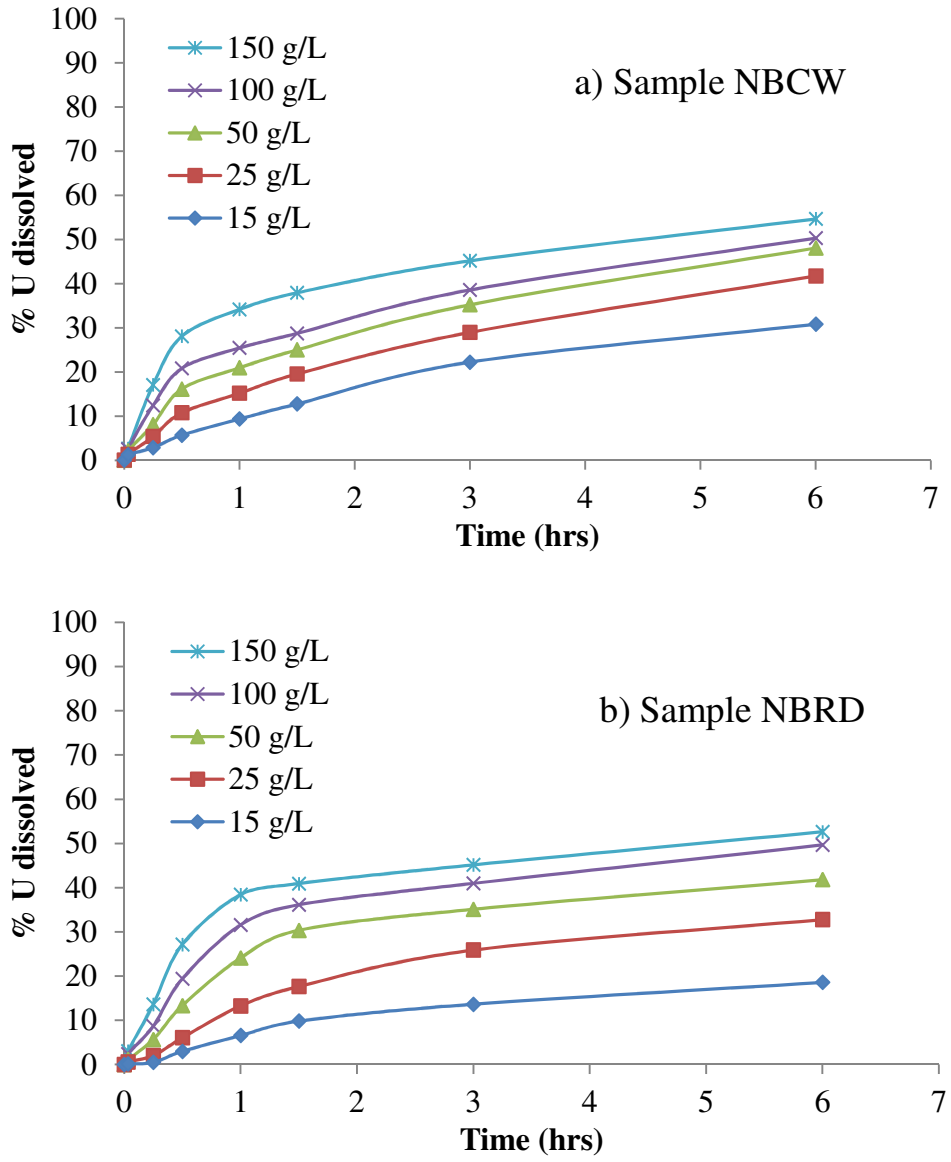

Figure 5.5: % U dissolved *vs.* time for tests conducted different acid concentrations. Plot a) shows the data for sample NBCW, plot b) the data for sample NBRD.

The uranium dissolution from brannerite kinetics for the tests conducted using varying acid concentrations were analysed to investigate the order of the dissolution under these conditions. The results of this analysis (Figure 5.6) showed that the kinetics of dissolution of uranium for both the NBCW and NBRD samples were most closely fitted by first order kinetic equations. The result suggests that the natural brannerite samples are undergoing a mechanism which is similar when the temperature is increased.

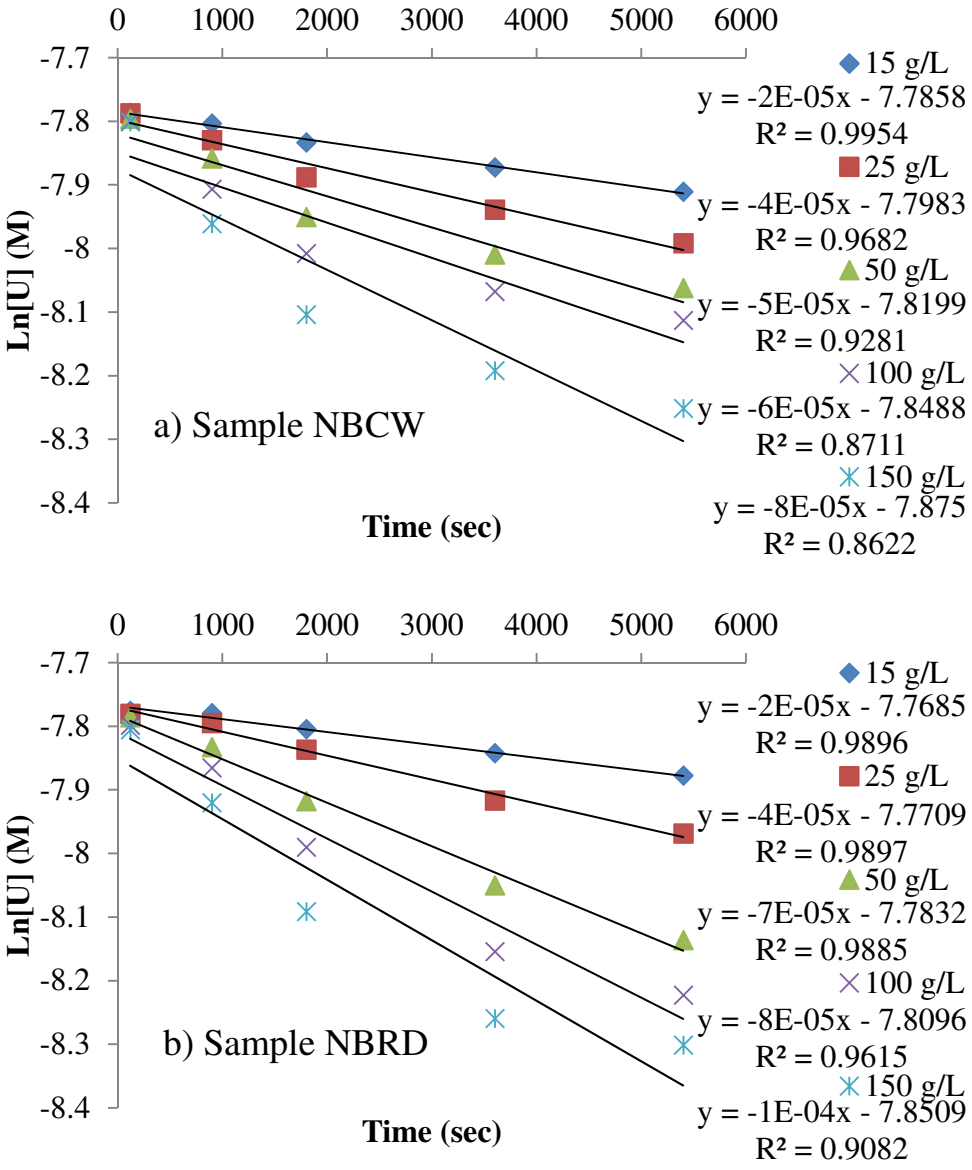

Figure 5.6: Plot of Ln [U] *vs.* time for the dissolution of uranium at various acid concentrations. Plot a) shows the data for sample NBCW, plot b) the data for sample NBRD.

5.3.1.3. Effect of [Fe(III)] and [H_2SO_4] using a high reaction temperature (95°C).

Previous results determined after increasing parameters such as the acid strength, oxidant concentration and temperature have demonstrated that all three parameters have the potential to significantly increase uranium extraction from brannerite. In the following section, the leach temperature is raised to 95 ºC whilst studying; a) the effect of varying the Fe(III) oxidant concentration and, b) the acid strength. Results from these tests are discussed below.

Increasing oxidant concentration – the conditions used in the tests to investigate the effect of varying [Fe(III)] at a higher temperature were as follows: an initial slurry concentration of 100 mg/L (as U), an acid concentration of 15 g/L, and a solution ORP of between 600-650 mV. Results in Figure 5.7a show that for sample NBCW, the addition of between 3 g/L and 12 g/L of Fe(III) causes a significant increase in the rate of uranium dissolution in the first hour of leaching where ~ 19 % of uranium was released for the system containing 3 g/L Fe(III) compared to ~ 38 % for the system containing 12 g/L Fe(III). It can also be seen that for the system containing 12 g/L Fe(III) (the maximum amount of oxidant tested), ~ 56 % of the uranium in the NBCW was dissolved after 6 hours. A comparison of the results obtained on the influence of [Fe(III)] at 50 °C (Figure 5.2a) versus 95 °C demonstrate that [Fe(III)] has a greater influence on the dissolution of NBCW when a higher reaction temperature is used with an overall increase of ~ 13 % U. For sample NBRD (Figure 5.7b), similar effects were observed with ~ 53 % of the uranium dissolved after 6 hours. Compared to the equivalent experiment conducted at 50 °C (Figure 5.2b), this represents an increase of ~ 18 % U extracted.

This effect is also seen in synthetic brannerite (section 4.3.2.4 in Chapter 4) where exact conditions of T = 95 °C, [H_2SO_4] = 15 g/L, [Fe(III)] = 3-12 g/L, ORP = 600-650 mV were used. An observation of an increased rate of uranium extraction can be seen in the first hour of leaching where ~ 7 % of uranium is released for the system containing 3 g/L Fe(III) compared to ~ 14 % for the system containing 6 g/L Fe(III). It can also be seen that for the system containing 12 g/L Fe(III) ~ 35 % of the uranium in the synthetic brannerite was dissolved after 6 hours. These results are consistent with the results obtained for natural brannerite (an increase in [Fe(III)] increases the U dissolution), yet the dissolution rate for synthetic brannerite is still significantly slower than the amorphous natural brannerite.

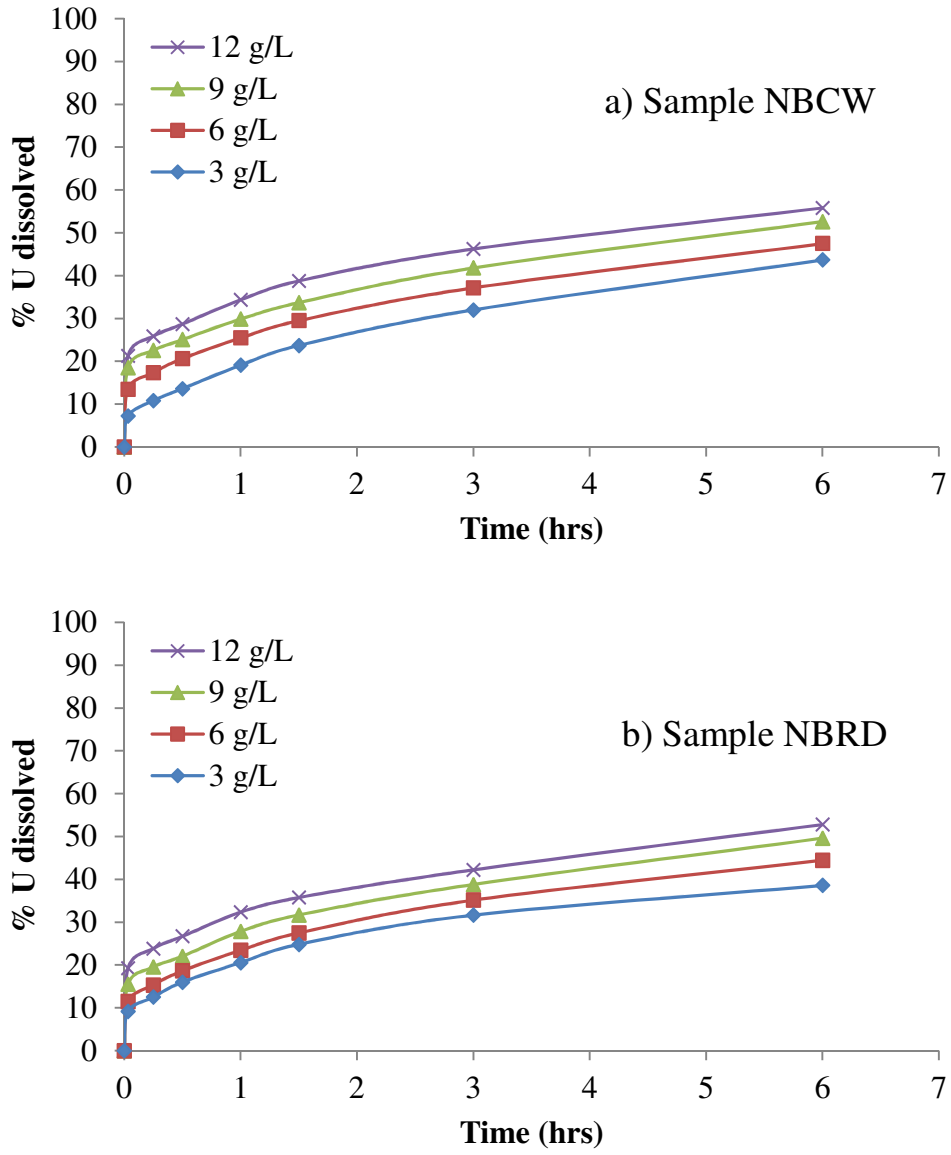

Figure 5.7: % U dissolved *vs.* time for tests conducted at 95 °C to examine the effect of varying [Fe(III)]. Conditions used: an initial slurry concentration of 100 mg/L (as U), an acid concentration of 15 g/L, and a solution ORP of between 600-650 mV. Plot a) shows the data for sample NBCW, plot b) the data for sample NBRD.

Increasing acid concentration – results from high temperature dissolution tests examining the effect of increasing acid concentration are shown in Figure 5.8. The data show that increasing [H_2SO_4] led to significant increases in brannerite dissolution. The maximum uranium dissolution measured after 6 hours at the highest acid strength of 150 g/L was ~ 61 % U (for both samples). This is compared to only 50 % U extracted at the same acid concentration (also for both samples) when the leach tests were conducted at 50 ºC (Figure 5.5).

Furthermore at 95 °C for synthetic brannerite at the similar acid conditions (section 4.3.2.4 in Chapter 4, an increase in the [H_2SO_4] from 15 to 150 g/L led to a significant growth in dissolution from 16.23 % to of 64.31 %, which is slightly higher than natural brannerites at ~ 61 % U for both NBCW and NBRD. These results clearly show that there is a similar mechanism of dissolution for synthetic brannerite compared with natural brannerite at higher temperatures and elevated [H_2SO_4].

Differences in leaching rates for the natural vs. synthetic brannerites – results suggest that synthetic brannerite has a significantly slower dissolution rate with respect to the natural brannerite samples that have been leached at temperatures of 50 °C. [Fe(III)] only has a significant effect on the dissolution of synthetic brannerite at higher temperatures. Natural brannerite at a temperature of 50 °C shows a significant increase in U dissolution. For both synthetic brannerite and natural brannerite an increase in dissolution is observed when an increase in [H_2SO_4] is used. A major observation is seen when synthetic brannerite and natural brannerite leaching rates become similar at conditions of high [H_2SO_4] and high temperature (95 °C). This observation demonstrates that there must be a mechanism change that brannerite undergoes to achieve faster and higher dissolution rate.

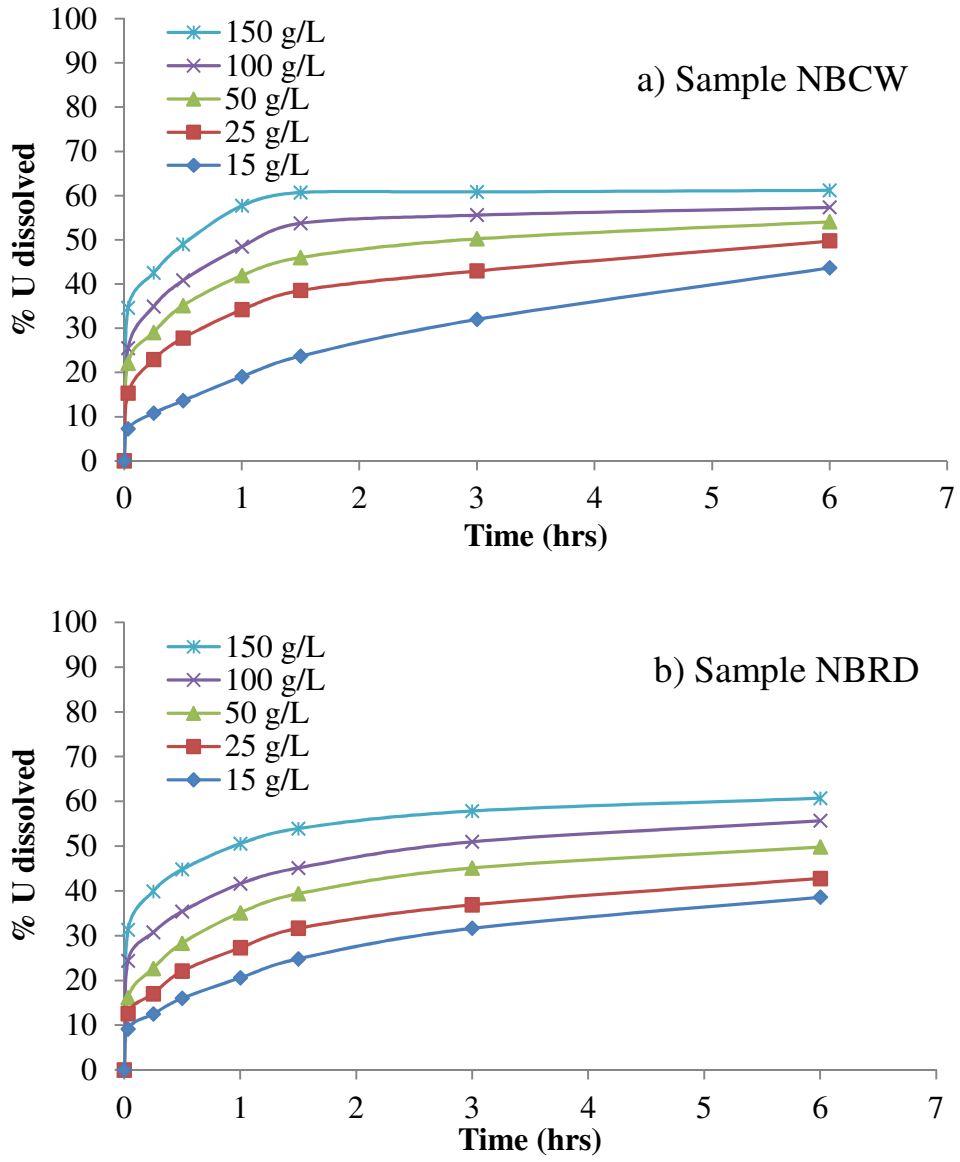

Figure 5.8: % U dissolved *vs.* time for tests conducted at 95 °C to examine the effect of varying acid concentration. Conditions used: an initial slurry concentration of 100 mg/L (as U), the oxidant concentration kept constant at 3 g/L (as [Fe(III)]), and a solution ORP of between 600-610 mV. Plot a) shows the data for sample NBCW, plot b) the data for sample NBRD.

Based on the results observed for the influence of increased [Fe(III)] and [H_2SO_4] on natural brannerite dissolution at 95 °C, it was decided to investigate the influence of [Fe(III)] under conditions of both high [H_2SO_4] (150 g/L) and high temperature (95 °C).

Previous results varying each parameter individually have demonstrated that maximum uranium extraction should occur when all three are maximised. The results from the tests are presented in Figure 5.9. As anticipated, the dissolution rate increased with increasing [Fe(III)] over the range tested (3 g/L to 12 g/L) with ~ 60 % U dissolved from both samples when 3 g/L of [Fe(III)] was used, whereas ~ 75-80 % of the uranium dissolved at 12 g/L Fe(III). Note that the dissolution of uranium in both tests containing 12 g/L Fe(III) appeared to reach equilibrium values for uranium dissolution as there was no significant change observed in the extent of dissolution after 3 hours total leach time.

Previous test results from Chapter 4 indicated for synthetic brannerite under similar conditions that ~ 37 % of uranium dissolved from synthetic brannerite when 3 g/L of [Fe(III)] was present, whereas at 12 g/L Fe(III) ~ 65 % of the uranium dissolved. The dissolution of synthetic brannerite in the test containing 12 g/L Fe(III) also most likely reached equilibrium at a value of ~ 65 % as there was no significant change in the extent of dissolution after 3 hours, which is similar to natural brannerite test in Figure 5.9.

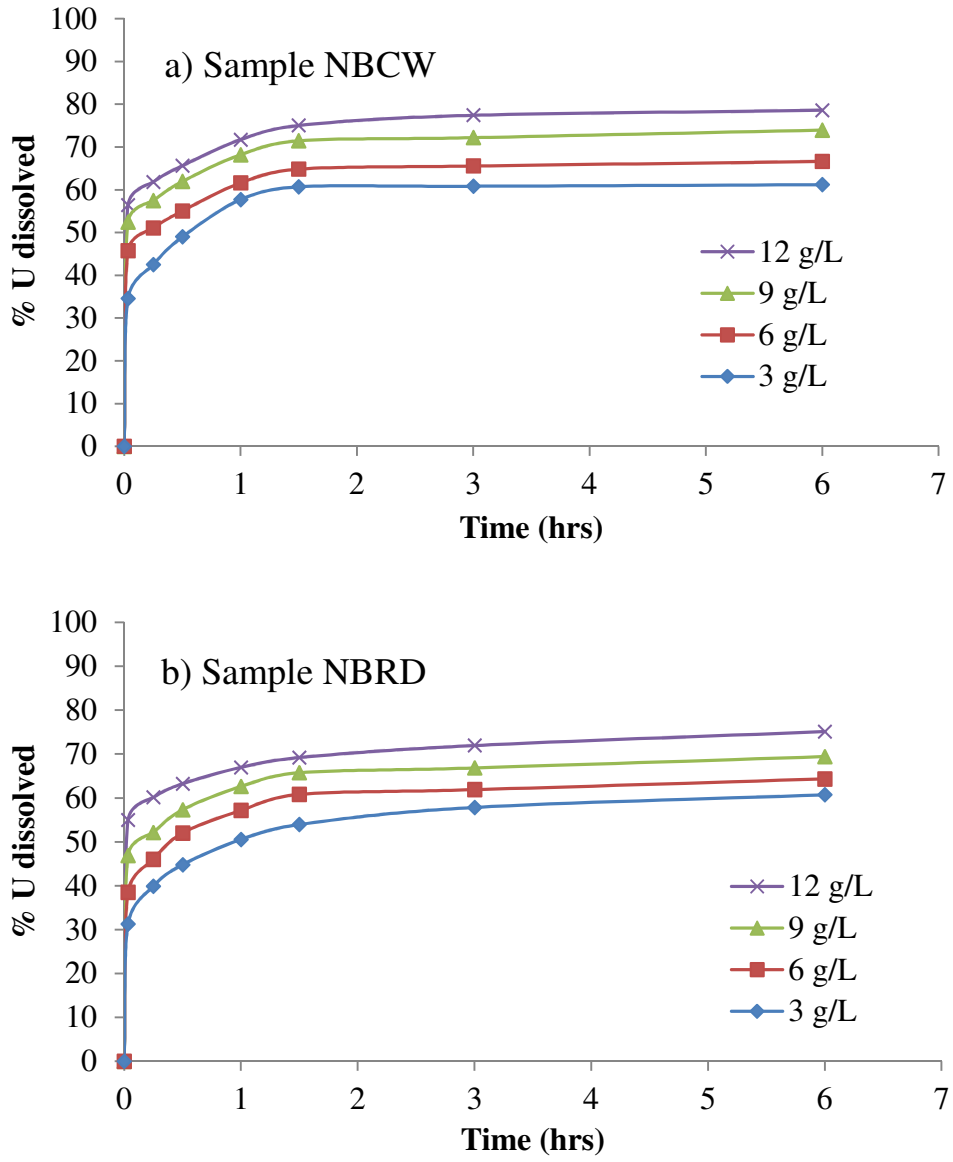

Figure 5.9: % U dissolved *vs.* time for tests conducted at 95°C and an acid concentration of 150 g/L to examine the effect of varying [Fe(III)]. Conditions used: an initial slurry concentration of 100 mg/L (as U), and a solution ORP of between 600-610 mV. Plot a) shows the data for sample NBCW, plot b) the data for sample NBRD.

EPMA mapping analysis was performed on selected residues from the samples leached at the acid concentration of 150 g/L and a temperature of 95 °C in order to locate residual brannerite grains and examine their distribution; to examine the chemical homogeneity of the brannerite grains, and; to determine if any other mineralogical changes such as

dissolution/removal of some gangue components had occurred. The samples examined were NBCW residues from tests conducted using Fe(III) concentrations of 3 g/L and 12 g/L (to enable a comparison between the best and worst performed samples) and also residue remaining from sample NBRD that was dissolved using an Fe(III) concentration of 3 g/L.

Map results showing the distribution of phases together with a corresponding map showing the distribution of the key elements Ti, Th and U are provided in Figure 5.10. Results for the 12 g/L Fe(III) experiment using the NBCW sample (Figure 5.10a), indicate a large amount of TiO_2 deposition had occurred, consistent with leaching of uranium and subsequent formation of TiO_2 (Eqn. 1). Texturally dense brannerite grains appear not to have been as affected by the leach solution with only minor occurrences of TiO_2, ususally associated with pores and/or fractures. The mechanism of attack by the leach solution is evident in the large brannerite particle at the left of Figure 5.10a where dissolution initially occurs at the margins of the grain causing a ragged outer surface and associated precipitation of fine-grained TiO_2. Further leaching results in the brannerite grains being nearly completely leached of uranium resulting in near full conversion of the original brannerite particle to TiO_2. Gangue particles, largely comprising oxides and silicates, appear not to have been affected by the leach solution. In addition, other U- and Th-containing phases present in the sample such as betafite ($(Ca,U)_2(Ti,Nb,Ta)_2O_6(OH)$) and thorutite ($(Th,U,Ca)Ti_2(O,OH)_6$) also have remained largely untouched by the leach solution.

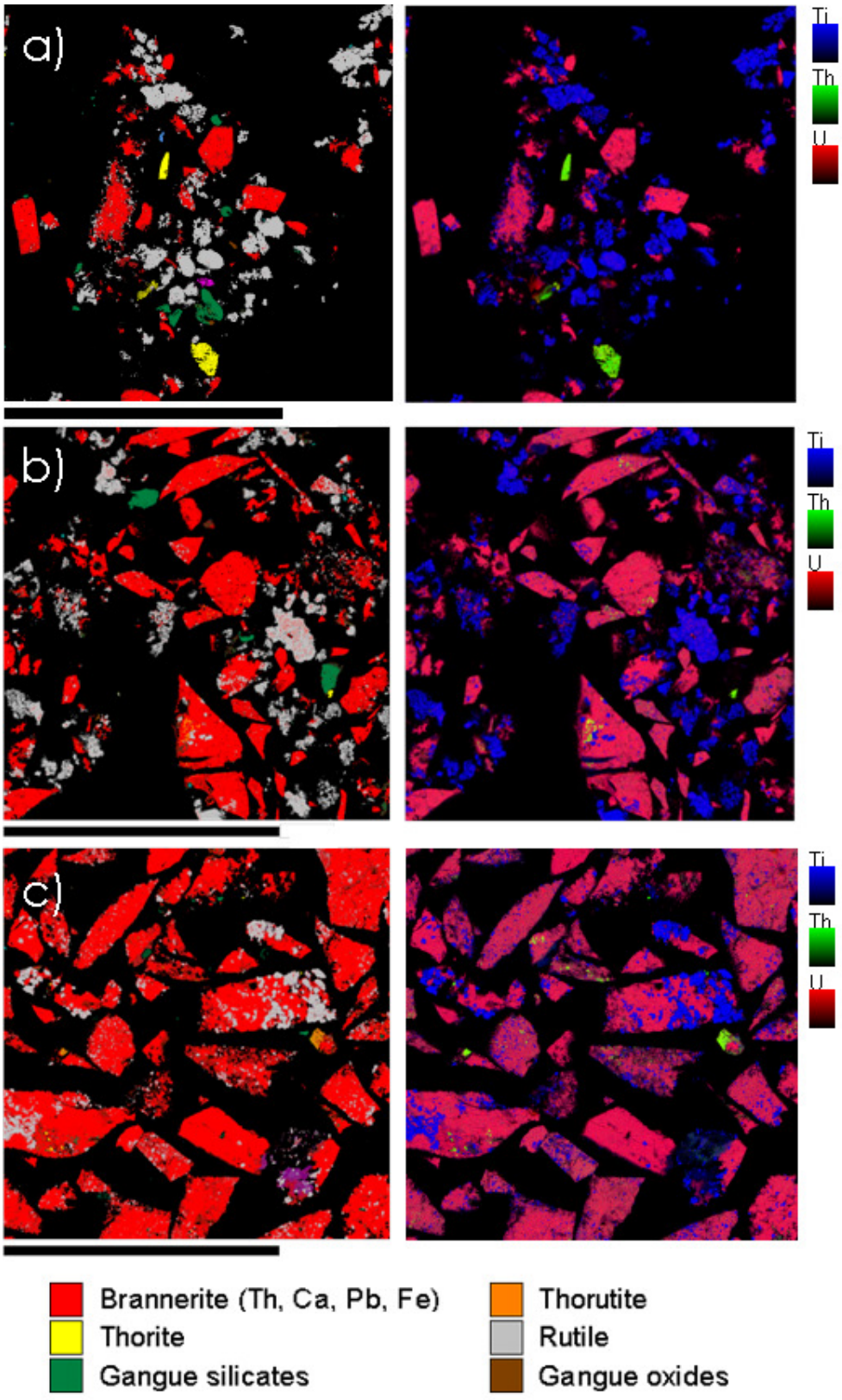

Figure 5.10: EPMA maps for the leached residues showing mineral phases identified after samples were leached at the acid concentration of 150 g/L, a temperature of 95 °C and Fe(III) concentrations of 3 g/L and 12 g/L. Image a) is sample NBCW leached at 12 g/L Fe(III),

image b) is sample NBCW at 3 g/L Fe(III), and image c) is sample NBRD at 3 g/L Fe(III). For each phase-patched map there is a corresponding Ti/Th/U map showing the distribution of these three key elements. The scale bar for each image is 500 µm.

Compared to the NBCW sample leached at 12 g/L Fe(III), the residue from the 3 g/L Fe(III) leach test shows evidence for considerably more dense, unleached brannerite particles remaining. Although it is recognised that particle densities within the mapped areas are different between Figures 5.10a and 5.10b, a wider examination of both leach test residues confirmed the presence of more unreacted brannerite remaining in the the 3 g/L Fe(III) leach test sample. This observation is consistent with the results above which indicate that higher levels of oxidant lead to increased dissolution of uranium from brannerite (see Figure 5.7). It is noted however, that where the original natural brannerite particles have been significantly altered, either through alteration via processes involving hydrothermal fluids or through metamictisation, at the high acid strength and temperatures used in these experiments, even low oxidant concentrations appear to be sufficient to cause almost complete extraction of uranium leaving behind almost monominerallic TiO_2 (see the predominatly TiO_2-rich particle at the right of centre in Figure 5.10b).

The NBRD residue from the sample leached at 3 g/L Fe(III) exhibited simlar textures and mineralogical changes as noted for sample NBCW leached at 3 g/L Fe(III) and did not show signs of having undergone significant levels of uranium extraction (Figure 5.10c). While individual brannerite grains have embayed and ragged rims suggestive of partial attack by the leach solution, for the most part the inner regions of the grains still appeared texturally dense with only minor development of TiO_2 (after extraction of uranium). When examined in more detail under higher magnification (not shown), the textures of these

grains appeared to be microporous and microfractured. These regions were coated/filled by TiO_2 indicating the leachant was able to penetrate to some degree, but did not result in complete extraction.

Observations from the NBCW and NBRD residues remaining after leaching strongly suggests that texture plays an integral role in determining the extent of uranium extraction in naturally-occurring brannerites. Brannerite grains that are less porous, less altered, and less affected by metamictisation (i.e. more crystalline) are less susceptible to leaching under mild conditions. In these materials, harsher leaching conditions likely involving elevated temperaures, high acid strengths and high levels of oxidant will be required.

5.3.2. Effect of brannerite crystallinity

Previous experiments to study the effect of metamictisation on the chemical durability of synthetic and natural brannerites in acidic solutions indicated that natural brannerite provided approximately one order of magnitude higher uranium release rates compared to synthetic materials (Zhang et al., 2006). These data suggested that the process of metamictisation may lead to enhanced brannerite dissolution rates.

To examine the effect of recrystallisation on uranium extraction, experiments were conducted on natural brannerite samples that had been heat treated to restore their crystallinity and then leached under the most extreme leach conditions used in the current study i.e. an acid concentrationof 150 g/L H_2SO_4, an Fe(III) oxidant concentration of 12 g/L, T = 95 °C, and an initial U slurry concentration of 100 mg/L. Results are shown in Figure 5.11 and these indicate that for both samples, no significant dissolution of recrystallised natural brannerite occurred even under these harsh leach conditions.

Maximum U extraction was < 10 % for both samples indicating that the annealing of the radiation damage through thermal recrystallisation significantly depresses uranium extraction from brannerite.

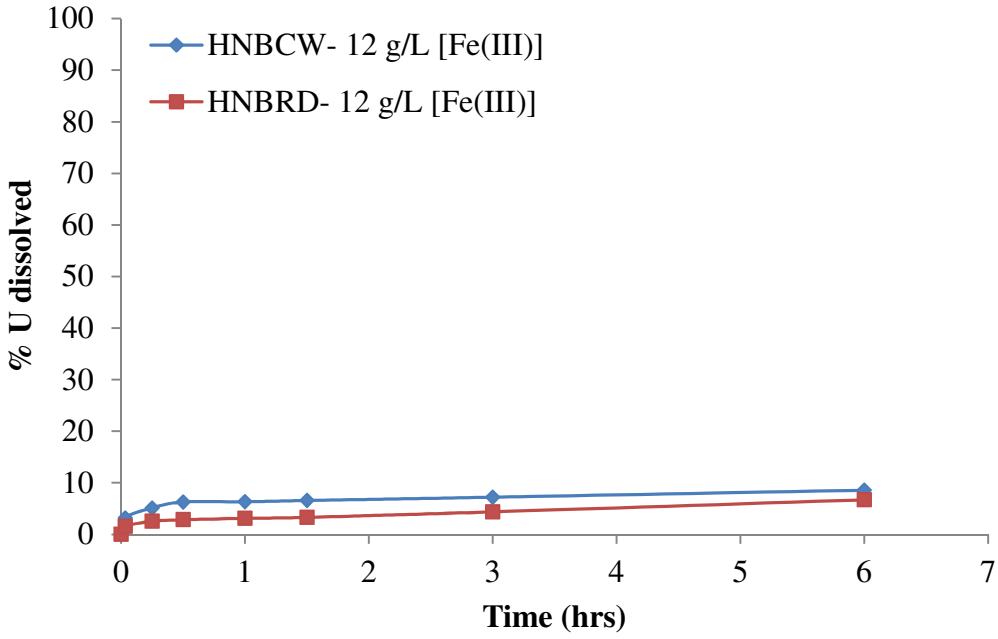

Figure 5.11: % U dissolved *vs.* time for the heat-treated samples HNBCW and HNBRD in solutions containing an Fe(III) concentration of 12 g/L and an acid concentration 150 g/L. Inset plot shows in more detail the data for time < 1.5 h. Both experiments were conducted at a leach temperature of 95 °C (ORP 600-610 mV).

EPMA mapping analysis was performed on the leached residue from sample HNBCW in an attempt to understand the chemistry, mineralogy and texture of the brannerite grains remaining. These results are shown in Figure 5.12. The most obvious difference between heated and unheated NBCW samples was that; a) there has been extensive recrystallisation accompanied by significant phase segregation in the heated sample, b) while large particles in the HNBCW seem porous, examination under higher magnification indicates particles are comprised of small, euhedral, dense brannerite particles. These observations of the

leached sample are consistent with the results obtained in Chapter 3, where a detailed knowledge of the unleached sample after heat treatment to 1200ºC was obtained. The extensive recrystallisation of the brannerite to produce clusters of 2-3 µm sized, prismatic grains as well as significant migration of elements were also observed (section 3.3.4 in Chapter 3), with a notable difference in the heated brannerite, which contained less Si, less Ca and significantly less Pb. These elements were not to be stabilised in the high temperature brannerite with the Ca and Si being incorporated into a Ca silicate mineral phase and the Pb and Si into a Pb-rich aluminosilicate film at grain boundaries. In addition, a thorianite–uraninite $(Th,U)O_2$ phase present in the unheated sample was decomposed into a ThO_2 phase and a UO_2 phase after heating while larger gangue mineral phases such as rutile present in the unheated natural sample remained unaffected by the heating process, which is discussed in greater detail in section 3.3.4 in Chapter 3.

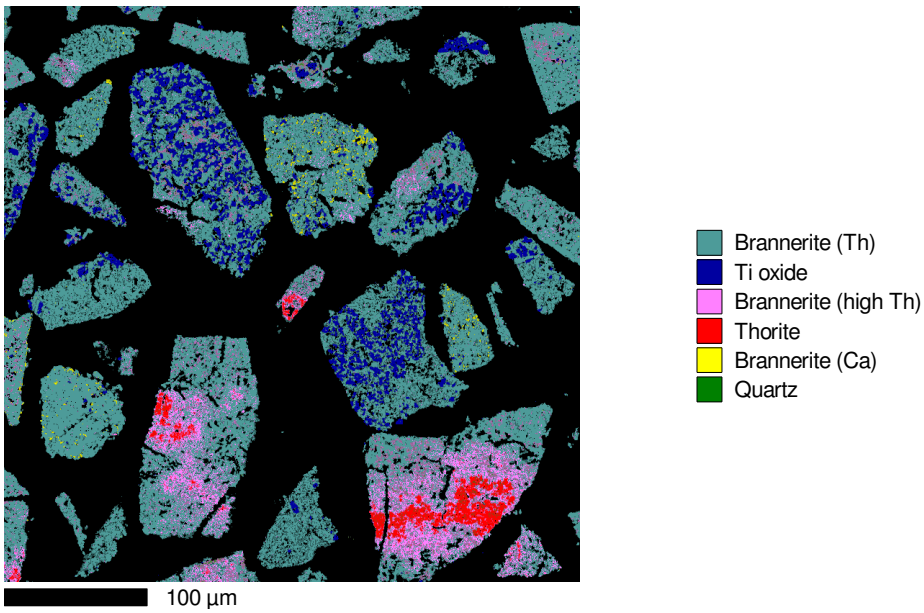

Figure 5.12: EPMA map for the leached residues from the heat-treated samples HNBCW leached at an [FeIII] of 12 g/L, an [H_2SO_4] of 150 g/L and a temperature of 95 °C.

Based on the EPMA map results, the changes in dissolution rates between the natural Crockers Well ore and the heat treated sample is likely attributable to a combiantion of effects. These include: a) different levels and types of impurities within the brannerite and, b) the crystallinity of the sample. For the former, recrystallisation of amorphous natural brannerite through high temperature annealing results in the formation of UO_2 particles among the recrystallised brannerite grains and the formation of Pb-rich aluminosilicate films at grain boundaries and triple points (Zhang et al., 2006). Both are readily leachable using acidic solutions and the low U extraction results are likely reflecting the solubility of UO_2. The most important effect of uranium extraction however, appears to be associated with the degree of crystallinity. Based on a comparison of leach test results comparing heat treated versus natural brannerite samples it is concluded that uranium can be readily extracted from brannerite if the brannerite is highly metamict and has additionally undergone some degree of alteration. The combination of a disrupted crystalline lattice in association with partial leaching and hydration of the brannerite contribute to making the brannerite more reactive than unaltered material.

5.4. Conclusions

Results showed that the effect of increasing [Fe(III)], [H_2SO_4], and temperature was to increase the solubility of uranium from brannerite. Uranium extraction levels were similar for both samples as each parameter was varied, with the slight differences attributable to small variations in brannerite chemistry and/or degree of alteration withinthe two samples.

Maximum uranium extraction rates of ~ 80 % U were achieved using an [Fe(III)] of 12 g/L, at 150 g/L [H_2SO_4] and a temperature of 95 °C. These conditions are more extreme than required for leaching uranium from other U-bearing phases such as uarninite and coffinite but refelect the more refractory nature of the chemically and more structurally complex brannerite. Samples that were heat treated to 1200 ºC to restore crystallinity performed much worse under identical conditions, with maximum uranium extraction rates of < 10 % U recorded. The lower extraction rates were attributed to the heat treatment causing chemical and structural (recrystallisation) changes to the brannerite.

Uranium recovery processes from brannerite are not straightforward with the efficiency of uranium recovery being greatly influenced by the mineralogical characteristics of the ore. Natural brannerites, while less susceptible to uranium extraction than other U-bearing minerals, can achieve high uranium extraction rates providing i) acid strength, oxidant strength and temperatures are maintained at elevated levels (compared to those traditionally used for uraninite leaching), and, b) the brannerite has not undergone any post crystallisation, high temperature modification (e.g. metamorphism), that is likely to cause significant recrystallisation of the sample.

5.5. References

Colella, M., Lumpkin, G.R., Zhang, Z., Buck, E.C. and Smith, K.L., 2005. Determination of the uranium valence state in the brannerite structure using EELS. XPS, and EDX. Phys. Chem. Minerals, 32, 52-64.

Finch, R.J. and Murakami, T., 1999. Systematics and paragenesis of uranium minerals. . Uranium: Mineralogy, Geochemistry and the Environment. Reviews in Mineralogy, 38, 91-180 pp.

Gogoleva, E.M., 2012. The leaching kinetics of brannerite ore in sulfate solutions with iron(III). Journal of Radioanalytical and Nuclear Chemistry, 293, 185-191.

Goldney, L.H., Canning, R.G. and Gooden, J.E.A., 1972. Extraction investigations with some Australian uranium ores. In: The AAEC Symposium on Uranium Processing, 20-21 July 1972, Paper V, AAEC/E238, (Australian Atomic Energy Commission), Lucas Heights, Australia.

Hester, K.D., 1979. Current developments at Rio Algom, Elliot Lake. CIM Bulletin, 72, 181-188.

Ifill, R.O., Cooper, W.C. and Clark, A.H., 1996. Mineralogical and process controls on the oxidative acid-leaching of radioactive phases in Elliot Lake, Ontario, uranium ores: II-Brannerite and allied titaniferous assemblages. CIM Bulletin, 89, 93-103.

La Rocque, E. and Pakkala, E., 1979. Current leaching and product recovery practice at Denison Mines Limited. CIM Bulletin, 72, 172-176.

Lottering, M.J., Lorenzen, L., Phala, N.S., Smit, J.T. and Schalkwyk, G.A.C., 2008. Mineralogy and uranium leaching response of low grade South African ores. Minerals Engineering, 21, 16-22.

Macnaughton, S.J., Ring, R.J., Day, A., Collier, D.E. and Tan, L.K.P., 1999. Optimisation of the leach conditions for a copper/uranium ore. In: Mishra, B. (Ed.), EPD Congress, Proceeding of Sessions and Symposia Minerals, Metals and Materials Society. The Minerals, Metals and Materials Society, 1999, San Diego, California.

Merritt, R.C., 1971. The Extractive Metallurgy of Uranium. Colorado School of Mines Research Institute, Colorado. 576p.

Muralikrishna, N., Mohanty, K.B. and Viswamohan, K., 1991. Extraction of uranium from refractory type of ores- A case study of brannerite from Ramsingpura, Sikar District, Rajasthan, India. Exploration and Research for Atomic Minerals, 4, 203-208.

Ram, R., Charalambous, F., Tardio, T. and Bhargava, S.K., 2011. An investigation on the effects of Fe (Fe^{II} & Fe^{III}) and oxidation reduction potential on the dissolution of synthetic uraninite (UO_2). Hydrometallurgy, 109 (12).

Ring, R.J., 1979. Leaching characteristics of Australian uranium ores. Proceedings Australasian Institute of Mining and Metallurgy, 272, 13-23.

Zhang, Y., Lumpkin, G.R., Li, H., Blackford, M.G., Colella, M., Carter, M.L. and Vance E.R., 2006. Recrystallisation of amorphous natural brannerite through annealing: the effect of radiation damage on the chemical durability of brannerite. Journal of Nuclear Materials, 350, 293-300.

Chapter 6

Conclusions and Future work

A summary of the work conducted in this thesis and the major results achieved have been provided. A brief summary of future work than can be conducted as a result of this work is also listed.

6.1. Conclusions

Natural brannerite and natural brannerite bearing ore – characteristics / mineralogy

X-ray diffraction analysis confirmed that the unheated samples of NBCW and NBRD were X-ray amorphous and therefore had undergone radiation-induced metamictisation. The crystallinity of the brannerite was restored upon calcination of the samples to 1200 °C for 24 hours in air. For the Crockers Well sample, recrystallisation began at temperatures as low as 800 °C while the Roxby Downs sample did not begin to show evidence of brannerite recrystallisation until an annealing temperature of 900 °C was reached.

Raman spectroscopy indicated that the effect of metamictisation was to make the peaks broad and of low intensity. After calcination, the Raman peaks were sharpened and intensified due to the increased crystallinity. Analysis of the natural brannerite samples by SEM and EPMA indicated that both samples contained exhibited complex, heterogeneous microstructural features. In each sample (NBCW and NBRD), the brannerite was Th-rich (~ 8-10 wt % Th) indicating partial solid solution between brannerite and thorutite ($ThTi_2O_6$) and was thoroughly mixed with uranothorite ($[Th,U]SiO_4$) and a solid solution of thorianite-uraninite ($[Th,U]O_2$). Typical gangue mineral phases in the samples included: rutile (distributed as fine-grained crystals throughout the Th-brannerite and uranothorite dominated particles), quartz, aluminosilicates, unidentified REE-containing phosphates, zircon, titanates and apatite.

After heat treatment the natural brannerite samples (HNBCW and HNBRD), generally contained less Si, less Ca and significantly less Pb. These elements appeared not to be stabilised in the high temperature brannerite with the Ca and Si being incorporated into a Ca silicate mineral phase and the Pb and Si into a Pb-rich aluminosilicate film at grain

boundaries. Furthermore, both heated natural brannerite samples contained a high-Th brannerite (up to 22-30 wt % Th). The thorianite-uraninite phase in the unheated samples was decomposed into separate ThO_2 and UO_2 phases after heating.

X-ray diffraction analysis of the 'high grade' brannerite leach feed sample (brannerite bearing ore) from the Olympic Dam deposit in South Australia indicated that the sample was high in quartz, iron oxides and feldspar potassium. No X-ray diffraction pattern for brannerite could be identified. EPMA mapping investigations determined very low quantities of brannerite within a quartz grain.

Synthetic brannerite

Synthetic brannerite (UTi_2O_6) was successfully synthesised. The prepared sample was characterised extensively using X-ray diffraction (XRD), scanning electron microscopy (ESEM), elemental mapping analysis and X-ray photoelectron spectroscopy (XPS) to determine the purity and homogeneity of the sample. It was concluded that the prepared sample was primarily brannerite with trace levels of UO_2 occurring on the surface. The sample was also highly homogenous, with uniform distributions of uranium and titanium. The primary oxidation state of the synthesised brannerite was determined to be U^{4+}.

Dissolution studies conducted on synthetic brannerite demonstrated that under parameters that are commonly used to leach / process uranium minerals no significant uranium dissolution occurred (T = 50 °C, $[H_2SO_4]$ = 15 g/L, [Fe(III)] = 3-12 g/L and ORP = 650-700 mV). However if a reaction temperature of 95 °C is used under the following conditions; $[H_2SO_4]$ = 15 g/L, [Fe(III)] = 3-12 g/L and ORP = 600-650 mV; there is a significant increases in the dissolution rate, with the system containing 12 g/L Fe(III) at the higher reaction temperature of 95 °C, ~ 35 % of the uranium in the synthetic brannerite

was dissolved after 6 hours. The results obtained on the influence of [Fe(III)] at 50 °C and 95 °C clearly show that [Fe(III)] only influenced the dissolution of synthetic brannerite when a higher reaction temperature is used (for systems having an [H_2SO_4] of 15 g/L).

Investigations into the influence of [H_2SO_4] on the dissolution of synthetic brannerite at five differing acid concentrations of 15, 50, 100, 150 and 200 g/L (H_2SO_4) showed to have a significant influence on dissolution at 50 °C and 95 °C in solutions containing 3 g/L Fe(III). This influence is however significantly higher at a reaction temperature of 95 °C, which is evidently consistent with a combined effect of acid and temperature and can be seen when a direct comparison of results from tests conducted at a temperature of 50 °C. For example, if an increasing [H_2SO_4] from 15 g/L to 50 g/L led to an increase in uranium dissolution from 2.59 % to 5.87 %. Whereas at a temperature of 95 °C and increasing [H_2SO_4] from 15 to 50 g/L led to an increase in dissolution from 16.23 % to 49.11 %. In addition to these results, at a reaction temperature of 95 °C, increasing the [H_2SO_4] from 15 to 200 g/L led to a significant increase in dissolution from 16.23 % to of 80.23 %. Synthetic brannerite dissolution most closely follows first order kinetics under the following conditions (T = 95 °C, [H_2SO_4] = 15 – 200 g/L), [Fe(III)] = 3 g/L).

An investigation into determining if H_2SO_4 alone at the higher reaction temperature of 95 °C, in the absence of Fe(III), was conducted to determine if the significant influences of [H_2SO_4] identified may have been due to a dissolution mechanism that did not involve Fe(III). The results indicated that no significant dissolution occurs at 95° C with a high acid concentration of [H_2SO_4] = 150 g/L in solution containing no Fe(III) and therefore the significant influence of [H_2SO_4] on brannerite dissolution clearly relies on the presence of Fe(III) in solution.

An investigation was undertaken to determine if the decreases in rate of synthetic brannerite dissolution that were observed in a number of tests was predominantly due to

decreasing brannerite slurry concentration.X-ray photoelectron spectroscopy (XPS) was used to determine if any significant changes on the surfaces of the leached brannerite particles and compared to that of the fresh brannerite particles. The results showed no significant changes to the surface of either leached to fresh brannerite particles. Tests conducted on synthetic brannerite residues combined with fresh synthetic brannerite showed that decreases in dissolution rates observed during the dissolution of synthetic brannerite were predominantly not due to decreasing brannerite slurry concentration and were most likely due to one or more of the following; changes in surface composition / surface passivation, changes in surface morphology and changes in particle size.

Investigations into the electrochemical properties of synthetic brannerite in [H_2SO_4] solutions were studied in a carbon paste electrode. Electrochemical methods were used to determine if synthetic brannerite was undergoing any type of passivation effect hindering the surface. The results showed that [H_2SO_4] has a predominate effect on the anodic dissolution rate of brannerite. The voltametric scans at a range of temperatures showed that the surface of the brannerite is liable to passivate, with the solution temperature and acid concentration key players in the behaviour of the surface. Acid concentrations above 100 g/L are required to prevent the onset of a passive region at moderate over-potentials, and promote facile dissolution.

The tafel curves results showed that acid concentrations from 15 to 50 g/l H_2SO_4 display limited leaching, with only a modestly active region corresponding to dissolution. H_2SO_4 concentrations of 100 to 150 g/L show a well-defined active region, ranging from approximately 0.45 to 0.55 V vs Ag/AgCl, where dissolution proceeds readily, but further scanning in the anodic direction leads to surface passivation, and a rapid drop off of the dissolution current.

An investigation into the surface of the synthetic brannerite -CPE sample was undertaken using EDX analysis after scanning for several minutes shows that the surface concentration of U relative to Ti is significantly decreased, indicating that a TiO_x passivating layer is responsible for the limited leaching of brannerite in commonly employed leaching conditions. ICP-MS analysis of the electrolyte solution after electrochemical leaching revealed that approximately 10 times the concentration of U dissolved when compared to Ti.

The apparent activation energies for the brannerite leaching in this active area were calculated to be approximately 50 kJ/ mol when the concentration of the acid was above 100 g/L. This apparent activation energy drops to approximately 30 kJ/mol for regions at which passivation is seen in the polarisation curves.

Natural brannerite dissolution

Results showed that the effect of increasing [Fe(III)], [H_2SO_4], and temperature was to increase the solubility of uranium from brannerite, (which agreed with the trends observed for the dissolution tests conducted for synthetic brannerite). Uranium extraction levels were similar for both samples as each parameter was varied, with the slight differences attributable to small variations in brannerite chemistry and/or degree of alteration within the two samples.

Maximum uranium extraction rates of ~ 80 % U were achieved using an [Fe(III)] of 12 g/L, at 150 g/L [H_2SO_4] and a temperature of 95°C. These conditions are more extreme than required for leaching uranium from other U-bearing phases such as uraninite and coffinite but refelect the more refractory nature of the chemically and more structurally complex brannerite. Samples that were heat treated to 1200 ºC to restore crystallinity performed much worse under identical conditions, with maximum uranium extraction rates

of < 10 % U recorded. The lower extraction rates were attributed to the heat treatment causing chemical and structural (recrystallisation) changes to the brannerite.

Uranium recovery processes from brannerite is not straightforward with the efficiency of uranium recovery being greatly influenced by the mineralogical characteristics of the ore. Natural brannerites, while less susceptible to uranium extraction than other U-bearing minerals, can achieve high uranium extraction rates providing i) acid strength, oxidant strength and temperatures are maintained at elevated levels (compared to those traditionally used for uraninite leaching), and, b) the brannerite has not undergone any post crystallisation, high temperature modification (e.g. metamorphism), that is likely to cause significant recrystallisation of the sample.

6.2. Future work

- Studies on the synthesis, characterisation and dissolution of various doped brannerites such as $UCaTi_2O_6$, $UCeTi_2O_6$ and $UThTi_2O_6$ – This will enable the influence of brannerite composition on dissolution to be determined, which in turn could assist in the selection of brannerite bearing ores to mine / process and /or the reaction conditions to use for treating ores containing brannerite of certain compositions

- An investigation into the effects of various anions and cations on synthetic brannerite dissolution – Uranium leach slurries contain numerous soluble species that may impact the dissolution of brannerite hence studies in this area of interest

- An investigation into the effect of [Fe(III)] : [Fe(II)] ratio on synthetic brannerite dissolution – This will determine the influence of Fe_{TOT} (Fe^{III}/Fe^{II}) and what role the oxidation reduction potential has on the dissolution of synthetic brannerite

- Electrochemical studies on natural brannerite and synthetically doped brannerites – This will enhance the role various impurities may play in the dissolution rate of natural brannerites and synthetically doped brannerites

- An in depth investigation on the passivation layer of synthetic brannerite and natural / heated natural brannerite – This investigation will enhance the chemical knowledge of the passivating layer that hinders uranium extraction from brannerite and may lead to overcoming that barrier

- Investigation of standard parameters on high grade ore tailings (seeding of synthetic brannerite into ore tailings) – This study will lead a gaining a greater understanding on the effect that re-leaching tailings will have on the overall uranium extraction

- Studies on the alkaline leaching on synthetic brannerite and natural brannerite – To determine if alkaline conditions are more suitable for the optimum extraction of uranium from synthetic brannerite

- Bio-leaching studies on synthetic brannerite, doped brannerite and heated natural brannerite – To use an environmentally friendly leaching technique, bio-leaching, in order to extract the uranium from synthetic brannerite, doped brannerite and heated natural brannerite